UNIVERSITÀ
DEGLI STUDI
DI PADOVA

SEDE AMMINISTRATIVA: Università degli Studi di Padova
DIPARTIMENTO DI ASTRONOMIA

Scuola di Dottorato di Ricerca in Astronomia

- Ciclo XXIII -

STELLAR EVOLUTION CODE WITH ROTATION

Direttore della Scuola: Dott. Giampaolo PIOTTO

Supervisor: Ch.mo Prof. Cesare CHIOSI

Dottoranda:
Jasna KRIVIČIĆ

1 Febbraio 2012

Abstract

There is a lot of observational and theoretical evidence that rotation crucially affects stellar structure and stellar evolution in particular for massive stars. Rotation influences the life of stars in several ways. For instance, centrifugal forces reduce the effective gravitational attraction, but also certain mixing processes of chemical elements can be induced by rotation, and mass loss can be altered. Within this thesis we describe the implementation of differential rotation in a stellar evolution code. Because of theoretical considerations stars are assumed to establish a rotation law with constant angular velocities on isobaric surfaces (shellular rotation). In this case the one-dimensional, spherical stellar structure equations can be modified to account for differential rotation including structural deformations of the star. By this approach the description of a stellar object is formally kept one-dimensional and one can utilize the numerical infrastructure of an existing "nonrotating" stellar evolution code. As a basis we use the Padova stellar evolution code, which is prepared and tested by us for the purposes of this work. In this thesis we present details about the development of additional numerical modules for treating rotation and how these extensions are implemented in an existing code. Moreover, we show the first results of our new implementation, which also includes a prescription of mass loss taking into account the effects of rotation. We discuss the obtained evolutionary tracks for rotating massive stars and compare our findings with results available in the literature. As far as a comparison is meaningful because of different stellar models and different degrees of sophistication in the modelling of additional physical processes, we observe the same effects of rotation as have been reported in the literature. For instance, on the main sequence the effective temperature is reduced for rotating models with respect to their nonrotating

counterparts. Rotating stars essentially mimic the behavior of nonrotating but slightly less massive stars. Our work explores the effects of rotation for varied stellar masses, varied chemical compositions and different initial rotation rates. In addition, the role of overshooting in rotating models is investigated. Finally, we indicate plans for future work, which includes numerical developments, the consideration of further physical processes as well as the computation and detailed analysis of a larger set of models.

Riassunto

Esistono numerose evidenze sia sperimentali che teoriche riguardanti l'importanza della rotazione sulla struttura ed evoluzione delle stelle e in particolare di quelle massicce. Limitandoci ad alcuni aspetti pi importanti, la rotazione grazie alla presenza delle forze centrifughe riduce l'effetto della forza gravitazionale, induce complicati processi di mescolamento delle abbondanze chimiche, e altera l'effetto della perdita di massa per vento stellare. In questa tesi, descrivo quanto fatto per introdurre la rotazione differenziale nelle equazioni di struttura delle stelle e nel codice numerico di Padova per il calcolo dei modelli stellari. La teoria permette di descrivere le stelle in presenza di rotazione mediante una legge di rotazione con velocità angolari costanti sulle superfici isobare (shellular rotation). In questo modo le equazioni di struttura in simmetria sferica radiale possono essere facilmente modificate per tener conto della rotazione differenziale e delle deformazioni strutturali indotte dalla rotazione stessa. In questo modo la descrizione di una stella pu ancora essere fatta in formalismo unidimensionale (sola coordinata radiale). Grazie a questa drastica semplificazione del problema, la struttura formale e contenuto fisico del codice numerico sviluppato per modelli non rotanti puo essere utilizzata anche in presenza di rotazione. Il codice utilizzato quello in uso a Padova, il quale stato opportunamente modificato per includere la rotazione. In questa tesi descrivo in dettaglio la parte di codice esplicitamente scritta per trattare la rotazione e come questa si inserisca e si integri nella rimanente parte del codice di struttura stellare. Illustro i primi risultati ottenuti assieme alla prescripzione per perdita di massa da vento stellare adottata in presenza di rotazione. Discuto i modelli evolutivi per stelle massice con rotazione e confronto i rilutati ottenuti con quelli esistenti in letteratura sullo stesso argomento. Considerando le differenze esistenti fra modelli

stellari simili calcolati da diversi autori, quanto ottenuto in presenza di rotazione perfettamente compatibile con quanto già noto in letteratura. Per esempio, durante la fase di sequenza principale, la temperatura effettiva dei modelli rotanti pi fredda rispetto a quella del caso non rotante. Le stelle in rotazione essenzialmente mimicano il comportanto di stelle non rotanti e di massa inferiore. Nella tesi esploro gli effetti dell rotazione al variare della massa stellare, della composizione chimica e di diversi tassi di rotazione iniziale. Inoltre studio l'effetto dell'overshooting convettivo in presenza di rotazione. Finalmente, brevemente presento e illustro i possibili sviluppi futuri per quanto riguarda la metodologia numerica, l'inclusione di ulteriori processi fisici e il calcolo di dettagliate griglie di modelli evolutivi.

Contents

CHAPTER 1

Introduction

"Epur si muove" said Galileo Galilei when claiming that the Earth is rotating. The same can also be said about stars, where the effects of rotation are much larger than on the Earth. The study of stellar rotation began about 1610, when Galileo recognized sunspots as being associated with the visible surface of the Sun and measured the rotation rate of this star by observing their motions across the solar disc. Christopher Scheiner was the first who noticed, around 1630, that the rotation rate at higher Sun's latitudes is slower. The equatorial regions rotate faster (with a period of about 25 days) than the polar regions which complete a cycle in 30 days. This so-called "differential rotation" is a property of gaseous bodies like stars (Jupiter shows also differential rotation), but its physical mechanism is still a topic of research. Stellar rotation is an example of an astronomical domain that has been studied for several centuries and in which the developments are rather slow.

The actual observation of the phenomenon of rotation needed to wait until stellar spectroscopy improved sufficiently to quantitatively observe the shape of stellar spectra lines. While Otto Struve is generally credited with being the "father of stellar rotation", seminal work by numbers of astronomers early in the 20th century laid a broad foundation for the quantitative determination of stellar rotation. The unambigous demonstration of the existence of stellar rotation awaited Rossiter's [144] explanation of an anamoly in the radial velocity curve β Lyrae as resulting from the axial rotation of the eclipsed star during the

eclipse. The systematic covering of the eclipsed disk yields shifts in the cetar of spectral lines during the eclipse resulting from apparent changes in the mean line-of-sight motion of the rotating eclipsed star. This effect, which is yet to described for any star by an ab initio model, is still generally known as Rossiter Effect and is considered to be first direct confirmation that stars do rotate.

1.1 Theoretical approachs of stellar rotation

The effects of rotation are considered in numerical codes since the seventies by Kippenhahn et al. [84] and by Endal & Sofia [51]. Further progress has been made by Zahn (1992) [179] and by Maeder& Zahn [114] who in particular took into account turbulent mixing. An important series of papers has been published by the Geneva group which have worked out many details of rotational effects in stellar evolution (see Maeder & Meynet [110] and references therein). Beside the Geneva group differential rotation has been investigated by Heger using codes developed by Langer (STERN) and by Woosley and Weaver (KEPLER) (see Heger & Langer [71] and Heger et al. [72]). In the early 2000s both groups have implemented magnetic fields in their codes (e.g. Heger et al. [73], Maeder & Meynet [112]). Heger have included the effects of magnetic fields according to the formula from Spruit [155] and the others were using general equations for the transport by Tayler-Spruit dynamo. Both groups find that the effects of magnetic fields are important but that non surface enrichment is produced durig the main sequence. Rotational mixing has been examined to explain certain observations and we will see this more in detail in a following section.

1.2 Observational evidence for stellar rotation

1.2.1 Rotation rates

The spectroscopic measurement of the widnening of line profiles (Slettebak et al. [151]) is the most direct method to determine the rotation rate of stars. This is due to the Doppler shif of light emanating from different regions of the stellar surface. Because of the rotational motion some parts of the stellar surface move towards the observer (spectral line is blue shifted) while others recede (spectral line is red shifted). The orbital motion of binary star is measured in a similar way, but in that case the Doppler shift of the lines affects the whole surface of the star and the result is a variation of the Doppler shift with time. In the case of stellar rotation light with different amounts of Doppler shift reaches us at the same time and therefore the spectral line appears broadened. In both cases only that part of the motion which is parallel to the line of sight causes a

measurable Doppler shift, while the movement perpendicular to the line of sight only causes the quadratic Doppler shift and it is not measurable for "normal" stars. This is, only the fraction $v \cdot sin(i)$ of the rotational velocity, v, parallel to the line of sight can be measured, where i is the inclination angle of the rotation axis relative to the "plane" of the sky. The inclination angle is known only in the exceptional case of eclipsing binaries. Unfortunately, these are mostly close binary systems and the rotation rate might be affected by their interaction, like tidal forces or mass exchange. Therefore, the true equatorial rotational velocities must be deconvolved from a sample of stars using a statistical method to get approximate mean values. For dwarf single late B and early O stars the typical mean rotation rates are found to be about 200 km/s, as it was find by Fukuda [58], Howarth et al. [76]. This is about 40% to 50% of their break-up velocity. Fukuda also poined out that some of the stars actually rotate close to their break-up velocity so that the emission lines in Be stars in general show higher mean rotation rates and that typical average rotation rates can reach as high as 400 km/s.

A more recent study performed by Huang & Gies [77], as we can see in Fig. 1.1, shows the disitribution of velocities for 496 stars with types 09.5 to B8 and masses between 3 and 20 $M_{\odot}$. The average velocity is 190 km/s after correction for the projection angle $sin(i)$ multiplied by $4/\pi$ to correct for random orientation effects.

Interoferometric observations with the Very Large Telescope Interferometer (VLTI) has allowed to reproduce the shape of a star where we can see that rotation makes the star shape oblate. In Fig. 1.2 we can see the shape reconstruction of the rapidly rotating Be star Achernar with a ratio $R_e/R_p \approx 1.5$ (Domiciano de Souza et al. [42]) A recent analysis of the data by Carciofi et al. [26] confirmed that the observations agree well with a rigidly rotating star at 99.2 % of its break-up velocity within the Roche model (see chapter 5). VLTI observations (Domiciano de Souza et al. [42]) of the fast rotating star Altair ($M \approx 1.8M$) confirm a gravity-darkening as predicted by the von Zeipel theorem (see chapter 3). This is also supported by further studies of Altair (Peterson et al. [136]) which rotates at 90% of its breakup angular velocity.

1.2.2 Stellar winds

The deviation of stellar mass loss from spherical symmetry is another indication for stellar rotation. One example are the non-spherical winds observed for O and B stars, Be and B[e] stars. This asphericity can be reflected in the line profiles, e.g. the P-Cygni profiles, for mass losing hot stars, in a polarization of the light and in excess in the infra-red and radio flux (Fullerton [59]). The

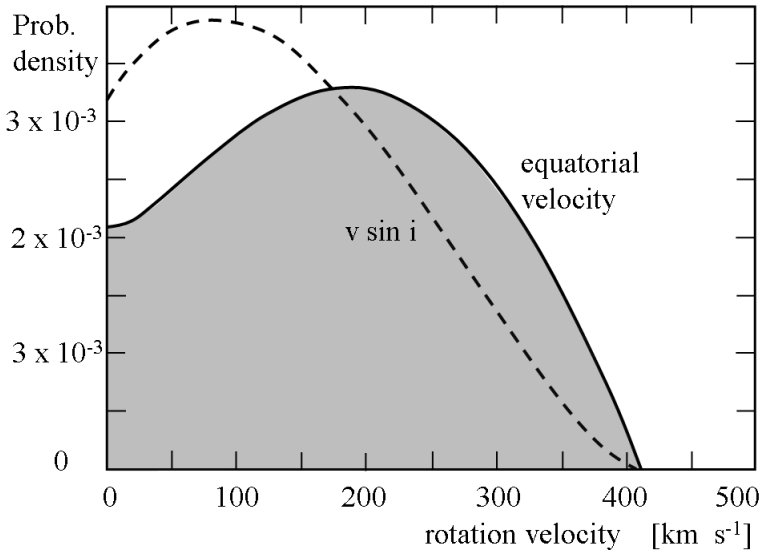

Figure 1.1— Probability density by km/s if rotation velocities for 496 stars with OB-types stars [77]

combined effects of a stellar wind and non-neglibible rotation can range from a small density contrast between equator and pole, to the formation of a wind compressed region in the equator, or even to a wind compressed disk. [16]

The morphology of observed planetary nebulae can be explained by different scenarios, such as binarity or interacting winds. Langer, Garcia-Segura & McLow [97] used the wind compressed disc model by Bjorkman & Casinelli [16] to tie the nebular structure to its formation and the evolution of the central star, In their proposed scenario, at the moment of the Luminouse Blue Variables (LBV) outbursts, which occur when the star reached its critical rotation, a slow dense equatorial wind is followed by a fast, almost spherical wind.

Alternatively, stellar rotation can produce strongly anisotropic mass loss. It was first noticed by Owocky & Gayley [134] that in a star rotating near the critical Ω limit the equatorial gravity darkening of the stellar radiation field can lead naturally to a bipolar wind outflow. This concept has been further developed by Maeder & Desjacques [107] to the conclusion that stellar winds from rotating stars show two main components: a fast, low density wind, produced by a higher T_{eff} and gravity at the poles, and an equatorial disc with a slow, dense wind, produced by a stronger opacities at the equator. Such a scenario

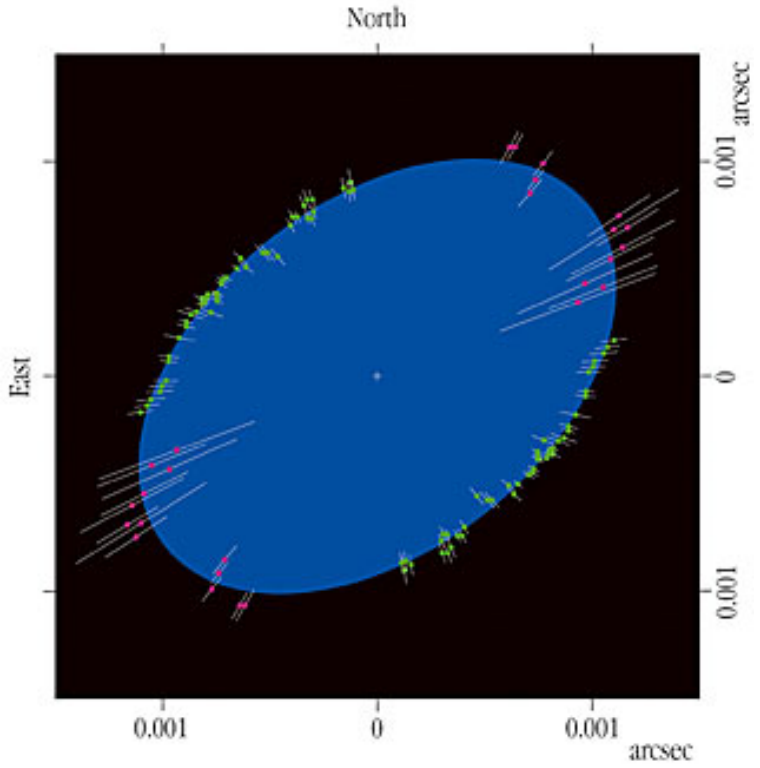

Figure 1.2— Shape reconstruction of the rapidly rotating star Archernar, as deduced from observations from the VLT Interferometer. Figure taken from [42]

well explaines the wind asymmetries found for many LBVs in the UV and from spectropolarimetry, but also produces models that morphologically well match the observations. In Fig. 1.3 we show the comparison between a simulation from Maeder & Desjacques [107] with $T_{eff} \simeq 30000K$ which generates an elliptical nebula, here compared with the LBV nebula around AG Carinae (right panel). It is also shown that at lower temperatures, $T_{eff} < 25000K$, the presence of a bi-stability limit at the equator generates an equatorial disc, such as in the case of η Carinae (left panel).

The "hour glass" nebula around η Carinae (Weis et al. [168])or the bipolar shape of many planetary nebulas are just some of the examples that show remarkable rotationally symmetric structures and might be best explained by rotation. The same explanation is valid for the ring system around Supernova

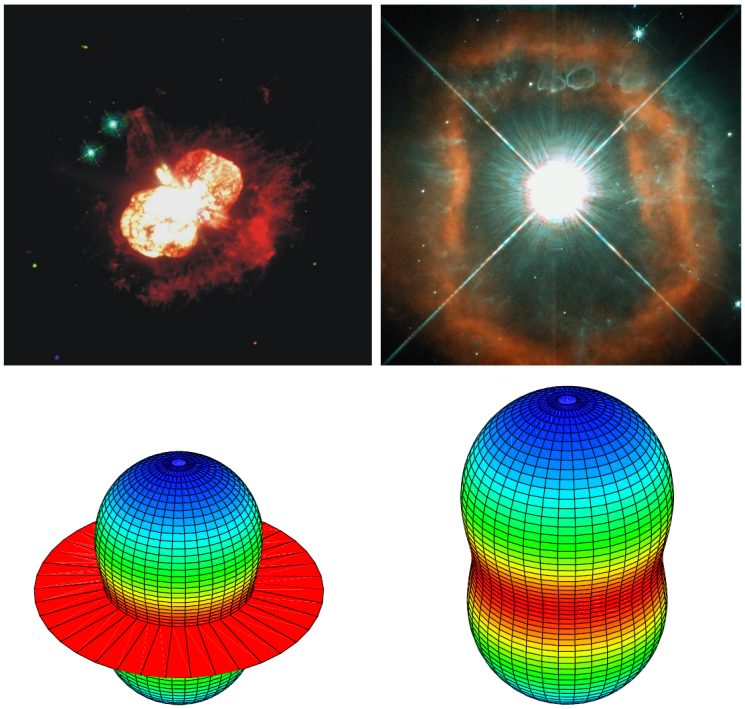

Figure 1.3— Comparison between simulated and observed structures of nebulae. Figures are taken from [107] and [168]

1987A as we can see on the Fig. 1.4 or the ring found around the blue supergiant Shear25.

1.2.3 Surface abundances

Chemical abundances are very powerful tests of the internal evolution, and they give strong evidence in favor of some additional mixing processes in O- and B-type stars, in supergiants, and in red giants of lower mass.

Striking surface abundance anomalies of massive stars comprise an enrichment of nitrogen, accompanied by low values of carbon and oxygen. Much evidence of He and N excesses in main sequence O-type and early B-type have been reported by a number of authors (e.g. Gies & Lambert et al. [63], Herrero et al. [74]). All fast rotators among the O-stars show some He excesses (Herrero et al. [74], Lyubimkov [103]). These abundance patterns are typical for hydrogen burning, and the coressponding processes take place only several

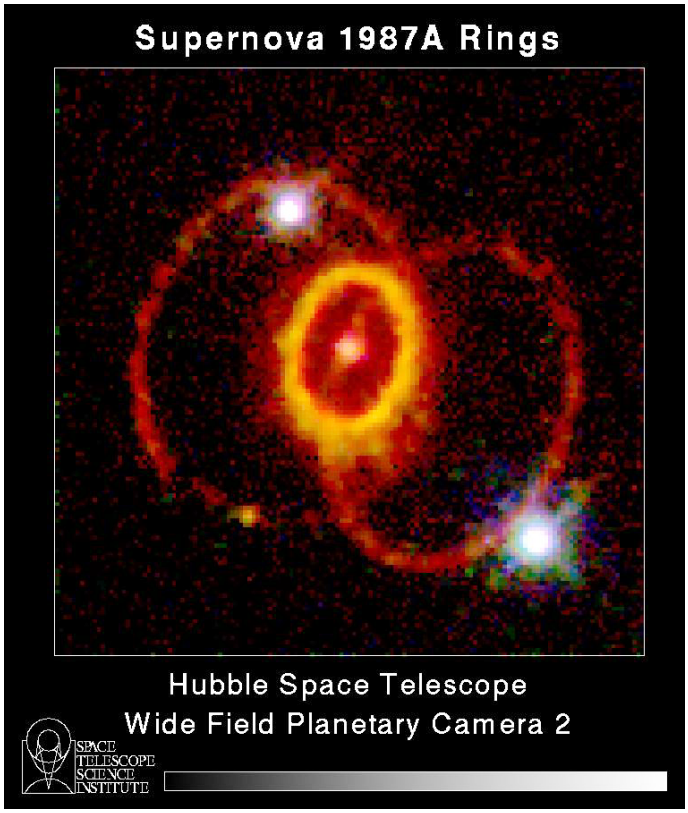

Figure 1.4— Optical imagine of the supernova remnant of SN1987A. Picture taken from www.spacetelescope.org/images/

solar masses below the surface, which is too deep to be uncovered by stellar winds during the main sequence evolution. The amplitudes of N enrichments at the end of the main sequence phase in massive stars are a reference point telling us the importance of mixing.

The boron abundances in five B-stars on the main sequence were found to be smaller than the cosmic meteoric value by a factor of at least 3 or 4 (Venn et al. [163]). Boron depletion occurs in stars that also show N excess; this suggests that the rotational mixing occurs throughout the star (Fliegner et al. [54]).

In table bla we replicate an compilation of [106] summarizing the nitrogen excess for different classes of stars in the Milky Way, in the Large Magellanic Cloud and in the Small Magellanic Cloud. These measurements provide evidence that rotational mixing plays an important role in massive stars. The ni-

Table 1.1— Nitrogen excess [N/H] observed in the Milky Way, the Large Magellanic Cloud and the Small Magellanic Cloud. The second row gives the corresponding metallicity.

Types of stars observed	Milky Way 0.02	LMC 0.008	SMC 0.004
O stars	0.8-1.0	-	1.5-1.7
B dwarfs $M < 20\ M_{\odot}$	0.5	0.7-0.9	1.1
B giants, supg. $M < 20\ M_{\odot}$	-	1.1-1.2	1.5
B giants, subg. $M > 20\ M_{\odot}$	0.5-0.7	1.3	1.9

trogen enrichment at the end of the main sequence phase leads to the following conclusions. In general, more massive stars show stronger nitrogen enhancement. Furthermore, taking into account the metallicities of the three galaxies the nitrogen excess is larger at lower metallicities. Besides, one recognizes an increasingly stronger enrichment as the stars evolve, constitent with the picture of rotationally induced mixing. Considering $v \sin(i)$ some authors found the tendative behavior that of a stronger mixing efficiency for higher values of $v \sin(i)$ (see e.g. Huang & Gies [77] and references in [106]).

The observations of abundances in supergiants lead to the following conclusions. Helium and nitrogen excesses seem to be the rule among OB supergiants and only a small group of the "peculiar" OBC stars has the normal cosmic abundances (Walborn [166]). An excesses of helium, sometimes called the "helium discrepancy", and corresponding excesses of N have been found by a number of authors (for more deteils see Maeder & Meynet [110]). Evidence of highly CNO-processed material is present for B supergiants in the range of 20-40 $M_{\odot}$. (McEarlean et al. [120]). Values of [N/H], the difference in log with respect to the solar values, amounting to 0.6 dex have been found for B supergiant around 20 M $M_{\odot}$ (Venn [162]). Such values agree with the enrichments found in the ejecta of SN 1987A (Fransson et al. 1989). The values of [N/H] for galactic A-type supergiants around 12 M $M_{\odot}$ lie between 0 and 0.4 dex ([162]). Very few abundance determinations exist in yellow and red supergiants. Some excess of N with respect to C and O has been found by Luck (1978) [102]. Barbuy et al. [7] found both enrichments and normal compositions among the slow rotating F-G supergiants. The dilution factor in the convective envelope of red giants and supergiants is so large that it is not possible from the rare data available to draw any conclusions about the presence of additional mixing (Denissenkov [41]).

All these above surface abundance peculiarities, which lead to discrepancies

with standard evoultionary models of massive star can be recovered by introducing one major effect of stellar rotation: the mixing of matter in the envelopes of massive main sequence stars (Langer et al. [96], Meynet & Maeder [124], Heger & Langer [71] It explains the enrichment of species produced deep inside the stars, and the depletion of fragile species, by transporting processed matter to the stellar surface.

But we need to mention the study of Hunter et al. [81] where the chemical compositions for 135 B-type stars in the Large Magelanic Cloud is presented with a broad range of rotational velocities (up to $\sim$ 350 km/s). This was the first significant abundance analysis of rapidly rotating stars early B-type stars and they utilised the nitrogen abundances to testing the theory of mixing, finding the theory to be unable to explain several aspects of the sample. Most of the outliers left cannot be used to test the rotation induced mixing , because they are evolved stars or known binaries. For the remaining one needs another explanation than pure rotational mixing. Brott et al. [23] confirmed quantitatively the result of Hunter et al. [81]. A conclusive assessment of the role of rotational mixing in massive stars requires a quantitative analysis that also accounts for the effects of binarity and magnetic fields.

1.2.4 Asteroseismology

Unlike its surface properties, the internal structure of a star, including its internal rotation, is not directly accessible to observations. Given that global helioseismology led to a huge step forward in the accuracy of the internal structure model and of the transport processes inside the Sun, asteroseismology aims to obtain similar improvements for different types of the stars by means of their oscillations. Stellar oscillations indeed offer a unique opportunity to probe the internal properties and processes, because these affect the observable frequencies. The confrontation between the frequencies measured with high accuracy and those predicted by models gives insight into the limitations of the input physics of models and improves them. In fact, stellar oscillation frequencies are the best diagnostic known that can reach the required precision in the derivation of interior stellar properties. Rotation also modifies the frequencies of the star's modes of oscillation (e.g. Gough [66]). An adequate seismic modelling of rotation inside stars therefore is within reach with high precision measurements and mode identifications of stellar oscillations.

In the past years, solar-like oscillations have been observed for a handful of stars either from the ground by using stabilized spectrographs developed for extra-solar planets searches or from photometric data obtained from space (e.g. Bedding & Kjeldsen [9]). While these asteroseismic observations mainly

focused on solar-type stars, solar-like oscillations have also been detected for a few red giants (e.g. Frandsen et al. [55]). These first detections together with the recent clear identification of non-radial oscillations of many red giants star (G-K giants) with CoRoT (De Ridder et al. [39]) stimulated the theoretical study of the asteroseismic properties of red giants stars and of the effects of various physical processes on the modelling of these stars. Some of Kepler's biggest surprise have been in its sounding out of red giants. Observations of gravity-mode period spacings in red giants permit a distinction between red giants burning helium in the core and those still only burning hydrogen in the shell. Bedding et al. [10] used high precision photometry obtained by the Kepler spacecraft over more than a year to measure oscillations in several hundred red giants. They find many stars whose dipole modes show sequences with approximately regular period spacings. These stars fall into two clear groups allowing the distinction between hydrogen shell burning stars (period spacing mostly $\sim$50 seconds) and those that are also burning helium (period spacing $\sim$100 to 300 seconds).

Beck et al. [8] reported an incresing rotation rate from the surface of the star to the stellar core in the interiors of red giants, using the rotational frequency splitting of recently detected "mixed modes". Information about angular momentum distribution is inaccessible to direct observations, but it can be extracted from the effect of rotation on oscillation modes that probe the stellar interior. By comparison with theoretical stellar models it was concluded that the core must rotate at least ten times faster than the surface. This observational result confirms the theoretical prediction of a steep gradient in the rotation profile towards the deep stellar interior and the standard model of red-giant formation, sun-like stars flinging their shallower layers outwards while their cores contract. Basic physics demand that angular momentum is conserved, so the outer layers must slow down their rotation and the contracting core must speed up, just as observed.

Some β Cep stars have been studied asteroseismically with data from intensive ground-based observational campaigns (Aerts, [1]). These studies placed limits on convective core overshooting and demonstrated the presence of non-rigid internal rotation (Aerts et al. [2]), in addition to identyfying constraints on the internal structure, opacities and abundances. With the new level of precision provided by Kepler, it is possible to examine the suspected presence of solar-like oscilaltions in β Cep stars (Belkacem et al. [12]). The detection of more pulsation modes is the key to detailed analyses of internal rotation. New methods using rotational mode splittings and their asymmetries have been developed by Suárez et al. [158], and might help to test theories describing angular momentum redistribution and chemical mixing due to to rotationally induced

turbulence. The analysis of "hybrid" p and g mode pulsators will result in tighter constraints on stellar structure, particularly on opacities (Handler et al. [70]). This increased understanding of β Cep stars through asteroseismology can provide useful information about the chemical evolution of the Universe. β Cep stars, which pulsate in modes of low radial order and with periods of about 2-7 hours, are ideal for determining the interior structure and compositions of stars of about 10 $M_{\odot}$, precursors of type II supernovae.

These project, and others further into the future, covering stars across the HR diagram will provide an extensive observational basis for investigating stellar interiors.

1.3 Theory versus observation

1.3.1 The ratio blue to red

The problem of the number ratio B/R of blue to red supergiants is one of the most severe in stellar evolution. As stated by Kippenhahn & Weigert [87] about stars in blue loops in the He-burning phase, the present phase is "... a sort of magnifying glass, revealing relentlessly the faults of calculations of earlier phases". The observations of nearby galaxies show that there are much more red supergiants at metallicities lower then solar, so that the B/R ratio decreases steeply with decreasing metallicity [80].

There were no sets of models which correctly predict the observed trend of decreasing B/R with decreasing Z, as emphasized by Langer & Maeder [98]. The comparisons generally show that the models with Schwarzschild's criterion (with or without overshooting) may reproduce the observed B/R at solar metallicity, while they fail at lower Z. At the other extreme, the models with the Ledoux criterion and those with semiconvection reproduce well B/R at the metallicities of the SMC, but they fail at higher Z. This shows, that at least in part, the problem is related to the size of the core and to the mixing efficency outside the core.

Other effects, such as mass loss, convection, opacities and metallicities play also a role. In particular, the growth of mass loss favours the formation of more red supergiants in the He-burning phase. However, the B/R problem in the SMC cannot be solved by mass loss, because the mass loss rates at lower Z, as in the SMC, are smaller than in the Galaxy and this produces fewer red supergiants.

In the work of Maeder & Meynet [111] it was shown that in this case rotation plays an important role. They found that the B/R ratios are much smaller for higher initial rotation velocities. This agrees with the fact that rotation favours the formation of red supergiants and reduces the lifetime in the blue. It was

noticed that for a $\bar{v} = 200km/s$ a B/R ratio of about 0.6 is well corresponding to the range of observational values. This is studied in more detail in Maeder & Meynet [111]. Here we just mention that when an extended intermediate convective zone is associated to the H-burning shell, the stars tends to stay in the blue part of the HR diagram. Rotational mixing tends to reduce the extension of this intermediate convective zone and thus to accelarate the redwards evolution in the HR diagram. The larger He-core in the rotating models means that a larger fraction of the total luminosity is made in the core. This means that the H-burning shell in the rotating case leads to a decrease of its H-content and opacity, and this also contributes to reduce the importance of the convective zone associated with the H-burning shell.

Therefore models with rotation well account for the long standing problem of the large numbers of red supergiants observed in low Z galaxies.

1.3.2 Current problems with Wolf-Rayet stars

Wolf-Rayet (WR) stars play a very important role in astrophysics as signatures of star formation in galaxies and starbursts, as injectors of chemical elements and of the radioactive isotope 26-Al, as sources of kinetic energy into the interstellar medium and as progenitor of supernovae and, likely as progenitors of long soft γ-ray bursts. One can identify certain subclasses of WR stars (WC, WN and WO stars) according to their spectra (see chapter 5 for details) The number of WC and WN stars increases with metallicity, for more details we refer to the reviw by Massey 2003 [117]. Many attempts have been performed to reproduce this observed trend: for instance the enhanced mass loss rate models of Maynet & Maeder. [109] provided a good agreement for solar and higher than solar metallicity but produced too few WN stars in metal poor regions. The inclusion of rotation together with reduced mass loss rates accounting for the effects of clumping improved the situation in the metal poor region, but produced too many WN stars at solar and higher metallicities (Meynet & Maeder [127]). Eldridge & Vink [49] show that models that include the mass loss metallicity scaling during the WR phase closely reproduce the observed decrease of the relative population of WC over WN stars at low metallicities. However, such models severely underestimate the fraction of WR to O-type stars. In that case, to improve the situation, a high proportion of WR stars originating from mass transfer in close binaries should be assumed at all metallicities. For instance at solar metallicity about 75% of the WR stars should be produced in close binary systems (Eldridge et al. [48]).

The WN/WC number ratio depends also on other factors, in particular on the evolutionary scenario. In Meynet & Maeder [125], the most massive

rotating stars enter into the WR regime already during the MS phase. This feature has good and bad effects. On the one hand, it allows these models to well reproduce the variation of the number fraction of WR to O-type stars since it significantly increases the WR lifetimes. On the other hand, it produces very long WN phases since the star enters into the WR phase having still a huge H-rich envelope. As a consequence, too low values for the WC/WN ratio are obtained at solar and higher metallicities.

In Meynet & Maeder [125], [127] the hypothesis has been made that when a star enters into the WR stage during the MS phase, it avoids the Luminous Blue Variable phase. Actually stars may behave differently. It may well be that a star which becomes a WR star during the MS phase, enters an LBV phase after the core H-burning phase, and then evolves back into the HR regime, When this evolutionary scenario is followed, reasonable values for both the WR/O and the WC/WN ratios are obtained. Indeed the ratios of WR/O and of WC/WN given by these models at solar metallicity are 0.06 and 0.9 which compares reasonably well with the observed values of 0.1 and 0.9 respectively (Meynet et al. 2008 [122]). Both ratios are not reproduced by the nonrotating models to which similar scenarios is applied. This ilustrates the possible key role that the LBV phase may play in shaping the WC/WN ratio.

1.3.3 Progenitors of supernovae

The famous example of a Type II supernovae event is the supernova which occured on February 23, 1987 in a LMC, a companion galaxy of the Milky Way, and was cataloged as SN 1987A. It was the by far closest supernova since centuries and opened unprecedented possibilities for observations and for testing of theoretical models. However, to the surprise of the scientific community, the stellar progenitor of this supenovae was a blue supergiant (Gilmozzi et al. [64]) with an effective surface temperature of more than 15 000 K and a radius of several tens times of our sun. In contrast, according to theoretical modelels and analyses of many type II supernova light curves most of the type II supernovae progenitor stars are expected to be red supergiants, which have effective temperature of 3 000 to 4 000 K and radii of several hundreds of thousands times that of our sun at the instant of the explosion (Eastman et al. [43]). Therefore, SN 1987A might be an exception to a normal case. One important influence on the properties of the star at the end of its evolution is its initial composition, i.e., the matter the stars forms from, which is different in the less evolved LMC than in the vicinity of our sun.

A completely unexpected, spectacular feature of the SN 1987A was a nebulae system of three rings around it as we can see on Fig. 1.4, which originates

from the presupernova star and was ionized by the flash of the supernova explosion. The presence of the ring structures around SN 1987A (Burrows et al. [24]), which likely result from the axisymmetric inhomogeneities in the stellar wind ejected by the progenitor (e.g. Martin & Arnett [116]), and the high level of nitrogen enchancements in the circumstellar material (e.g Fransson et al. [56]) are features that may be a hint that rotation played an important role in the evolution of the progenitor star of this supernova and can eventually be important in the evolution of many massive stars. Woosley et al. [176] suggested that any mechanism that reduces the helium core while simultaneously increasing helium in the envelope would favour a blue supernova progenitor. Such an expectation follows from the theoretical models by Hirschi et al. [75] for rotating stars at higher masses; the rotating models are more luminous and evolve to RSG phase before the ignition of He burning, which result in higher mass loss rates, the loss of most of the H envelope before the termination of He burning, and an evolution towards the blue before the terminal points. This presupernova rotating model of a $20M_{\odot}$ can end its life in the blue, but the model star has a low hydrogen content and would probably result in a IIb or Ib SN rather than a type II.

1.3.4 The type Ib and Ic supernovae

Type Ib supernovae are core-collapse supernovae whose spectrum shows no hydrogen lines. The spectra of type Ic supernovae shows no hydrogen and helium lines (e.g. Wheeler et al. [171]). The progenitors of these core collapse supernovae are thus believed to be stars stripped of their original H-rich envelope for type Ib's and also of their He-rich envelope for Ic's. Progenitors are therefore naked stellar cores as for instance Wolf-Rayet stars (WR). The observed frequency at solar metallicity of type Ibc supernovae is about 20% the frequency of type II supernovae (Cappellaro et al. [25]) which represents a significant fraction of core collapse supernovae.

In Fig. 1.5 we can see the different supernovae types expected for various initial metallicities as given from rotating models by Georgy et al. [61]. From the graphic it can be observed that the number fraction of type Ibc to type II should increase with metallicity. This is an effect of the stronger winds at higher metallicities, which favor the formation of H-free stars at the end of their evolution. The expected increase of the Ibc/II ratio has been shown by Prantzos & Boissier [139]. Comparing the theoretical ratios obtained from single stars with the observed ones, a good fit is obtained only for the rotating models computed by Georgy et al. 2009 [61] and Meynet & Maeder [127].

It is important to point out that an observed trend can also be reproduced

by invoking close binary star evolution (Eldridge et al. [48]). In this scenario, the hydrogen rich envelope is removed either through a Roche lobe overflow process or during a common envelope phase, producing a WR star.

Two very differnt models (single stars with rotation and close binary evolution with mass transfer are both able to give a reasonable fit to the data. As a matter of fact both scenarios probably contribute to the observed populations of type Ibc supernovae. However, it would be interesting to know their relative importance and how their relative importance changes with metallicity. Predictions of single star models for the variations with metallicity of the separate ratios of type Ib/II and of Ic/II are discussed in Georgy et al. [61].

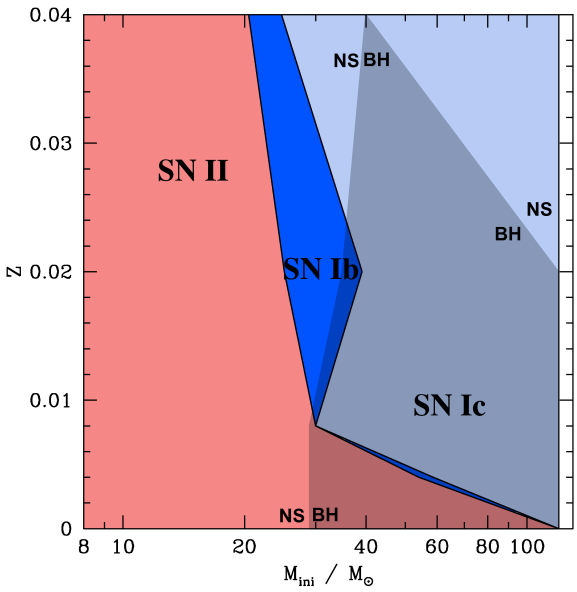

Figure 1.5— The different supernovae types expected for various initial metallicities as given from rotating models. Figure taken from [61].

1.3.5 The progenitors of long soft Gamma Ray Bursts

Collapsar model proposed by Woosley (1993) [173] is the most promising model for the prognitors of the long soft Gamma Ray Bursts (GRBs). In this model, a long GRB is the product of the evolution of a massive star, which at the end of their evolution produces a fast rotating black hole. In addition, for the GRB to be visible, the massive star should have lost its envelope. This model

received a strong support when observations showed that there is a connection between long-soft GRB events and type Ic supernovae (Woosley & Bloom [174]). The two discoveries that revolutionized this field were SN1998bw/GRB980425 (Galama et al. [60]), the first discovery of an explosion that produced both a GRB and a SN, and SN2003dh/GRB030329 (Stanek et al. [156]). In more distant GRBs, although the afterglows (electromagnetic radiation resulting from the interaction between the outflow of the GRB and the interstellar medium) are usually observed, the supernovae are intrinsically much fainter and hence are often undetected. This confirmed the collapsar model, involving a compact, rotating hydrogen deficient massive progenitor, i.e. a WR star (MacFayden & Woosley [104]). Rotation is critically important since the collapsar model involves highly collimated jets produced along the polar axes, arising from a dense, equatorial accretion disc feeding the central black hole. The dense stellar winds from WR stars hinder the direct measurments of rotational velocities, but polarimetry suggests negligible deviations from spherical symmetry in most solar metallicity WR stars. An unsolved challange to evolutionary models involves the requirement of high angular momentum within the WR core in the collapsar model. Evolutionary models allowing for magnetic fields involve cores that are sufficiently spun down before collapsing, in most models either due to shear between the slowly rotating envelope and the core or due to loss of angular momentum during the WR phase as a result of its high mass loss rate. These permit the observational rotational rates of young pulsars (e.g. a period of 33 ms for the Crab pulsar) to be reproduced. However, collapsars would require an order of magnitude shorter periods of 2ms (Woosley & Heger [175]).

1.4 Our work

As we outline at the begining of this chapter stellar rotation is a crucial property of stars not yet explored in full detail observationally nor theoretically. Observations prove that stars rotate. However, their concrete rotation profile throughout the star is not easily accessible by observation. But there are for instance hints that stellar cores rotate substantially faster than the surface layers as we discussed in the context of astroseismology. Based on these facts one should conclude that stellar rotation is a key ingredient in understanding stellar evolution theoretically and to connect stellar models with observations.

Considering its importance the treatment of stellar rotation is still somewhat lagging behind in to date stellar models. Only a few research groups have implemented stellar rotation in their evolution codes, although an inclusion of stellar rotation should be obligatory for the above mentioned reasons. In particular, it is known that stellar rotation is important for the evolution of

massive stars. Here we also emphasizes that the theoretical modelling of stellar rotation is crucial for the consideration of massive stars as progenitors for supernova explosions where rotation may play a non-negligible role in particular in the context of long gamma-ray bursts where according to theoretical models rotation is highly important.

Given these facts the consideration of stellar rotation in stellar models is highly desrable. It is the purpose of the project presented in this thesis to implement stellar rotation in the existing Padova stellar evolution code, which up to now did not consider rotational effects. The main focus is put on massive stars because these stellar objects are thought to be most affected by stellar rotation. The first challenge and important step on the way to an implementation with rotation however is to prepare a version of the existing code in a way that it can be used for stellar modelling without rotation but taking into account the latest developments in the input physics (like neutrino reactions, nuclear reactions rates and opacities) and to test and run this version successfully. The code which is the basis for the inclusion of rotation, is outlined in chapter 2. The results of calculations with this code are presented in chapter 4 where we obtained evolutionary tracks for very massive stars with different metallicities without rotation. The implementation of rotation as the main subject of this work is explain in chapter 3. Here we discuss the underlying equations and, since according explainations are not available in the literature, we spend particular effort for a thorough description of the numerical scheme developed within this project for implementing stellar rotation. Finally, in chapter 5 we show the first results of our new implementation includiong stellar rotation, which opens an avenue for future work. The outlook to future projects is described in chapter 6 together with a summary and the conclusions of our work.

CHAPTER 2

Basic stellar structure equations and their Numerical implementation

This chapter is thought to give an overview of the basic equations describing stellar evolution without discussing too many details in order to capture the main features. There is a wealth of literature availabe where detailed discussions can be found. Furthermore, in this chapter we sketch the numerical methods which are used to solve the resulting set of equations. The presentation in this chapter will be on a rather basic level because it is supposed to set the stage for the main work of this thesis which is presented in chapter 3, where we will describe in detail how the equations summarized in this chapter are modified in order to treat stellar rotation and how the existing numerical modules of the code are extended to solve the resulting set of modified stellar structure equations.

2.1 Equations of stellar structure and evolution in spherical symmetry

Here we present in brief the common equations of stellar evolution in spherical symmetry, this means for sufficiently slowly rotating stars without magnetic fields. This essentially implies that any quantity of interest (for instance the density, the pressure, the temperature and so on) is solely a function of the radial coordinate r. These quantities however will change in time. But, as long as a star does not encounter a very rapid evolutionary phase (like explosive burning) or heavy pulsations, the stellar fluid can be considered to be

hydrostatic equilibrium because all relevant timescales are much longer than the hydrodynamical timescale

$$\tau_{hydro} \approx \sqrt{\frac{R^3}{GM}}. \tag{2.1}$$

This is an estimate for the time a star needs to dynamically adjust to a new structure. Under the assumption of hydrostatic equilibrium the pressure P at some point r inside the star is given by

$$\frac{dP}{dr} = -\frac{\rho(r)GM(r)}{r^2} \tag{2.2}$$

with the density $\rho(r)$ and the mass $M(r)$ enclosed by a sphere with the radius r. Here, G denotes the gravitational constant.

Moreover, it is assumed that the mass of a star is conserved, which by considering a thin shell reads

$$dM(r) = 4\pi\rho(r)dr \tag{2.3}$$

and can be integrated to

$$M(r) = \int_0^r dM(r). \tag{2.4}$$

Alternatively, one may express the equation of mass conservation as

$$\frac{dM(r)}{dr} = 4\pi\rho(r). \tag{2.5}$$

Beside the conservation of mass, also the conservation of energy needs to be fulfilled. Denoting the energy flux through a sphere with radius r with $L(r)$, one can deduce that this flux changes as

$$\frac{dL(r)}{dr} = 4\pi\rho(r)\left(\epsilon_n - \epsilon_\nu + \epsilon_{grav}\right) \tag{2.6}$$

with the specific energy production rate by nuclear burning ϵ_n. Furthermore, this equation takes into account energy losses by neutrinos, which are given by ϵ_ν as the loss rate per unit mass and unit time. Beside these microphysical sources and sinks of energy, a star can loose or gain energy by changing its inner structure (expansion or contraction), because mechanical work can be converted in heat. This effect is subsumed by ϵ_{grav}. Note that all energy rates on the right-hand side of (2.6) are functions of the temperature, the density and the chemical composition, as for instance the efficiency of certain nuclear reactions is highly dependent on the thermodynamical properties.

In addition to the above equations for the pressure, the mass shells and the luminosity, one have to specify the equation of energy transport because the efficiency of energy transport determines the temperature profile of a star. the concrete form depends on whether energy is transported by radiation or by convection. In the case of radiative transport the equation for the temperature profile takes the form

$$\frac{dT}{dr} = -\frac{3\kappa\rho}{4acT^3}\frac{L(r)}{4\pi r^2} \tag{2.7}$$

with the opacity κ and the radiation constant a. For energy transport by convection equation (2.7) has to be replaced by

$$\frac{dT}{dr} = \left(1 - \frac{1}{\gamma}\right)\frac{T}{P}\frac{dP}{dr} \tag{2.8}$$

where γ is the ratio of the specific heats c_P/c_V.

At this point it is important to note that all quantities appearing on the right-hand sides of the equations 2.2, 2.5, 2.6, 2.7 and 2.8 are functions of the temperature, the density and the chemical composition. The density is determined by the pressure, the temperature and the chemical composition through the equation of state. (Here, we do not discuss the term ϵ_{grav} which contains a time derivative, but see any textbook on stellar evolution.)

In order to obtain for a given chemical composition a solution to the equations governing the stellar structure, one has to specify appropriate boundary conditions. Of course, in the center $r = 0$ of the star one sets $L(0) = 0$ and $M(0) = 0$. At the surface R of the star $M(r)$ equals the prescribed mass M of the star. In addition to these requirements the solution of the stellar interior needs to match a solution for the stellar atmosphere (see e.g. Kippenhahn & Weigert [87] for details and chapter 3), where one applies the Stefan-Boltzmann law

$$L = 4\pi R^2 \sigma_B T_{eff}^4 \tag{2.9}$$

with the Stefan-Boltzmann constant σ_B.

Given appropriate boundary conditions and a given chemical composition one can in principle solve the set of stellar structure equations to obtain profiles of the pressure, the temperature, the mass and the luminosity (neglecting the time dependent term ϵ_{grav}). However, it turns out to be very useful to perform a change of the variables. Commonly, in stellar evolution one adopts a Lagrangian point of view. Then, the mass inside a sphere $M_r = M(r)$ is promoted to an independent variable, and all quantities are expressed as a function of this Lagrangian coordinate M_r. For this transformation one makes use of

equation (2.5) and obtains for the hydrostatic equilibrium

$$\frac{dP(M_r)}{dM_r} = -\frac{GM_r}{4\pi r^4(M_r)}. \tag{2.10}$$

The equation for the mass conservation turns now into an equation determining the position r of a given mass shell

$$\frac{dr(M_r)}{dM_r} = \frac{1}{4\pi r^2(M_r)\rho(M_r)}. \tag{2.11}$$

The energy balance is now given by

$$\frac{dL_r(M_r)}{dM_r} = \epsilon(M_r) \tag{2.12}$$

subsuming energy production and loss in only one term ϵ. Finally, the equation for the energy transport reads in the new coordinates

$$\frac{dT(M_r)}{dM_r} = -\frac{GM_rT(M_r)}{4\pi r^4(M_r)P(M_r)}\nabla. \tag{2.13}$$

In the case of radiative energy transport, we use

$$\nabla = \nabla_{rad} = \frac{3}{16\pi Gac}\frac{\kappa_R L_r P}{M_r T^4} \tag{2.14}$$

where the Rosseland opacity provides a frequency averaged opacity. In the case of convective energy transport one uses

$$\nabla = \nabla_{ad} = \frac{d\ln(T)}{d\ln(P)}_{ad}. \tag{2.15}$$

Which nabla to use is decided by the Schwarzschild criterion, which determines whether the stellar fluid is unstable to convection. Note that also other choices are possible (see e.g. Kippenhahn & Weigert [87]). We note that thermal conductivity can be implementated with a "total" opacity given by

$$\frac{1}{\kappa_{tot}} = \frac{1}{\kappa_{rad}} + \frac{1}{\kappa_{cond}} \tag{2.16}$$

where one defines

$$\kappa_{cond} = \frac{4acT^3}{3\rho K} \tag{2.17}$$

with the conductivity K.

One recognizes that all quantities on the right-hand sides of the above equations depend only on the mass shell, the pressure, the luminosity, the temperature and the chemical composition. As mentioned, the equation of state, the opacity, the energy production and the ∇ are entirely determined by these variables. Hence, the resulting system is essentially one-dimensional though the involved dependencies may be rather complicated and may require some numerical schemes, for instance for interpolating in an eqaution of state table. (Note that the term ϵ_{grav} contains a time derivative, which is implemented implicitly.)

At this point one may wonder how stars actually evolve since the above equations do not contain any time dependence except for ϵ_{grav} which is often negligible. The system indroduced above in principle only determines the stellar structure. In order to understand how a star evolves one has to consider the nuclear burning taking place in the stellar interior. This nuclear burning provides energy and changes the chemical composition of the matter by depletion of fuel and the production of nuclear ashes. These processes are the driving force that moves a star through the Hertzsprung-Russell diagram. Comparing the relevant timescales one finds that the nuclear timescale is the most important. This timescale is given by the available energy reservoir by nuclear reactions divided by the luminosity and turns out to be longer than the Kelvin-Helmholtz timescale, which characterizes the contraction and cooling of a gas cloud. Moreover, both timescales exceed significantly the hydrodynamical timescale (2.1) of a star. This fact has been already taken into account in equation (2.2) where hydrostatic equilibrium is imposed. The comparison of timescales justifies to advance a stellar model entirely through the evolution of the chemical composition.

The chemical composition of stellar matter is described by mass fractions X_i of certain nuclei. For a nucleus with mass m_i, the mass fraction is defined by the particle number n_i per volume via

$$X_i = \frac{m_i n_i}{\rho} \tag{2.18}$$

with the density ρ.

The mass fractions are given at every mass shell and generally change in time. Here the particular advantage of the Lagrangian scheme becomes obvious because in an Eulerian frame any expansion or contraction of a mass shell would imply a change of the composition, which has to be taken into account accordingly. Of course, the chemical composition "vector" has to fulfill the normalization condition

$$\sum_i X_i = 1. \tag{2.19}$$

In cases, where the chemical composition is changed entirely by nuclear reactions, the evolution of the composition "vector" is given by

$$\left(\frac{dX_i}{dt}\right)_{nuc} = \frac{m_i}{\rho}\left[\sum_j r_{ji} - \sum_k r_{ik}\right]. \tag{2.20}$$

Here r_{ji} is the reaction rate, that is, the number of reactions per unit volume per second, of a reaction that produces species i, and r_{ik} is the reaction rate of a reaction that destroys i. This expression must be evaluated for each nucleus i in all mass shells of a star. In addition, one finds the energy generation rate per unit mass as it is used in the equation of the energy conservation (equation (2.12)) via

$$\epsilon_{nuc} = \sum_{p,q} \epsilon_{p,q} = \frac{1}{\rho}\sum_{p,q} r_{pq} e_{p,q}. \tag{2.21}$$

The sum runs over all reactions that transform a nucleus p into a nucleos q releasing an energy $e_{p,q}$.

The above expression for the changes of the chemical composition do not hold for convective regions because there instantaneous mixing is assumed. In this case the chemical composition of the whole convective zone is evolved according to

$$\left(\frac{dX_i}{dt}\right)^{conv}_{nuc} = \frac{\int_{conv}\left(\frac{dX_i(M_r)}{dt}\right) dM_r}{\int_{conv} dM_r}. \tag{2.22}$$

The integrals are taken over the whole convective region and the compositional changes $\frac{dX_i(M_r)}{dt}$ for every layer in the convective zone are evaluated.

We stress that equation (2.20) is extendable to account for various mixing processes. Then, additional terms are added on the right-hand side of equation (2.20), which describe microscopic diffusion and turbulent mixing. Furthermore, mixing due to stellar rotation can be implemented in the same way. Note that the additional terms involve first or second order spatial derivatives which requires special care in the numerical treatment. In this context we refer to Salasnich [147] where the implementation of a Crank-Nicoloson scheme is described, which allows a stable evolution. Note that this approach requires to solve a set of linear equations.

After discussing the time evolution of stellar models we now turn to the question how to numerically risolve the stellar structure equations. It is important to note that as argued above a stellar evolutionary model can be considered as a sequence of equilibrium stellar structure models.

2.2 Basic numerical schemes in stellar evolution

This section is devoted to briefly sketch the numerical methods underlying the implementation. Here we focus on a general description of the numerical scheme for solving the stellar structure equations in the spherical, nonrotating case because this scheme is used as the basis for the inclusion of stellar rotation. The according adaptions and extensions, which are required to treat stellar rotation, are described in detail in chapter 3. We also note that there are a number of excellent textbooks available to which we refer the reader for details. For instance, many details on the numerical implementation of stellar evolution codes can be found in Kippenhahn & Weigert [87]. Furthermore, the "Numerical recipes" [140] provides a general review of numerical schemes.

As has been argued above, the equations governing the evolution can be decoupled from the set of equations determining the stellar structure. Here we focus on the latter as the main difficulty in stellar evolution models. Formally one has to solve a boundary-value problem. Before discussing the actual implementation we recall some basic procedures for solving systems of nonlinear equations. Additional information can be found in [140].

A standard procedure for solving nonlinear equations is the Newton method, which can be employed to computed iteratively the root of a one-dimensional nonlinear function. Given a function $f(x)$ the task is to solve

$$f(x) = 0. \tag{2.23}$$

The derivative $f' = \frac{df}{dx}$ can be obtained analytically. Given any guess value x^0 that approximates the unknown root x^{root} with $f(x^{root}) = 0$, one can obtain successively better approximations to x^{root} by the iteration

$$x^{i+1} = x^i - \frac{f(x^i)}{f'(x^i)}. \tag{2.24}$$

If an appropriate start value has been chosen, the procedure typically converges within a few steps (see any textbook on numerical methods, a graphical intuitive understanding of the procedure by the behavior of tangentials can be found in most references).

This method for solving nonlinear equations can be readily generalized to more dimensions. Bold symbols are supposed to be vector quantities and the task is to find a solution to the following vector equation

$$\mathbf{f}(\mathbf{x}) = \mathbf{f}(x_1, \ldots, x_n) = \begin{pmatrix} f_1(x_1, \ldots, x_n) \\ f_2(x_1, \ldots, x_n) \\ \vdots \\ f_n(x_1, \ldots, x_n) \end{pmatrix} = \begin{pmatrix} 0 \\ 0 \\ \vdots \\ 0 \end{pmatrix}. \tag{2.25}$$

In order to compute the solution numerically, one has to set up the Jacobi matrix

$$\mathbf{Df}(\mathbf{x}) = \begin{pmatrix} \frac{\partial f_1}{\partial x_1}(\mathbf{x}) & \frac{\partial f_1}{\partial x_2}(\mathbf{x}) & \cdots & \frac{\partial f_1}{\partial x_n}(\mathbf{x}) \\ \frac{\partial f_2}{\partial x_1}(\mathbf{x}) & \frac{\partial f_2}{\partial x_2}(\mathbf{x}) & \cdots & \frac{\partial f_2}{\partial x_n}(\mathbf{x}) \\ \vdots & \vdots & & \vdots \\ \frac{\partial f_n}{\partial x_1}(\mathbf{x}) & \frac{\partial f_n}{\partial x_2}(\mathbf{x}) & \cdots & \frac{\partial f_n}{\partial x_n}(\mathbf{x}) \end{pmatrix}. \tag{2.26}$$

By means of this matrix a iteration step is performed in the following way

$$\mathbf{x}^{i+1} = \mathbf{x}^i - \left(\mathbf{Df}(\mathbf{x}^i)\right)^{-1} \cdot \mathbf{f}(\mathbf{x}^i). \tag{2.27}$$

Note that first the Jacobi matrix has to be evaluated at $\mathbf{x}^i$, and then the inverse of this matrix has to be computed. Formally, this procedure is analog to (2.24). Of course, choosing an appropriate start value for the iteration is crucial. This guess vector should be already sufficiently "close" to the actual solution. We also note that the Jacobi matrix can become quite large and appropriate methods for the inversion of the matrix have to be used that eventually take advantage of the particular structure of the Jacobi matrix.

With these considerations we are prepared to outline the basic ideas of the Henyey method for solving the four stellar structure equations (2.10) to (2.13). The "trick" is essentially to formulate the whole problem in a way that the above sketched multi-dimensional Newton method can be employed.

Inspecting the equations under consideration, we find that they can be written as

$$\frac{dy_i}{dM_r} = f_i(y_1, ..., y_4, M_r) \text{ with } i = 1, ...4. \tag{2.28}$$

with $y_1 = P$, $y_2 = r$, $y_3 = L_r$, and $y_4 = T$. These equations are not yet in the form of (2.25). To this end we discretize the equations by considering them at discrete values in the M_r-range. Setting up a grid of mass shells M_r^j one can turn the differential equations into difference equations. Here j runs from 1 to some number N with $M_r^1 = M$ and $M_r^N = 0$. (Actually the first mass shell is not loacted at the stellar mass but at a slightly lower mass where we fit an atmosphere solution.) With these choices equation (2.28) can be rewritten as

$$0 = \frac{y_i^j - y_i^{j+1}}{M_r^j - M_r^{j+1}} - f_i(y_1^{j+1/2}, ..., y_4^{j+1/2}) \tag{2.29}$$

where we used finite differencing for approximating the derivative. The right-hand sides f_i should be evaluated in a way to provide an average value what we indicate by $y_i^{j+1/2}$. Note that this equation is not only set up for each quantity i but also for all grid points $j = 1...(N-1)$. Hence, we turned a set

of differential equations into a relatively large system of in general nonlinear equations. The numerical scheme for solving this system as it is done in our code has been described above. This system of equations deserve two more comments. First of all, appropriate boundary conditions have to be imposed at the edges of the mass interval and thus extend the system of equations (see for instance Kippenhahn & Weigert [87] for details). Moreover, it is important how the single equations of the system are arrange because this determines the structure of the so-called Henyey matrix. Typically it is computed in a way that only elements close to the diagonal are nonzero, which is advantageous for the inversion of the matrix.

We also note that the start values for every iteration process are given by the solution of the stellar model of the previous time step. Since changes within this time are typically small, a small number of iterations is sufficient to obtain a converged solution. Furthermore, we mention that in the code somewhat different variables are implemented that are more suited for a numerical treatment. The corresponding equations can be easily derived from the stellar structure equations presented in this chapter. Details are given in chapter 3, where we describe the concrete implementation taking into account stellar rotation.

2.3 Input physics

Finally, we summarize some features of the input physics of our code such as the used opacities, the neutrino losses, the nuclear reactions and the equation of state. We refer to Salasnich [147] for more details.

The opacities employed in our code are the ones provided by the OPAL group which, are available in the web (http://opalopacity.llnl.gov/existing.html). A description of these calculations can be found in Rogers & Iglesias [143]. At temperatures below $log\ T < 4$ the opacities are supplemented by the molecular opacities of Alexander & Ferguson [4]. For the transition between the two regimes a certain interpolation scheme is employed (see Weiss & Schlattl [170]). Moreover, in the very high temperature regime ($log\ T \geq 8.7$), we use data by Weiss et al. [169]. Beside these, we use the conductive opacities of Itoh et al. [82] assuming electron-degeneracy.

As described above, our stellar evolution code requires as an additional input the energy generation by nuclear reactions and losses due to neutrino emission. The neutrino rates are the ones provided by Haft et al. [69]. The nuclear network of our code includes nuclei from hydrogen up to magnesium. The according reaction rates of the pp chain and the CNO cycle are taken from Caughlan & Fowler [27] with a few corrections due to more recent investigations (see Bertelli et al. [15] for details).

Furthermore, in order to close the system of equations describing stellar structure and evolution one has to supply an equation of state. Above 10^7 K the gas is fully ionized and electron degeneracy becomes important which is taken into account by the equation of state (Kippenhahn et al. [85], Kippenhahn et al. [88]). Furthermore, Coulomb interactions are taken into account at higher densities following Girardi et al. [65]. At lower temperatures the "MHD" equation of state is adopted (see Mihalas et al. [128] and references therein).

2.4 Convection

Convection is one of the most important physical processes for mixing in stars. At present convection remains a source of uncertainity in stellar model computations. In our stellar models, convection is treated with the Schwarzschild criterion for stability. Usually energy transport in the outer convection zone of stars is described according to the mixing-length theory (MLT) of Böhm-Vitense (1958) [18]. The basic idea is to model the complicated pattern of structure and motion of convective elements by a suitable mean element with suitable velocity. In reality, convective elements may have noticeable different scales. On the contrary, the ideal elememts of the MLT all possess the same physical properties if generated at a certain radial distance r from the center. Each of this is supposed to travel, on average, over the distance Λ (defined as the mixing length), and disolve into the surrounding medium losing its identity. By assumption, the dimensions of the average elements are assumed to be equal to Λ, the mixing length, and the shape of the elements is not specified. There are two characteristic lengths: the mixing length and the dimension of the element (in the MLT both are assumed to be equally proportional to the local pressure scale height, with the proportionality coefficient taken as a free parameter to be fixed by comparing model results with observations. It is worth to notice that this kind of parameters exist also in some sophisticated models of stellar convection (e.g. Xiong [177]). An ideal self-consistent theory of convection should derive those typical scales from first principles instead of assuming them as parameters. We adopt the same value as in Bertelli et al. [14] for the MLT parameter ($\alpha = 1.68$), calibrated by means of the solar model.

2.4.1 Overshoot

The extension of the convective regions, either cores or envelopes, is determined by the presence of convective overshoot. Core overshoot is determined my means of the formalism developed by Bressan et al. [21], which seeks for the layer at which the velocities (rather then the acceleration) of convective elements become zero and expresses the mean free path of these as $l = \Lambda_C H_P$ (H_P being

the pressure scale height). The choice of the free parameter Λ_C determines the extent of overshooting across the border of the classical core (determined by the Scharzschild criterion). Other authors (see below) fix the extent of the overshooting zone to be at the distance $d = \Lambda_C H_P$ from the border of the convective core (Schwarzschild criterion).

The Λ_C paramater in Bressan's et al. [21] formalism is not equivalent to others found in the literature. For istance, the overshooting extension determined by $\Lambda = 0.5$ with the Padova formalism roughly corresponds to the parameters adopted by the Geneva group, $d = 0.25 H_P$ by Schaller et al. [148] and $d = 0.1 H_P$ above the convective border by Ekström et al. [46]. The efficiency of overshoot at the bottom of convective envelopes is taken from Alongi et al. [5]. For massive stars this value is equal to $\Lambda_e = 0.7$. We recall that the question of the overshooting efficency in stars of different masses is still a matter of debate (see Deng & Xiong [40]).

2.5 Mass loss

Mass loss has a crucial effect on the evolution of massive stars. It was well established that mass loss by stellar winds cannot be neglected (see Chiosi & Maeder [30]). Kudritzki & Puls [91] describe extensively winds from hot stars. The rate of which massive star lose mass is so high that the entire envelope can be removed, with profound consequences for their location in Hertzsprung-Russell diagram, their surface chemical abundances, their evolution as supernovae precursors and their contribution to the galactic enrichment. Therefore, the evolution of all stars with initial mass $M \geq 6 M_\odot$ is calculated in presence of mass loss by stellar wind using the de Jager et al. [38] relationship for all stages from the main sequence to the so called Jager limit. Beyond this, the mass loss rates are increased to $10^{-3} M_\odot yr^{-1}$ as indicated by observational data from Luminous Blue Variables (LBV). For the WNL stages, which are supposed to start when the surface abundance of hydrogen falls below $X = 0.4$ we apply the mass loss rate by Maeder [105], while the phases of WNE e WC are treated according to the formulation of Langer [93].

The rates incorporate the dependence on metallicity given by Kudritzki et al. [90]

$$\dot{M}_Z = \left(\frac{Z}{Z_\odot} \right)^{0.5} \dot{M}_{Z_\odot}. \tag{2.30}$$

We note that the most used prescriptions for the RSG phase given by de Jager et al. [38] have been confirmed observationally (Crowther [34], Mauron & Josselin [119]), which justifies their use in our code.

2.5.1 Changes of the mass loss rates $\dot{M}$ with rotation

We briefly highlight how the mass loss is implemented in our new code in order to take into account the effects of rotation on this physical process. Theoretical considerations lead to the conlusion that mass loss should be enhanced by rotation Friend & Abbott [57]. In our code we use a prescription by Langer [95])

$$\dot{M}(v) \;=\; \dot{M}(v=0)\left(\frac{1}{1-\frac{v}{v_{\rm crit}}}\right)^{\xi} \tag{2.31}$$

where $\xi \simeq 0.5$. The critical velocity for break up (see chapter 5) is denoted by $v_{\rm crit}$.

CHAPTER 3

Implementation of rotation

Astonishing progress has been made towards understanding stellar evolution in the past fifty years. In spite, of an enormous number of studies of spherical models, however, relatively little attention has been paid to the role of rotation and which therefore remained an important unknown in the theory of stellar structure and evolution for a long period. Basically, there are two reasons for the neglect of rotation in most previous investigations: one of this is that dropping the assumption of spherical symmetry leads to a substantional increase in the numerical complexity of the equations of stellar structure. The other is that spherically symmetric (i.e. nonrotating) models have been sufficent in explaning the relevant observational data like the mass-luminosity relationship, HR diagrams of clusters, etc. Over the recent years, however a number of serious discrepancies between current models and observations have been noticed. They particularly concern the helium and nitrogen abundances in massive O- and B-type stars and in giants and supergiants, as well as the distribution of stars in the HR diagram at various metallicities.

3.1 Rotation during the years

Developments in the domain of stellar rotation have been rather slow. A few of early works apply to real stars, becasue in general gaseous configurations were not considered, and no account was taken of the radiative energy transport. The general equations of rotating stars in radiative equilibrium were first formulated

by Milne [129]. Solutions are obtained on the basis of truncated expansions in the small parameter $\epsilon = \Omega^2 R^3/GM$, which is the ratio of the centrifugal force to gravity at the equator. It is shown that a star will appear hotter at the poles than at the equator.

Von Zeipel [165] properly demonstrated that the conditions of mechanical and radiative equilibrium are, in general, incompatible in a uniformly rotating barotrope. Vogt [164] and Eddington [44] in order to resolve the so-called von Zeipel paradox, pointed out independently that the small departures from spherical symmetry in a rotating star lead to unequal heating along the polar and equatorial radii. This in turn causes a large-scale flow of matter in meridian planes passing through the rotation axis. Eddington [45] claimed that the timescale of the thermally-driven currents is of the order of the Kelvin-Helmholtz time, $t_{KH} = GM^2/RL$, where L is the total luminosity of the star. This incorrect result has misled the people for more then twenty years.

Krogdahl [89] has shown that, to $0(\epsilon)$, the angular velocity Ω and the circulation velocity $\vec{u}$ take the form $\Omega = \Omega(\omega_0 + \epsilon\omega_1 + ...$ and $\vec{u} = \epsilon\vec{u_1} + ...$, where Ω_0 is a constant. In an attempt to solve a differential equation, derived from the Navier-Stokes equation,

$$\frac{\partial}{\partial t}(\Omega\omega^2) + \vec{u} \cdot \nabla(\Omega\omega^2) = F_\Psi + L_\Psi \tag{3.1}$$

that describes the evolution of the angular velocity which incorporates frictional force and a term accounting for the Lorenz force in the case of the presence of a prescribed magnetic field, he tried to do it analytically with $\partial/\partial t = L_\Psi = 0$ and prescribed an overly restrictive condition on the circulation pattern. Yet, this was the first consistent formulation of the problem, because it shows that some kind of viscous action must be retained so as to obtain self-consistent solutions.

It is claimed by Gratton [67] that the circulation pattern in a uniformely rotating, inviscid radiative envelope consists of two distinct cells separated by the particular level surface over which $\Omega^2 = 2\pi G\rho$. This artificial result, which does not apply to realistic stellar models, was independently found by Öpik [131]. Schwarzschild [150] resolved the von Zeipel paradox by choosing the rotation law so that the vector $\vec{u}$ identically vanishes in the models. As was shown by Aikawa [3] these steady, inviscid models are somewhat arbitrary because their rotation law depends on a free constant. Moreover, one must bear in mind that there is no obvious reason to expect rotating stars to select zero-circulation configurations. In fact, because these inviscid baroclinic models are always unstable with respect to nonaxisymmetric motions, the slighest disturbance will generate three-dimensional motions and, as a result, a large-scale meridional circulation will commence.

Sweet [160] was the first to show that the circulation caused by a slow solid-body rotation is quadrupolar in its structure, e.g., $u_r = \epsilon u(R) P_2(cos\theta)$, where P_2 is the Legendre polynomial. The meridional flow consists of a single cell, with interior upwelling at the poles which is compensated by interior downwelling at the equator. He also showed that the timescale of these currents is of the order of t_{KH}/ϵ, thus correcting Eddington's (1929) wrong estimate. It was also found that

$$u_r \propto 1 \text{ and } u_\theta \propto \frac{1}{R-r} \tag{3.2}$$

as $r \xrightarrow{a} R$ near the surface, and

$$u_r \propto \frac{1}{r-R_C} \text{ and } u_\theta \propto \frac{1}{(r-R_C)^2} \tag{3.3}$$

as $r \xrightarrow{a} R_C$ near the core-envelope interface. Hence, this inviscid solution does not satisfy the essential boundary condition

$$\vec{n} \cdot \vec{u} = 0, \tag{3.4}$$

at the two boundaries where $\vec{n}$. is the outer normal. This condition merely expresses the fact that, without mass loss, the currents must flow along the boundaries. Moreover, with $\partial/\partial t = F_\Psi = L_\Psi = 0$ and Ω = constant, it is evident that one cannot satisfy equation (3.1). The transport of specific angular momentum by the meridional currents remains always unbalanced (Randers [141])

Mestel [121] argued that the presence of chemical inhomogeneities will considerably restrain the circulatory currents, unless the star is on the verge of equatorial break-up. This suggestion is quite plausible since, as one knows form the empirical evidence, most stars do not mix extensively in their radiative interior as they evolve away from the main sequence. It is also suggested that (laminar) viscous boundary layers could form near the core and the surface, thus preventing the unwanted singularities in equations (3.5) and (3.3). Unfortunately, neither at the core nor at the surface a satisfactory boundary-layer analysis has been made.

Baker & Kippenhahn [6] found that when the prescribed rotation law is nonuniform, one gets instead of equation (3.5)

$$u_r \propto \frac{1}{(R-r)^n} \text{ and } u_\theta \propto \frac{1}{(R-r)^{n+1}} \tag{3.5}$$

as $r \xrightarrow{R}$ near the free surface, where n is the effective polytropic index. This result is a mathematical property that has no physical content, but it is important to remember that condition (3.4) is not satisfied, and that the transport

of angular momentum always remains unbalanced because these authors have also let $\partial/\partial t = F_\Psi = L_\Psi = 0$ in equation (3.1).

The newly proposed solutions rests essentially on the a dynamical linkage between eddy-like and/or wave-like motions, called anisotropic turbulence, because they are predominantly two-dimensional and the mean flow (i.e., the differential rotation and concomitant meridional currents). To be more specific, because strict radiative equilibrium prevents a rotating star from being a barotrope, the main idea is that the chemically homogeneous parts in a radiative envelope are filled with small-scale transient motions that are caused by the ever-present barotropic-baroclinic instabilities. This anisotropic turbulence, in turn, generates thin thermo-viscous boundary layers so that the circulation velocities do not become infinitive and may satisfy condition (3.4) at the boundaries of the radiative envelope. Simultaneously, the turbulent friction F_Ψ acting on the differential rotation can be made to balance the transport of angular momentum in equation (3.1).

Therefore, by taking into account the so-called eddy/wave-mean flow interaction in a stellar radiative zone, one can combine, the far-reaching but incomplete contributions that were originally made by Krogdahl [89], Sweet [160] and Mestel [121] and that we presented in this section, into a single, coherent framework.

3.2 Methods used to investigate effects of rotation

Rotation may effect the equations of stellar structure in four ways as has been pointed out by [50].

- Centrifugal forces reduce the effective gravity at any point but not on the axis of rotation. This affects the equation of hydrostatic equilibrium and must be taken directly into account.

- The centrifugal force is not, in general, parallel to the force of gravity, therefore, equipotentials surfaces are not longer spheres and the spherical relationships between the radius, enclosed volume, and surface area of an equipotential surface cannot be used. All the equations except the equation for adiabatic convective equilibrium need to be changed.

- Because the radiative flux varies with the local effective gravity (the Von Zeipel effect, 1924), the radiative flux is not constant on an equipotential surface. This enters directly into the radiative equilibrium equation and may affect the stability to convection by changing the radiative temperature gradient.

- Rotation may inhibit certain modes of convective motions and, therefore, directly affect the criterion for convective stability (Randers [142], Cowling [33]). In addition, not all angular momentum distributions are stable, and this can lead to convection in regions which are stable to purely thermal convection (Wasiutynski [167]). In this way rotation is inducing some mixing processes.

The first three effects were incorporated into the equations of the stellar structure equations by Kippenhahn & Thomas [86] and this is the method on which we will also base the implementation of the rotation in our stellar evolution code and that we will analize in detail in the following sections. But before we want to give an owerview of several different methods that have been used in the past to investigate the effects of rotation. Perturbation techniques, as those of Chandrasekhar [28] and Sweet & Roy [159], which have been applied to polytropes or other highly simplified stellar models, we will not include here.

3.2.1 Kippenhahn-Thomas method

The method of Kippenhahn & Thomas [86] for computing the internal structure of nonspherical stars was based on the assumption that the force per gram causing the deviations from spherical symmetry is conservative. The main idea of this method is to replace the usual spherical stratification, which prevails in nonrotating stars, by a rotationally deformed stratification. This method applies when the effective gravity (the gravity decreased by the effect of centrifugal forces) can be derived from a potential, i.e. when the problem is conservative, which occurs for solid body rotation or for constant rotation on cylinders centered on the axis of rotation. In this case structural variables, pressure P, density ρ and temperature T keep a constant value on the equipotential. Like this the problem can be kept one-dimensional. The method has also the advantage that in a spherical stellar structure code small changes have to be made to obtain non-spherical stellar models. This method was similar to the one of Faulkner et al. [52] in the case of purely rotating stars with the exception that it was not necessary to use the division into the two zones.

This method was applied in most subsequent work with minor differences. Endal & Sofia [50] interpolated in tabular data to find the shapes of the equipotential surfaces, while Pinesonneault [138] integrated the relevant equation from the center to the surface using a fourth-order Runge-Kutta method. Once the shapes of the surface is known, the average values of the local gravity acceleration and its inverse on an equipotential surface are needed to find the rotational correction terms for the equations of stellar structure. To determine this quantities Endal & Sofia divided the potential into three parts: Ψ_s, the spherically

symmertic part of the gravitational potential, Ψ_r, the cylindrically symmetric potential directly due to rotation and Ψ_d, the cylindrically symmetric part of the gravitational potential due to distortion of the shape of the star. Unlike the method of Endal & Sofia, Pinesonneault directly integrated the distorted potential from the center to the surface.

The Kippenhahn-Thomas method is used by most of the other authors (Fliegner & Langer [53], Meynet & Maeder [123], Heger & Langer [72]) even when the internal rotation generally evolves towards laws that are non-conservative and when this method cannot be directly used. In the following sections we will see the assumptions that we need to adopt to use the Kippenhahn-Thomas method as Meynet & Maeder [123] did and that we will apply during the implemenatation of rotation into our code.

3.2.2 Double-Approximation Method

The method consists of dividing the star into two parts: a core which is assumed to be rotating slowly in comparison to the local critical velocity, and an envelope which contains a negligible amount of mass. First-order expansions in the rotation parameter are used in the core, and the Laplace equation is used for the potential in the envelope (the mass of the envelope does not contribute to the potential). For uniform rotation this is a valid approximation, but for differential rotation (rapidly rotating cores) the core approximation breakes down.

A number of investigators, Roxeburgh et al. [145] , Faulkner et al. [52], Stritmatter et al. [157], Sackmann & Anand [146], each of whom has introduced minor modifications, has used this method.

3.2.3 J^2 Method

A detailed description of the J^2 has been given by Papaloizou et al. [135]. The stellar structure equations used in the J^2 method are formally equivalent to those used in the Kippenhahn-Thomas method, so the only difference is in the evaluation of the total potential, Ψ. In the J^2 method, the Roche approximation has generally been used. The Roche approximation should break down in regions where the ratio of the mean interior density to the central density ($< \rho > /\rho_c$) and the ratio of angular velocity to critical angular velocity (ω/ω_{cr}) are both signifiant compared with unity. This will be the case for rapid differential rotation in the core.

3.2.4 Self-consistent-field Method

The self-consistent-field (SFC) method, as described by Ostriker & Mark [133], is primarily a method for obtaining accurate solutions of the total potential and hydrostatic equilibrium equations. The SFC method was combined with the complete stellar structure equations by Jackson [83]. Jackson's method was applied to differentially rotating stars on the upper main sequence by Bodenheimer [17]. In this method the stellar structure equations are evaluated on equipotential surfaces, as in the Kippenhahn-Thomas and J^2 methods. The primary difference is that the potential equation is solved much more accurately and the method is, as a result, very timeconsuming. This makes it unsuitable for evolutionary calculations, but it remained a very powerful method for testing more approximate techniques.

3.3 Differential rotation

A particulary interesting case of differential rotation is the so-called shellular rotation (Zahn [179]), with a rotation law where Ω is constant on isobaric shells and depending to the first order on the distance r to the stellar center,

$$\Omega(r, \vartheta) = \bar{\Omega}(r) + \Omega_2(r) P_2(cos\vartheta) \tag{3.6}$$

where P_2 is the second Legendre polynomial. It is supported by the study of turbulence in the Sun and the stars (Spiegel & Zahn [154]). Such a law results from the fact that differential rotation in radiative regions produces turbulence that is very anisotropic. It is much stronger in the horizontal direction than in the vertical direction, where stabilization occurs because of the stable temperature gradient. The horizontal turbulence enforces an essentially constant rotation rate on isobars, thus producing the preceeding law. We need to point out that the isobars are not spherical surfaces. There is an angle ϵ between the radial direction and the direction of the gravity or between a spherical shell and an equipotential as it can be seen in Fig. 3.1. As an example, in the Roche model at break-up rotation at a colatitude of $\vartheta = 45$ degrees this angle is 13 degrees. For lower rotation rates, it rapidly decreases, behaving like Ω^2. Therefore, if one writes the shellular rotation as $\Omega \approx \Omega(r)$, one should not consider the case of extreme rotation velocities.

In the case of shellular rotation, the centrifugal force cannot be derived from a potential and this case is clearly not conservative. Following Meynet & Maeder [123] we present here some clarifications on the implicit assumptions made when the Kippenhahn & Thomas method is used in the case of the shellular rotation law.

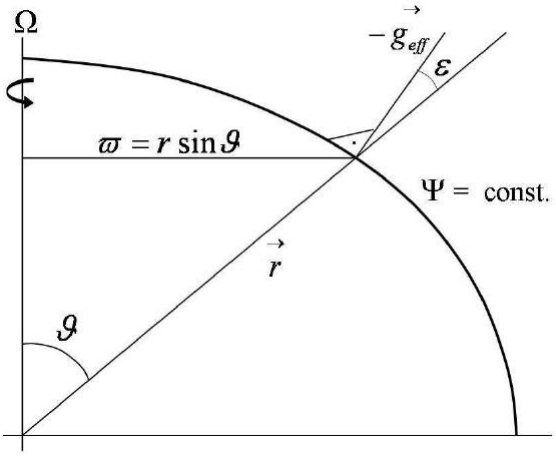

Figure 3.1— The angle ϵ is the angle between the vector radius and the normal $-\vec{g}_{eff}$ to an equipotential. Figure taken from [106]

First we will show the demonstration that for a shellular rotation law the surfaces Ψ_P given by the equation

$$\Psi_P = \Phi + \frac{1}{2}\Omega^2 r^2 sin^2\theta = \text{const.} \tag{3.7}$$

are isobars. The gravitational potential is defined by $\partial\Phi/\partial r = GM_r/r^2$ and $\Phi = -GM_r/r$ in the Roche approximation, which is used in all the derivations, r is the radius, Ω the angular rotation rate and ϑ the colatitude.

The components of the gradient of Ψ_P in polar coordinates r,ϑ are

$$\frac{\partial\Psi_P}{\partial r} = \frac{\partial\Phi}{\partial r} + \Omega^2 r sin^2\theta + r^2 sin^2\theta\Omega\frac{\partial\Omega}{\partial r}, \tag{3.8}$$

$$\frac{1}{r}\frac{\partial\Psi_P}{\partial\theta} = \frac{1}{r}\frac{\partial\Phi}{\partial\theta} + \Omega^2 r sin\theta cos\theta + r^2 sin^2\theta\Omega\frac{1}{r}\frac{\partial\Omega}{\partial\theta} \tag{3.9}$$

The hydrostatic equilibrium implies that

$$\vec{\nabla}P = -\rho\vec{g}_{eff} \tag{3.10}$$

where $\vec{g}_{eff}$is the effective gravity. Its components, in spherical coordinates are expressed by following equations

$$g_{eff,r} = \frac{\partial\Phi}{\partial r} + \Omega^2 r sin^2\theta, \tag{3.11}$$

$$g_{eff,\theta} = \frac{1}{r}\frac{\partial \Phi}{\partial \theta} + \Omega^2 r sin\theta cos\theta. \tag{3.12}$$

Thus, by comparing these terms and the derivatives of Ψ_P, one can write

$$\vec{g}_{eff} = \vec{\nabla}\Psi_P - r^2 sin^2\theta \Omega \vec{\nabla}\Omega. \tag{3.13}$$

Finally, the equation for hydrostatic equilibrium is thus

$$\vec{\nabla}P = -\rho(\vec{\nabla}\Psi_P - r^2 sin^2\theta \Omega \vec{\nabla}\Omega). \tag{3.14}$$

The vector $\vec{\nabla}\Omega$ is parallel to $\vec{\nabla}P$ because Ω is constant on isobars. The hydrostatic equation (3.14) implies the parallelism of $\vec{\nabla}P$ and $\vec{\nabla}\Psi$. Therefore, in this non-conservative case the surfaces defined by $\Psi = const.$ (3.7) are isobaric surfaces, but they are not equipotential and the star is said baroclinic. In the case of solid body rotation, isobars and equipotentials coincide and the star is barotropic. Thus, we can notice that the shape of the isobars in the case of a shellular rotation law are identical to the shape of equipotentials in a conservative situation.

Therefore, for shellular rotation one may choose to write the equations of the stellar structure on the isobars and use, with changes that we will show in the following, a method devised for the conservative case by Kippenhahn & Thomas [86], with the big advantage to keep the equations for stellar structure one-dimensional.

3.4 Derivations of stellar structure equation for rotating stars

The equations of stellar structure are useful to write in a form similar to that of the non-rotating case, that we explained in section 2.1 in order to minimize the modifications necessary for calculating rotating stars with shellular rotation. A radius r_P is associated to an isobar and it is defined by

$$V_P = \frac{4\pi}{3} r_P^3 \tag{3.15}$$

where V_P is the volume inside an isobar. For any quantity, q, which is not constant over an isobaric surface, a mean value is defined by

$$< q >= \frac{1}{S_P} \int_{\Psi=\text{const}} q d\sigma \tag{3.16}$$

where S_P is the surface of the isobar and $d\sigma$ is an element of this surface. The area of this surface is given by

$$S_P = . \int_{\Psi=\text{const}} d\sigma. \tag{3.17}$$

The difficulties of this method we will be analized in detail in the section 3.9 and now we will focus on the changes in the stellar structure equations following Meynet & Maeder [123].

3.4.1 Hydrostatic equilibrium equation

The effective gravity can no longer be defined as a gradient $\vec{g}_{eff} = -\vec{\nabla}\Psi$, since Ψ is not a potential. $\vec{\nabla}\Omega$ is parallel to $\vec{\nabla}\Psi$ and therefore can be expressed by

$$\vec{\nabla}\Omega = -\alpha\vec{\nabla}\Psi \text{ with } \alpha = |\frac{d\Omega}{d\Psi}|, \tag{3.18}$$

a scalar which depends only on Ψ. Replacing $\vec{\nabla}\Omega$ by this expression as a function of $\vec{\nabla}\Psi$ in (3.13), for the modulus of $\vec{g_{eff}} = (-g_{eff,r}, -g_{eff,\theta}, 0)$ we get the following expression

$$g_{eff} = (1 - r^2 sin^2\theta\Omega\alpha)\frac{d\Psi}{dn} \tag{3.19}$$

where dn is the average distance between two neighboring isobaric surfaces, ($dn = dr_P$).

The equation of hydrostatic equilibrium (3.14) becomes similarly

$$\frac{dP}{dn} = -\rho(1 - r^2 sin^2\theta\Omega\alpha)\frac{d\Psi}{dn}. \tag{3.20}$$

From this equation, one can immediately deduce that the quantity $\rho(1-r^2 sin^2\theta\Omega\alpha)$ is constant on an isobar.

The mass inside the isobar M_P needs to be used as independent variable and therefore the expression $\frac{d\Psi}{dM_P}$ needs to be found. Using (3.19) one can write

$$\begin{aligned} dM_P &= \int_{\Psi=\text{const}} \rho dn d\sigma = d\Psi \int_{\Psi=\text{const}} \rho\frac{dn}{d\Psi}d\sigma \\ &= \int_{\Psi=\text{const}} \rho\frac{(1 - r^2 sin^2\theta\Omega\alpha)}{g_{eff}}d\sigma. \end{aligned} \tag{3.21}$$

Since, $\rho(1 - r^2 sin^2\theta\Omega\alpha)$ is constant on isobars, one can easily integrate this equation by using the definition (3.16) and gets the following expression

$$\frac{d\Psi}{dM_P} = \frac{1}{\rho(1 - r^2 sin^2\theta\Omega\alpha) < g_{eff}^{-1} > S_P}. \tag{3.22}$$

Together with (3.20), one obtains

$$\frac{dP}{dM_P} = \frac{dP}{d\Psi}\frac{d\Psi}{dM_P} = \frac{-1}{< g_{eff}^{-1} > S_P}. \tag{3.23}$$

The quantity f_P is defined by

$$f_P = \frac{4\pi r_P^4}{GM_P S_P} \frac{1}{< g_{eff}^{-1} >} \tag{3.24}$$

and is equal to unity for a non-rotating star. With this definition the equation of hydrostatic equilibrium in Lagrangian coordinates finally can be written in the following form

$$\frac{dP}{dM_P} = -\frac{GM_P}{4\pi r_P^4} f_P \tag{3.25}$$

and we can notice that apart from the factor f_P, the equation keeps the same form as in the conservative case.

3.4.2 Continuity equation

Similarly, we want an equation equivalent to (2.11) for shellular rotation. According to (3.15), the volume of a shell between two isobars is

$$dV_P = 4\pi r_P^2 dr_P; \tag{3.26}$$

which can also be expressed by

$$\begin{aligned} dV_P &= \int_{\Psi=\text{const}} dn d\sigma = d\Psi \int_{\Psi=\text{const}} \frac{dn}{d\Psi} d\sigma \\ &= d\Psi \int_{\Psi=\text{const}} \frac{(1 - r^2 sin^2\theta \Omega\alpha)}{g_{eff}} d\sigma. \end{aligned} \tag{3.27}$$

By applying (3.16) one finally gets

$$dV_P = d\Psi S_P [< g_{eff}^{-1} > - < g_{eff}^{-1} r^2 sin^2\theta > \Omega\alpha]. \tag{3.28}$$

This expression together with (3.15) and (3.22) leads to

$$\frac{dr_P}{dM_P} = \frac{1}{4\pi r_P^2 \bar{\rho}} \tag{3.29}$$

with

$$\bar{\rho} = \frac{\rho(1 - r^2 sin^2\theta \Omega\alpha) < g_{eff}^{-1} >}{< g_{eff}^{-1} > - < g_{eff}^{-1} r^2 sin^2\theta > \Omega\alpha}. \tag{3.30}$$

The quantity $\bar{\rho}$ is not equal to $< \rho >$. Indeed $\bar{\rho}$ is obtained by averaging the density over the volume between two isobars, instead $< \rho >$ is an average performed on an isobaric surface.

3.4.3 Radiative transport

A star is a beautiful self-controlled nuclear reactor. If this reactor is rotating, the spherical symmetry is broken and therefore the density structure and energy transport are no longer the same at the equator and at the poles. The global self-control still can be mantained by producing some circulation of matter to compensate for the local deviations from the energetic equilibrium produced by rotation.

In a rotating star, locally, the vertical radiative transfer is expressed by equation

$$F = -\frac{4acT^3}{3\kappa\rho}\frac{\partial T}{\partial n} \tag{3.31}$$

where dn is the element of distance between two isobars and F is the radiative flux at a given point on an isobar. Taking into account that

$$\frac{\partial T}{\partial n} = \frac{\partial T}{\partial M_P}\frac{\partial M_P}{\partial \Psi}\frac{\partial \Psi}{\partial n} \tag{3.32}$$

where $\frac{\partial \Psi}{\partial n}$ is defined from equation (3.19) as

$$\frac{\partial \Psi}{\partial n} = \frac{g_{eff}}{(1 - r^2 sin^2\theta\Omega\alpha)} \tag{3.33}$$

and $\frac{\partial M_P}{\partial \Psi}$ from equation (3.22), it is found that

$$F = -\frac{4acT^3}{3\kappa\rho}\frac{\partial T}{\partial M_P}\rho < g_{eff}^{-1} > S_P g_{eff} \tag{3.34}$$

where S_P is the surface of the considered isobar.
Integrating over an isobar we get the following expression for the radiative transfer in a rotating star

$$L_P = -\frac{4ac}{3} < g_{eff}^{-1} > S_P^2 < \frac{T^3 g_{eff}}{\kappa}\frac{dT}{dM_P} > . \tag{3.35}$$

3.4.4 Convective transport

At a given point on an isobar, locally, in a convective region holds

$$\frac{\partial lnT}{\partial lnp} = \nabla_{ad}. \tag{3.36}$$

Taking the average over an isobar on both sides of this equality, implies that

$$< \frac{\partial lnT}{\partial lnp} > = < \nabla_{ad} > . \tag{3.37}$$

3.4.5 Conservation of energy

The net energy outflow dL_P from a shell comprised between the isobars Ψ and $\Psi + d\Psi$ is equal to

$$dL_P = \int_{\Psi=\text{const}} \epsilon \rho dn d\sigma = d\Psi \int_{\Psi=\text{const}} \epsilon \rho \frac{dn}{d\Psi} d\sigma \tag{3.38}$$

where ϵ is the net rate of energy production in the shell. Using (3.19) and the constancy of $\rho(1 - r^2 sin^2\theta\Omega\alpha)$ on an isobar leads to a

$$dL_P = d\Psi < \frac{\epsilon}{g_{eff}} > S_P \rho(1 - r^2 sin^2\theta\Omega\alpha). \tag{3.39}$$

Taking into account equation (3.22) and decomposing the energy rate into its nuclear, gravitational and neutrino components finally it can be written

$$\frac{dL_P}{dM_P} = \frac{< (\epsilon_{nucl} - \epsilon_\nu + \epsilon_{grav}) g_{eff}^{-1} >}{< g_{eff}^{-1} >} \tag{3.40}$$

which is the equation for energy production in a rotating star in equilibrium.

3.4.6 Stellar structure equations for rotating stars

Because of the non-constancy of the density and the temperature on isobars in the case of shellular rotation, one can notice that the equations presented above are not as simple as in the conservative case. They can be transformed into a form proposed by Kippenhahn & Thomas [86].

The continuity equation for the mass keeps its usual form if the quantity $\bar{\rho}$ is considered as a dependent variable instead of ρ, as it can be noticed from equation (3.29). One also needs to consider a mean temperature $\bar{T}$ obtained form the equation of state with the input variables $\bar{\rho}$, p and the chemical composition. Due to a strong horizontal turbulence the chemical composition is supposed to be homogeneous on an isobaric surface. The energy conservation equation and the energy transport equation are written using these mean values of the density and temperature, making the following approximations:

$$\frac{< (\epsilon_{nucl} - \epsilon_\nu + \epsilon_{grav}) g_{eff}^{-1} >}{< g_{eff}^{-1} >}$$

$$\approx \epsilon_{nucl}(\bar{\rho}, \bar{T}) - \epsilon_\nu(\bar{\rho}, \bar{T}) + \epsilon_{grav}(\bar{\rho}, \bar{T}) \tag{3.41}$$

and

$$< \frac{T^3 g_{eff}}{\kappa} \frac{dT}{dM_P} > \approx \frac{\bar{T}^3 < g_{eff} >}{\kappa(\bar{\rho}, \bar{T})} \frac{d\bar{T}}{dM_P}. \tag{3.42}$$

In convective regions, the temperature gradient is the adiabatic gradient and the average gradient is approximated by

$$< \frac{dlnT}{dlnP} >=< \nabla_{ad} > \approx \frac{dln\bar{T}}{dlnP} \tag{3.43}$$

With these changes of variables and approximations we recover the set of stellar structure equations given by Thomas & Kippenhahn [86]:

$$\frac{\partial P}{\partial M_P} = -\frac{GM_P}{4\pi r_P^4} f_P \tag{3.44}$$

$$\frac{\partial r_P}{\partial M_P} = \frac{1}{4\pi r_P^2 \bar{\rho}} \tag{3.45}$$

$$\frac{\partial L_P}{\partial M_P} = \epsilon_{nucl} - \epsilon_\nu + \epsilon_{grav} = \epsilon_{nucl} - \epsilon_\nu - c_P \frac{\partial \bar{T}}{\partial t} + \frac{\delta}{\rho} \frac{\partial P}{\partial t} \tag{3.46}$$

$$\frac{\partial lnT}{\partial M_P} = -\frac{GM_P}{4\pi r_P^4} f_P \min[\nabla_{ad}, \nabla_{rad} \frac{f_T}{f_P}] \tag{3.47}$$

where

$$\nabla_{ad} = \frac{P\delta}{\bar{T}\bar{\rho}c_P} \text{ (convective zones)} \tag{3.48}$$

$$\nabla_{rad} = \frac{3}{16\pi acG} \frac{\kappa l P}{m\bar{T}^4} \text{ (radiative zones)} \tag{3.49}$$

$$f_P = \frac{4\pi r_P^4}{GM_P S_P} \frac{1}{< g_{eff}^{-1} >} \tag{3.50}$$

$$f_T = (\frac{4\pi r_P^2}{S_P})^2 \frac{1}{< g_{eff} >< g_{eff}^{-1} >} \tag{3.51}$$

Partial derivatives have replaced total derivatives to allow for the fact that the quantities depend not only on M_P but also on time. Moreover, the involved simplifications used in order to derive these eqautions are no severe assumptions.

3.5 The equations for the stellar enevelope

The outer layers of a stellar model are treated seperately from the interior. Kippenhahn et al. [88] defined an envelope as the layers connecting the inner solutions to the atmosphere. Under the assumption of constant $L_r = L$, the only equation involving time dependencies is trival, and the remaining set of three now ordinary differential equations can be integrated explicitly.

Convection is treated non adiabatically, partial ionisation is treated in details and the ϵ's are considered to be zero in the envelope. The envelopes of massive hot stats contain only a few thousands of the total mass, therefore one may consider that the envelope rotates with a uniform angular velocity equal to that of the first (outermost) interior shell. Under such a conditions locally a solid roation law can be assumed. The independent variable M_P used in the interior is advantageously replaced by the pressure which in the outer parts of the stars covers a much wider range of values. Using the pressure as the independent variable, the equations of stellar structure become:

$$\frac{\partial ln r_P}{\partial ln P} = \frac{P}{r_P}\frac{\partial r_P}{\partial M_P}\frac{\partial M_P}{\partial P} = -\frac{r_P P}{G M_P \bar{\rho}}\frac{1}{f_P}, \tag{3.52}$$

$$\frac{\partial ln M_P}{\partial ln P} = \frac{P}{M_P}\frac{\partial M_P}{\partial P} = -\frac{4\pi r_P^4 P}{G M_P^2}\frac{1}{f_P}, \tag{3.53}$$

$$\frac{\partial ln T}{\partial ln P} = \min[\nabla_{conv}, \nabla_{rad}\frac{f_T}{f_P}]. \tag{3.54}$$

3.6 The Von Zeipel Theorem

Before examining in detail the equations for the atmosphere let us demonstrate the Von Zeipel theorem and his consequences. The von Zeipel theorem relates the radiative flux at some colatitude θ on the surface of a rotating star and the local effective gravity $g_{eff}(\Omega, \theta)$, as a function of the angular velocity Ω and θ. Considering first the case of a uniformly rotating star, the flux is

$$\vec{F}(\Omega, \theta) = -\chi\vec{\nabla}T(\Omega, \theta) \text{ with } \chi = \frac{4acT^3}{3\kappa\rho} \tag{3.55}$$

In a rigidly rotating star, the equipotentials and isobars coincide, so we have a barotropic case, and they are also surfaces of constant T and ρ. Therefore, using the equation of hydrostatic equilibrium this equation can be expressed as

$$\vec{F}(\Omega, \theta) = -\chi\frac{dT}{dP}\vec{\nabla}P(\Omega, \theta) = -\rho\chi\frac{dT}{dP}\vec{g}_{eff}(\Omega, \theta). \tag{3.56}$$

The effective gravity and pressure gradient are parallel. The term $(\rho\chi dT/dP)$ is constant on a given equipotential, and therefore the flux is proportional to the effective gravity on the equipotential. In order to estimate the coefficient of proportionality, the total luminosity $L(\Omega)$ on an equipotential of surface Σ is expressed by

$$L(\Omega) = \int_{\Sigma} \vec{F}(\Omega,\theta)d\vec{\sigma} = (\rho\chi\frac{dT}{dP}) \int_{\Sigma} \vec{\nabla}\Psi(\Omega,\theta)d\vec{\sigma} \tag{3.57}$$

By Gauss theorem, this provides with the Laplacian of Ψ given by

$$\nabla^2\Psi = 4\pi G\rho - 2\Omega^2 \tag{3.58}$$

the expression

$$L(\Omega) = \left(\rho\chi\frac{dT}{dP}\right) \int_V \nabla^2\Psi dV = \left(\rho\chi\frac{dT}{dP}\right) \int_V (4\pi G\rho - 2\Omega^2)dV. \tag{3.59}$$

The proportionality coefficient is therefore

$$\left(\rho\chi\frac{dT}{dP}\right) = \frac{L(\Omega)}{4\pi GM_r\left(1 - \frac{\Omega^2}{2\pi G\bar{\rho}_m}\right)} \tag{3.60}$$

where $\bar{\rho}_m$ is the average density within the level surface considered. This relation applies to any equipotential, but in general the von Zeipel theorem is considered at the surface of a star of total mass M and luminosity L.

Von Zeipel theorem can be expressed by the following equation

$$\vec{F}(\Omega,\theta) = -\frac{L}{4\pi GM^*}\vec{g}_{eff}(\Omega,\theta) \tag{3.61}$$

and it says that the radiative flux at the surface of a rotating star is proportional to the local effective gravity at the considered colatitude where

$$M^* = M\left(1 - \frac{\Omega^2}{2\pi G\bar{\rho_M}}\right) \tag{3.62}$$

and where $\bar{\rho}_M$ is the average stellar density. From g_{eff}, one obtains the radiative flux locally and therefore T_{eff} is written like

$$T_{eff}(\Omega,\theta) = \left(\frac{L}{4\pi\sigma GM^*}\right)^{\frac{1}{4}} [g_{geff}(\Omega,\theta)]^{\frac{1}{4}}. \tag{3.63}$$

Both the effective gravity and temperature vary over the stellar surface of a rotating star and influence the emergent spectrum. The equatorial regions

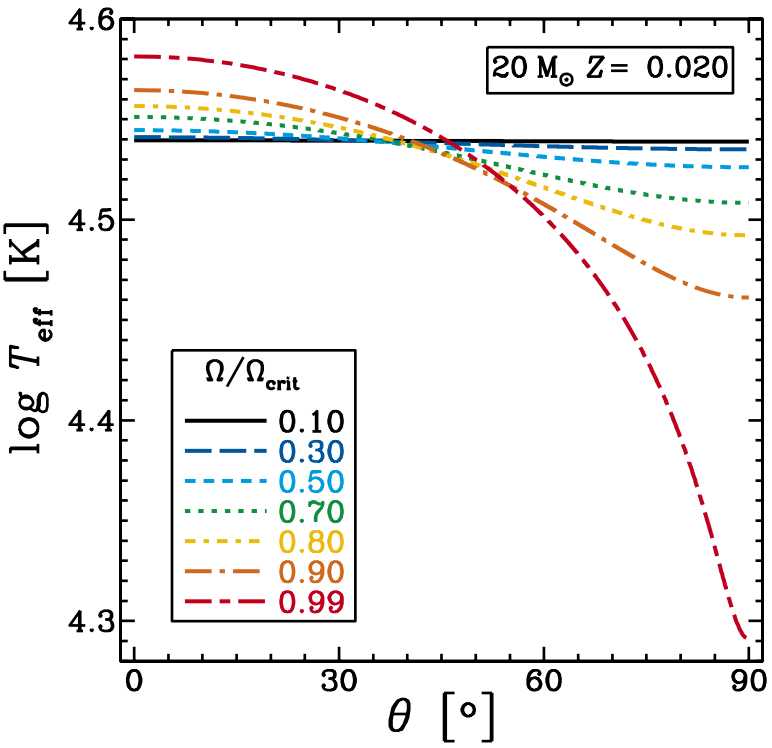

Figure 3.2— The local T_{eff} as a function of the colatitude θ for models of 20 $M_\odot$ on the ZAMS with various ratios Ω/Ω_{crit} of the angular velocity to the critical value. Figure taken from [47].

are fainter and cooler then the polar regions, which are brighter and hotter. This effect is called the gravity-darkening. Figure 3.2 shows an example of a considerable variations of T_{eff} over the surface of rotating stars.

The von Zeiplel theorem in a star with shellular rotation shows only minor differences with respect to equation (3.61) [106]. The differences, which essentially depend on the Ω gradient close to the surface, may slightly increase the contrast between the pole and the equator. Interferometric observations [42] of the fast rotating star Altair have confirmed the existence of gravity darkening as predicted by the von Zeipel theorem. More recent works [136] have confirmed a surface temperature distribution in this star in agreement with the von Zeipel theorem. Two dimensional models have tested the validity of the von Zeipel relation (Lovekin et al. [101]) but depending on the rotation laws, there are some small differences.

3.7 The equations for the atmosphere

In the atmosphere, the mass, the radius and the luminosity are supposed to keep constant values. Only the hydrostatic equilibrium equation and the radiative transfer equations must be solved. Considering that Ω is constant as a function of the depth and takes the same value as in the envelope. In such a case the effective gravity can be derived from a potential and one can write (3.20)

$$\frac{P}{\Psi} = -\rho \tag{3.64}$$

Taking into account the fact

$$\frac{dr_P}{d\Psi} = \frac{S_P < g_{eff}^{-1} >}{4\pi r_P^2} \tag{3.65}$$

that can be derived from expression (3.28) and (3.15), with $\alpha = \frac{d\Omega}{d\Psi} = 0$ one can obtain the following expression:

$$\frac{dP}{dr_P} = \frac{dP}{d\Psi}\frac{d\Psi}{dr_P} = -\rho\frac{4\pi r_P^2}{S_P < g_{eff}^{-1} >}. \tag{3.66}$$

Specifying the optical depth by $d\tau_P = -\kappa\rho dr_P$, one gets

$$\frac{dP}{d\tau_P} = \frac{1}{\kappa}\frac{4\pi r_P^2}{S_P < g_{eff}^{-1} >} \tag{3.67}$$

that can be transformed into

$$\frac{d\tau_P}{dlog_{10}P} = \kappa\frac{S_P < g_{eff}^{-1} >}{4\pi r_P^2} Pln10. \tag{3.68}$$

The equation of radiative equilibrium may be transfromed into a relation linking the temperature to the optical depth. P_{rad} is called the radiation presure and it can be defined as

$$\frac{dP_{rad}}{dn} = \frac{dP_{rad}}{d\Psi}\frac{\Psi}{dn} = \frac{P_{rad}}{dr_P}\frac{dr_P}{d\Psi} g_{eff}. \tag{3.69}$$

From equation (3.65), one gets

$$\frac{dP_{rad}}{dn} = \frac{S_P < g_{eff}^{-1} >}{4\pi r_P^2} g_{eff}. \tag{3.70}$$

In the diffusive approximation it can be written

$$\frac{dP_{rad}}{dr_P} = -\frac{\kappa\rho}{c}F \tag{3.71}$$

and with the expression (3.70), one gets

$$\frac{dP_{rad}}{dr_P} = \frac{4\pi r_P^2}{S_P < g_{eff}^{-1} >}\frac{\kappa\rho}{c}\frac{F}{g_{eff}}. \tag{3.72}$$

Using the formula for the optical depth given above yields

$$\frac{P_{rad}}{d\tau_P} = \frac{4\pi r_P^2}{S_P < g_{eff}^{-1} >}\frac{1}{c}\frac{F}{g_{eff}}. \tag{3.73}$$

Integrating form τ_P to the surface

$$P_{rad}(\tau_P) = \frac{4\pi r_P^2}{S_P < g_{eff}^{-1} >}\frac{1}{c}\frac{F}{g_{eff}}\tau_P + P_{rad}(0). \tag{3.74}$$

In the case the specific intensity can be considered as isotropic and having non-zero values only in the outward direction, it is found

$$\frac{cP_{rad}(0)}{F} = \frac{2}{3} \tag{3.75}$$

and therefore it can be expressed as

$$P_{rad}(\tau_P) = \frac{F}{g_{eff}c}\left[\frac{4\pi r_P^2}{S_P < g_{eff}^{-1} >}\tau_P + \frac{2}{3}g_{eff}\right]. \tag{3.76}$$

Using the theorem of von Zeipel that we explained above we write

$$\frac{F}{g_{eff}} = \text{const} = \frac{L}{S_P < g_{eff} >} \tag{3.77}$$

and thus the radiation pressure can be expressed by

$$P_{rad}(\tau_P) = \frac{L}{S_P < g_{eff>}c}[\frac{4\pi r_P^2}{S_P < g_{eff}^{-1} >}\tau_P + \frac{2}{3}g_{eff}]. \tag{3.78}$$

Defining T_{eff} by the expression

$$L = S_P\sigma T_{eff}^4 \tag{3.79}$$

one gets

$$P_{rad} = \frac{S_P \sigma T_{eff}^4}{S_P g_{eff} c} [\frac{4\pi r_P^2}{S_P < g_{eff}^{-1} >} \tau_P + \frac{2}{3} g_{eff}]. \tag{3.80}$$

With

$$P_{rad} = \frac{4}{3} \frac{\sigma}{c} T^4 \tag{3.81}$$

and introducing the expression for f_T one finally obtains

$$T^4(\tau_P) = \frac{3}{4} T_{eff}^4 \left[\frac{S_P}{4\pi r_P^2} f_T \tau_P + \frac{2}{3} \frac{g_{eff}}{< g_{eff} >} \right]. \tag{3.82}$$

3.8 Angular momentum

The equation of transport of angular momentum for shellular rotation in the vertical direction in Lagrangian coordinates is formulated by Zahn et al. [179].

$$\rho \frac{d}{dt} (r^2 \Omega)_{M_r} = \frac{1}{5r^2} \frac{\partial}{\partial r} (\rho r^4 \Omega U(r)) + \frac{1}{r^2} \frac{\partial}{\partial r} \left(\rho D r^4 \frac{\partial \Omega}{\partial r} \right) \tag{3.83}$$

where $\Omega(r)$ is the mean angular velocity at level r, $U(r)$ is the vertical velocity of the meridional circulation velocity and D is the diffusion coefficient due to the sum of the various turbulent processes. The factor 1/5 comes from the integration in the latitude. The angular momentum is conserved in the case of contraction or expansion. The first term on the right-hand side, corresponding to meridional circulation, is in advective term. The second term on the right-hand side, which corresponds to the diffusion processes, is a diffusive term. It can be noticed that advection and diffusion are different. The correct treatment of advection is very costly numerically because (3.83) is a fourth order equation, more details can be found in [179], for instance that the expression of $U(r)$ contains third order derivatives of Ω. This is the reason why some research groups treat meridional circulation in a diffusive way (Heger 2000 et al. [72]) with the risk of transporting angular momentum in the wrong direction, in the case that meridional circulation builds gradients.

The physics of meridional circulation are profoundly explained in Maeder [106]. For the purpose of explaining the implementation of rotation in the code at this point it is enough to know that the equation for the transfer of angular momentum should be solved and that in the case of "no wind " and for asymptotic regimes, the advection of angular momentum by the meridional currents is compensated by the diffusion of angular momentum through shear flows [179]. Therefore one can consider that the angular momentum per unit

mass in a given shell remains constant with time and this is how we are treating the problem of angular momentum.

The angular momentum of a given mass shell is computed as follows. The momentum of intertia of a mass shell (with the mass elements $\rho dnd\sigma$) is given by

$$dI = \int_{S_P} r^2 sin^2\theta \rho dnd\sigma = \int_{S_P} r^2 sin^2\theta \rho \frac{dn}{d\Psi} d\Psi d\sigma. \tag{3.84}$$

With equation (3.33) one obtains

$$dI = \int_{S_P} r^2 sin^2\theta \rho \frac{1 - r^2 sin^2\theta\Omega\alpha}{g_{eff}} d\Psi d\sigma, \tag{3.85}$$

which equals

$$dI = (1 - r^2 sin^2\theta\Omega\alpha)\rho \int_{S_P} r^2 sin^2\theta \frac{1}{g_{eff}} d\Psi d\sigma \tag{3.86}$$

because of equation (3.20) implying that the prefactor is constant on S_P and can be moved in front of the integral. Also, $d\Psi$ is constant between two isobars (an isobar equals a surface with Ψ =const.), which yields

$$dI = (1 - r^2 sin^2\theta\Omega\alpha)\rho d\Psi \int_{S_P} r^2 sin^2\theta \frac{1}{g_{eff}} d\sigma. \tag{3.87}$$

The integral is now expressed by the average over the isobar (see equation eq:q), so

$$dI = (1 - r^2 sin^2\theta\Omega\alpha)\rho d\Psi < \frac{r^2 sin^2\theta}{g_{eff}} > S_P. \tag{3.88}$$

Using equation(3.22) we find

$$dI = \frac{< r^2 sin^2\theta / g_{eff} >}{< g_{eff}^{-1} >} dM_P. \tag{3.89}$$

Defining now the specific angular momentum by means of the angular velocity and the moment of inertia we arrive at

$$j = \Omega dI = \frac{\Omega < g_{eff}^{-1} r^2 sin^2\theta >}{< g_{eff}^{-1} >}. \tag{3.90}$$

3.9 Genreal overview of the implementation of stellar rotation

This section describes details of our implementation of stellar rotation in the Padova stelar evoltuion code. In all the derivations the Roche model is used, so the gravitational potential is approximated by $\Phi = -GM_{\bar{r}}/\bar{r}$ where $M_{\bar{r}}$ is the mass inside the isobaric surface with a mean radius $\bar{r}$.

The basic equation describing the properties of mass shells, which are supposed to be isobars, is

$$\Psi_P(r,\theta) = \Phi + \frac{1}{2}\Omega^2 r^2 \sin^2\theta = \text{constant}. \tag{3.91}$$

Here $\Phi = \frac{-GM_P}{r}$ is the gravitational potential so that

$$-\frac{GM_P}{r} + \frac{1}{2}\Omega^2 r^2 \sin^2\theta = -\frac{GM_P}{r_{pol}}, \tag{3.92}$$

where we used the value of Ψ at the pole to fix the constant. So $-\frac{GM_P}{r_{pol}}$ is the parameter that characterizes a certain mass shell. Hence, a surface (in the following we will use the terms surface of an isobar or mass shell equivalently) is defined by the three parameters r_{pol}, the radius of the surface at the pole, M_P, the mass enclosed (the Roche model is adopted), and the angular velocity Ω. The equation for the surface itself, $r(\theta)$, is given only implicitly and can only be solved numerically. Moreover, a number of quantities that reflect properties of the deformed surface (3.92) can only be obtained numerically. In the following we will refer to these quantities as "derived quantities". They include f_P, f_T, the axis ratio $\frac{r_e}{r_{pol}}$ (with r_e being the radius at the equator), the surface area S_P, the volume V_P, the averaged effective gravity $< g_{eff} >$, the inverse of the effective gravity $< g_{eff}^{-1} >$, and the specific angular momentum j of a given mass shell. Note in particular that the enclosed volume of the deformed surface defines r_P by

$$r_P = \left(\frac{3}{4\pi}V_P\right)^{1/3}. \tag{3.93}$$

This basically is the principal challenge for the implementation of rotational effects (assuming shelluar rotation) in a stellar evolution code like the one of the Padova group. A stellar evolution code essentially solves numerically a set of differential equations for the pressure P, the radius coordinate r_P, the luminosity L_P and the temperature T as a function of the mass coordinate M_P (see presentation in chapter 2). The right-hand sides of the equations are in principle only dependent on P, r_P, L_P, T and M_P, though the actual dependence can be rather complicated including the implementation of an equation of state

and the opacities (assuming that the chemical composition and thus also the energy production is a function of the mass shell). This basic scheme remains unaltered also if stellar rotation is included. However, the underlying equations are changed as shown earlier in this chapter. In particular, for every evaluation of the right-hand side of the stellar structure equations one needs to know f_P and f_T as a function of r_P, M_P and either the angular velocity Ω or the specific angular momentum j that are assigned to a given mass shell. Thus, Ω and j are implicitly determined by M_P (details on the functional dependence and the underlying physics will be given below). Furthermore, one should bear in mind that some of the involved quantities have a more abstract meaning like for instance r_P being not a certain locus of a mass shell but being a measure for the volume of a deformed surface of an isobar.

The complication of the implementation of stellar rotation arises from the fact that f_P, f_T, and so on are derived properties of a deformed mass shell (i.e. numerically computed) expressed by equation (3.92), and during the evolution one is requesting $f_P, f_T, ...$ as depending on M_P and r_P, the latter being also a derived quantity from (3.92) and not a direct parameter entering (3.92). Note that the functional form of a mass shell is determined by (r_{pol}, M_P, Ω) (and not by r_P directly). Hence, the task is to determine the dependence of several quantities that can only be computed numerically from the surface equation parametrized by r_{pol}, M_P, and Ω. During the evolution this dependence will be invoked by an interpolation procedure using tables that express the functional dependence between (M_P, r_P, Ω or j) and f_T, f_P and so on. The tables are two-dimensional because the angular velocity or the specific angular momentum, respectively, are a function of M_P as discussed above. Details on the construction of the tables, the interpolation scheme and the implementation into the existing code are described in the following.

3.10 Details on the implementation of stellar rotation

It is important to note that two different tables have to be computed. The first one is used for the first stellar model only assuming that the star is uniformly rotating with a given constant angular velocity Ω supplied by the user. So the table entries depend only on r_P and M_P (two-dimensional table). Once the first stellar model is converged, the specific angular momentum of every mass shell is computed (see equation (3.90)) and assigned to the corresponding mass shell. As discuused above we assume that the angular momentum per unit mass of a given mass shell is conserved throughout the evolution. This means that a mass shell which expands in the course of the evolution slows down its rotation, or spins faster if it contracts. Therefore, the first table,

where a constant angular velocity has been assigned to a certain mass shell, cannot be used for the second and subsequent stellar models, since this would violate the conservation of angular momentum. Instead, one needs to compute a second table, where the specific angular momentum of a certain mass shell equals the specific angular momentum of this mass shell in the first stellar model. So one again ends up with a two-dimensional table because the specific angular momentum is fixed by the mass shell. (Note that the implementation of angular momentum transport would require to extend the table into a third dimension varying also the specific angular momentum of a given mass shell. This, however, is beyond the scope of this work (but see for instance , and the conservation of the specific angular momentum of each mass shell can be considered to be a fair approximation.)

3.10.1 Construction of the first table with constant angular velocity

In order to describe how to construct the first table, we start by outlining how to compute in general properties of a deformed mass shell which are entering the modified stellar structure equations (see section 3.4). While the surface $r(\theta)$ itself is determined implictily by (3.92), derived properties like $r_P, f_P, f_T, ...$ depend on quantities that are obtained from an integration over the surface. These quantities include the surface area itself (equation (3.17)), the volume (and therefore r_P, equation (3.15)), and variables which are averages over the surface (see equation (3.16)). To the latter group include the average of the effective gravity, the average of the inverse of the effective gravity (each computed via formula (3.16)), and more complicated expressions that are needed to determine the specific angular momentum (equation (3.90)). The computation of all these qunatities (except for the volume) is based on a numerical integration over the deformed surface in spherical coordinates with a discretezation in the θ-direction (polar angle) assuming axisymmetry around the rotation axis. All considered equations are of the type

$$I = \int_{\Psi=\text{const}} q d\sigma, \tag{3.94}$$

with some integrand q and the surface element $d\sigma$. The integration runs over a surface of constant Ψ expressed by equation (3.92), which implicitly gives $r(\theta)$.

Using the axisymmetry we write

$$\begin{aligned} I &= \int_{\Psi=\text{const}} q(r,\theta,\phi)d\sigma && (3.95)\\ &= \int_{\Psi=\text{const}} q(r,\theta,\phi)r^2\sin(\theta)d\phi d\theta && (3.96)\\ &= 2\pi\int_{\theta=0}^{\theta=\pi} q(r(\theta),\theta)r(\theta)^2\sin(\theta)d\theta && (3.97)\end{aligned}$$

and finally discretize

$$\begin{aligned} I &= 2\pi\int_{\theta=0}^{\theta=\pi} q(r(\theta),\theta)r(\theta)^2\sin(\theta)d\theta && (3.98)\\ &\approx 2\pi\sum_{i=1}^{n-1}[q(\theta_{i+1},r(\theta_{i+1}))r^2(\theta_{i+1})\sin(\theta_{i+1}) && (3.99)\\ &\quad +q(\theta_i,r(\theta_i))r^2(\theta_i)\sin(\theta_i)] && (3.100)\\ &\quad \times\frac{1}{2}(\theta_{i+1}-\theta_i) && (3.101)\end{aligned}$$

with

$$\theta_i = (i-1)\cdot\frac{\pi}{n-1}. \qquad (3.102)$$

Here, the composed trapezoidal rule has been employed (see [140]). For the actual implementation of equation (3.98), there still remains the difficulty to specify $r(\theta)$ determining the radial coordinate of the isobar as a function of the polar angle θ. This, however, can not be accomplished in closed form, but needs to be done numerically. To this end we write equation (3.92), which describes the deformed surface of an isobar depending on the parameters (M_P, r_{pol}, Ω), as

$$f(r) = \frac{GM_P}{r_{pol}} - \frac{GM_P}{r} + \frac{1}{2}\Omega^2 r^2\sin^2\theta_i = 0. \qquad (3.103)$$

Hence, the task reduces to find the root of this one-dimensional function for a given value θ_i, which can be easily achieved with a Newton iteration method for solving nonlinear equations (see chapter 2). Starting with a guess value r^0 for the root of function (3.103), one iteratievly computes

$$r^{j+1} = r^j - \frac{f(r^j)}{f'(r^j)} \qquad (3.104)$$

until sufficient convergence has been reached. The derivative of equation (3.103) reads

$$f'(r) = \frac{GM_P}{r^2} + \Omega^2 r\sin\theta_i. \qquad (3.105)$$

In the current implementation we use $r^0 = r_{pol}$ and find convergence typically after a few iterations. The convergence is checked by simply monitoring the relative change of r^j.

In summary we perform a numerical integraton for equations of the type (3.94) with an embedded Newton method to obtain $r(\theta_i)$ at every node θ_i. A similar procedure is used to compute r_P which is given by the volume $V_P = \frac{4\pi}{3} r_P^3$ inside a deformed surface. Here, the equation

$$V_P = \int_{\Psi=\text{const}} dV \tag{3.106}$$

is integrated numerically with

$$dV = r^2 \sin(\theta) d\phi d\theta dr. \tag{3.107}$$

Thus, one obtains the one-dimensional integral

$$\begin{aligned} V_P &= \int_{\Psi=\text{const}} r^2 \sin(\theta) d\phi d\theta dr & (3.108)\\ &= 2\pi \int_{\Psi=\text{const}} r^2 \sin(\theta) d\theta dr & (3.109)\\ &= \frac{2\pi}{3} \int_0^\pi r^3(\theta) \sin(\theta) d\theta, & (3.110) \end{aligned}$$

which can be solved with the same numerical method and it follows

$$r_P = \left(\frac{1}{2} \int_0^\pi r^3(\theta) \sin(\theta) d\theta \right)^{1/3}, \tag{3.111}$$

where again the parameters M_P, r_{pol}, Ω defining the deformed surface under consideration, enter through the definition of the surface equation in the Newton method.

The procedure outlined above is used in our implementation to compute derived quantities of an isobar from the parameters M_P, r_{pol}, Ω defining this surface sketched as follows

$$(M_P, r_{pol}, \Omega) \longrightarrow V_P, S_P, < g_{eff} >, < g_{eff}^{-1} >, < g_{eff}^{-1} r^2 sin^2(\theta) > \longrightarrow f_T, f_P, V_P, j$$

Here we use equations (3.106), (3.16) and (3.17) for the first step and equations (3.15), (3.90), (3.51) and (3.50) for the second step.

In the following we describe how the two tables are setup in our implementation. For the first table (constant angular velocity) we start by choosing an angular velocity which is supposed to be constant through out the star in the

first stellar model. Then, we use the structure of the corresponding non-rotating stellar model under consideration providing a grid of (M_P^{non},r_P^{non}) coordinates of this model, which serve as a rough estimate for the requested values of M_P, r_P of the rotating model. These values should be represented by the table. For every mass shell (value of M_P) we define a range 0.5 r_P^{non} ... 3 r_P^{non} and subdivide it into about 200 equally spaced intervals. The gridpoints of this range serve now as input values for computing the "derived quantities" and thus determine the extension of the table for this mass shell M_P. We now (arbitrarily) identify the values of the above r_P^{non}-range with the parameter r_pol, which is somewhat inconsistent, but sufficient to serve as an estimate for the range of the table, but it is just needed to have a rough idea about the involved ranges. The concrete values for the range and the spacing can be varied for different models but should simply ensure that the whole possible range of potentially invoked input values r_P and M_P is covered by the table with sufficient resolution. By this procedure a grid of (M_P, r_{pol}) values is set up (Ω =constant), and for every grid point we compute numerically the derived quantities f_P ,f_T, j, and, in particular, r_P(, which is used as an independent variable when the table is called for determining f_P, f_T, ...). We stress once more that r_P is actually used as an independent variable when the table is called, but since it can be obtained only numerically, it can not be used to setup the table but is rather implemented as an dependent variable of the table.

When this table is used for the computation of the first stellar model, for a given (M_P, r_P) dependent quantities like f_P and f_T are obtained from an interpolation. First the corresponding mass shell is loacted. Then we perform a one-dimensional interpolation using grid points with constant M_P covering the requested r_P. Note that for the interpolation the r_P-entries of the table are used. We implemented linear and 3rd order interpolation schemes. In practice, the table is not computed for every mass shell but only for about every 10th (concrete number varies for different models). Therefore, we implemented a more general scheme performing a two-dimensional interpolation in M_P- and r_P-direction. This is accomplished by successive one-dimensional interpolations in M_P- and r_P-direction and has the advantage that arbitrary M_P values can be requested, allowing also for a redistribution of the mass shells.

3.10.2 Setup of the second table with constant specific angular momentum

As discussed above we evolve the stellar models assuming that the specific angular momentum of every mass shell is conserved. Therefore, once the first model has converged, we compute the specific angular momentum of every

given mass shell and assign it to this shell (see equation (3.90)). Now, the second table for the rest of the evolution has to be constructed in a way that the specific angular momentum of a given mass shell remains constant. To this end we set up a grid of (M_P, r_{pol}) values as described above. Then, for every pair (M_P, r_{pol}) we search the value of the angular velocity in such a way that the specific angular momentum j of a mass shell defined by (M_P, r_{pol}, Ω) has the same value as the angular momentum that has been assigned to the given M_P value. Starting from a guess value of Ω we compute the properties of this mass shell including the specific angular momentum. Comparing the obtained specific angular momentum with the value assigned to the given mass shell, we increase or decrease the angular velocity Ω depending on whether the computed j is too low or too high. Furthermore, the step size for the new guess value of Ω is reduced whenever the deviation between computed and assigned specific angular momentum becomes larger in a subsequent step. By this procedure for every (M_P, r_{pol}) the angular velocty is determined which corresponds to a specific angular momentum equal to the one belonging to M_P in the first stellar model. Once this table is constructed, it is used throughout the subsequent evolution of the star employing the same interpolation scheme as detailed above.

Figure 3.3 shows a section of the table that has been constructed for constant angular momentum. Here, f_T is displayed as a function of the radial coordinate r_P. The deviation of f_T from unity is an indication for how strong the stellar structure equations are affected by rotation. The plotted lines belong to certain mass shells, i.e. certain values of M_P. The table was computed for a star with 10 $M_\odot$. One can see that the radial coordinate spans different ranges for different mass shells, because a mass shell initially located close to the center will not move to far from its origin. Furthermore, one can see that as a certain mass shell expands (following a certain line) f_T decreases, i.e. the effects of rotation become less important. this is clear becuase then the shell rotates slower because of the conservation of angular momentum. One can also recognize that the datapoints (crosses) are not equidistant, because the table was set up with equidistant r_{pol} values resulting in a different spacing in r_P-space.

3.10.3 Implementation of the atmosphere equations

The implementation of the equations describing the atmosphere requires a scheme similar to the one outlined above. As in the case of the stellar interior, the basic procedures for computing the atmosphere remains unaltered, though the equations need to be changed as summarized above in this chapter.

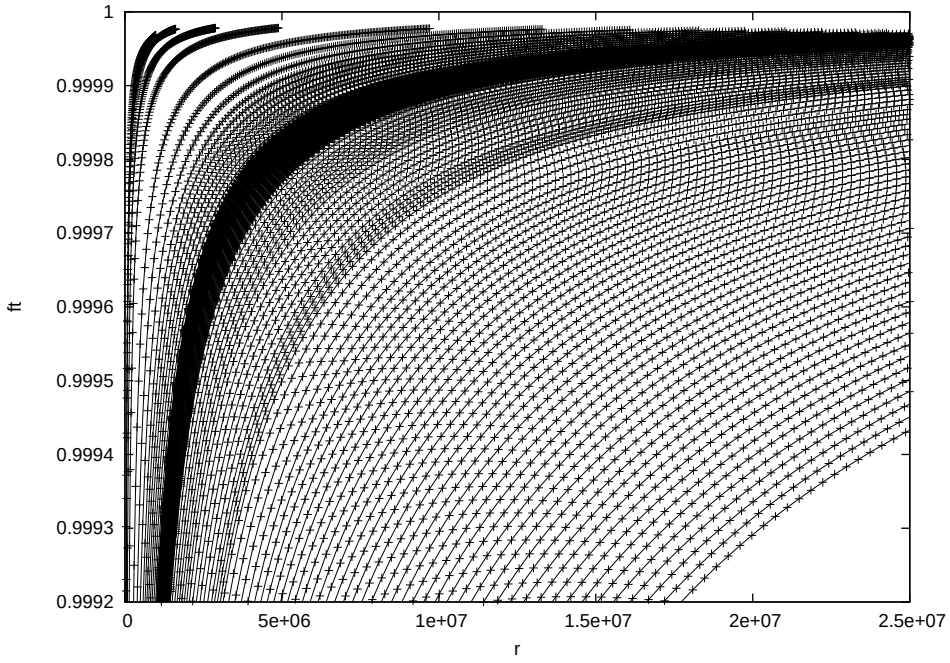

Figure 3.3— Dimensionless quantity f_T as a function of r_P in units of km. See main text for explanations.

For the atmosphere it is assumed that it rotates with a prescribed angular velocity which is equal to the outermost mass shell of the stellar interior. Inspecting the equations for the atmosphere (see section 3.7) one finds that they contain the "derived quantities" f_T, S_P, $< g_{eff} >$ and $< g_{eff}^{-1} >$, which are functions of M_P, r_P and Ω. Hence, one is again facing the task to determine these quantities, computed from the surface equation (3.92), as functions of (M_P,r_P,Ω) similar to the treatment of the stellar interior. Here, however, we do not use tables because relatively few evaluations are required. Instead, we compute the values directly on demand. For defining a deformed surface of a mass shell M_P and Ω are already given as prescribed values of the atmosphere. To uniquely define the surface (and to compute the derived quantities) only r_{pol} needs to be determined in a way that $r_P = (\frac{3V_P}{4\pi})^{1/3}$ as computed from the surface equals the prescribed r_P-value of the atmosphere. To this end we employ the same search algorithm as described above, but this time varying r_{pol} until the r_P values agree with sufficient accuracy.

3.11 Discretisation of the equations

The change of varaibles needs to be done before discretizing the equations.
$Q = ln(1 - M_P/M_f$ is the new mass coordinate
where M_f is the mass limit between the interior and the envelope of the star,
$P = lnP$ is the new pressure variable,
$T = ln\bar{T}$ is the new temperature variable,
$R = lnr_P$ is the new radius coordinate,
$RH = ln\bar{\rho}$ is the new density coordinate,
$CAP = ln\kappa$ is the opacity,
$S = ln(1 + L_P/(fL_{tot})$ is the new luminosity coordinate
where L_{tot} is the total luminosity of the star and
f is factor to ensure that $L_P/fL_{tot} > -1$ so that S is define. This factor is important when the neutrino energy losses are important.

Applying this change of variables to the equations presented in this and the previous chapter one gets the following formula for:

Energy conservation:

$$\frac{\partial S}{\partial Q} = -\frac{M_f}{fL_{tot}} e^{Q-S}(\epsilon_{nucl} - \epsilon_{nu} + \epsilon grav) \tag{3.112}$$

Momentum equation:

$$\frac{\partial P}{\partial Q} = \frac{GM_f^2}{4\pi} f_P e^{Q-P-4R}(1 - e^Q) \tag{3.113}$$

Mass conservation:

$$\frac{\partial R}{\partial Q} = \frac{M_f}{4\pi} e^{(Q-3R-RH)} \tag{3.114}$$

Energy transport equation:

Radiation:

$$\frac{\partial T}{\partial Q} = \frac{3M_f fL_tot}{256\pi^2\sigma} f_T(e^S - 1)e^{[Q+CAP-4(R+T)]} \tag{3.115}$$

Convection:

$$\frac{\partial T}{\partial Q} = \frac{GM_f^2}{4\pi} f_P e^{(Q-P-4R)}(1 - e^Q)\frac{\delta}{c_P} \tag{3.116}$$

Discretizing equations and by approximating the spatial derivatives in the middle of the mass zone one gets the following expressions in the code:
For energy conservation:

$$\frac{S(J1) - S(J)}{Q(J1) - Q(J)} + \frac{M_f}{fL_{tot}} e^{0.5(Q(J1)+Q(J)-S(J1)-S(J)}$$

$$\times \left(\sqrt{\epsilon_{nucl}(J1)\epsilon_{nucl}(J)} - \sqrt{\epsilon_{\nu}(J1)\epsilon_{\nu}(J) + \epsilon_{grav}} \right) = 0, \tag{3.117}$$

where
$\epsilon_{grav} = \frac{1}{4\delta t} e^{0.5(P(J1)+P(J)-RH(J1)-RH(J))} [-(RHT(J1) + RHT(J))$

$$\times (VP(J1) + VP(J)) + \left(\frac{RHT(J1)}{ADI(J1)} + \frac{RHT(J)}{ADI(J)} \right) (VT(J1) + VT(J))$$

Momentum equation:

$$\frac{P(J1) - P(J)}{Q(J1) - Q(J)} - \frac{GM_f}{4\pi} f_P e^{0.5(Q(J1)+Q(J)-P(J1)-P(J)-4R(J1)-4R(J))}$$

$$\times (1 - e^{0.5(Q(J1)+Q(J))}) = 0, \tag{3.118}$$

Mass conservation:

$$\frac{R(J1) - R(J)}{Q(J1) - Q(J)} + \frac{M_f}{4\pi} e^{0.5(Q(J1)+Q(J)-3R(J1)-3R(J)-RH(J1)-RH(J))} = 0, \tag{3.119}$$

Energy transport equation: Radiation:

$$\frac{T(J1) - T(J)}{Q(J1) - Q(J)} - \frac{GM_f^2}{4\pi} f_T e^{0.5(Q(J1)+Q(J)-P(J1)-P(J)-4R(J1)-4R(J))}$$

$$\times \left(1 - e^{0.5(Q(J1)+Q(J))} \right) 0.5(RAD(J1) + RAD(J)) = 0, \tag{3.120}$$

Convection:

$$\frac{T(J1) - T(J)}{Q(J1) - Q(J)} - \frac{GM_f^2}{4\pi} f_T e^{0.5(Q(J1)+Q(J)-P(J1)-P(J)-4R(J1)-4R(J))}$$

$$\times \left(1 - e^{0.5(Q(J1)+Q(J))} \right) 0.5(ADI(J1) + ADI(J)) = 0. \tag{3.121}$$

where $RHT = \partial RH/\partial T = -\delta$,
$ADI = \nabla_{ad}$ is the adiabatic gradient $\partial lnT/\partial lnP|_{ad}$,
$RAD = \nabla_{rad}$ is the radiative gradient $\partial lnT/\partial lnP|_{rad}$.

CHAPTER 4

Massive stars - models with mass loss and without rotation

Massive stars are the crossroads of any important astrophysical problem. Therefore, a proper understanding of thier evolutions is highly diserable. They are the main sources of UV radiation. By heating the interstellar dust they produce the far-IR luminosities of galaxies. They are the progenitors of blue supergiants, red supergiants, luminous blue variables (LBV), Wolf-Rayet stars, supernovae and black holes and also the main sources of nucleosynthesis. Massive stars are observable at large distances in the Universe either directly or by their signatures in the integrated spectrum of galaxies. Stellar winds and supernovae contribute almost equally to the injection of mechanical power and turbulence into the interstellar medium. The observations of starbursts have shown the major role of massive stars in the spectral and chemical evolution of galaxies.

4.1 The life of a massive star

Massive stars have an initial mass larger than $8\pm1\ M_{\odot}$ and their life is divided into several stages. The first stage is the formation of the star, which is not yet completely understood for massive stars. Current thinking is that they are formed either by the merger of smallar mass strars (Bonnell et al. [19]) or that they are formed by mass accretion that increases with the instant mass of the star (Behrend & Maeder [11]). Stellar evolution studies usually start on the zero age main sequence (ZAMS). During the main sequence (MS) the star

burns hydrogen into helium in its core. This is the longest stage of the life of the star ($\approx 90\%$ of the total lifetime) and it lasts for three to 15 million years for masses between 60 and 15 $M_{\odot}$, respectively. This is much shorter than the lifetime of the sun which is around nine billion years.

At the end of hydrogen burning, the core contracts and the envelope expands (effect called the "mirror effect"). The evolution of the envelope varies with the initial mass of the star and depends on mass loss.

In the core, contraction continues until the central temperature is high enough to start helium burning ($T_C \sim 1.5 \cdot 10^8 K$). He-burning lasts about 10% of the H-burning lifetime. During this stage, helium is transformed into carbon and oxygen. It is imortant to bear in mind and take it into account that He-burning is sensitive to the treatment of convection because the He-burning core grows in mass and faces a mean molecular weight (μ) gradient. He-burning is also sensitive to the rate of the nuclear reaction $^{12}C(\alpha,\gamma)^{16}O$ which competes with the triple-α reaction (transforming helium into carbon), Schlattl et al. [149].

The evolution of the massive stars in the H- and He-burning phases is heavily influenced by mass loss due to a radiative stellar winds. They are able to remove most of the initial stellar mass, leaving only bare cores (Wolf-Rayet stars) deprived of their envelopes.

Massive stars are often fast rotators and experience rotational mixing which transports elements to the surface, which are synthesized in the core. Observations show large nitrogen and helium enrichment, particularly in low-Z stars. Rotation also enhances the mass loss rates by stellar winds and creates anisotropic winds, which are stronger at the poles than at the equator.

We thus conclude that the physics and evolution of the massive stars are dominated by mass loss and by rotational mixing.

4.2 Evolutionary tracks with mass loss

In this chapter we will present evolutionary models calculated in the range from 10 $M_{\odot}$ to 120 $M_{\odot}$ for three different metallicity. We consider that stellar models are on the Zero Age Main Sequence (ZAMS) when chemically homogeneous stars begin their hydrogen burning and the gravitational energy production is less than about 1% of the total energy. Our models are evolved from the ZAMS, and the evolution is followed in detail through the entire hydrogen and helium burning phase until carbon ignition. The Padova group calculated different set of evolutionary models for massive stars in the past, but in the last fiftheen years the concentration of the group was put on low and intermediate stars and especially in the extension of stellar models and isochrones until the end

of the thermal pulses along the the asymptotic giant branch (TP-AGB) for all the masses up to $\sim 6M_{\odot}$ Marigo & Girardi [115]. With changes in the code during the years and with new input physics described in chapter 2 it is necessary to compute the new set of evolutionary models for nonrotating massive stars. We need to point out that the computation of massive stellar models is nuemrically more challenging than for intermediate and low-mass stars because of the treatment of the stellar atmosphere.

We encountered numerical difficulties with models with models in the mass range 25-60 $M_{\odot}$ during the cenral helium burning phase. Specifically, because of the mass loss, the steep discontinuity in the molecular weight caused by the intermediate convective core reaches the surface, and the models of the RSG phase could not reach the equilibrium configuration located far away in the blue side of the HR diagram. For masses greater than about $> 60M_{\odot}$ this was less of problem because mass loss is so efficient that the hydrogen rich envelope is soon peeled off and the star never enters the RSG phase.

The set of nonrotating massive stars is the base for investigating the effects of rotation once it is implemented in the code which is the main purpose of this thesis. The models of massive nonrotating stars can be used for different purposes. They can be considered as describing the evolution of slowly rotating stars, i.e. of the stars that rotate slowly enough so that their outputs are only a little affected by rotation. They allow comparisions with nonrotating evolutionary tracks that were published previously. Since the models are computed with exactly the same physics as will be employed for rotating stars, they offer a comparision basis for studying the effects of rotation.

We also point out that the increasing number of observed supernova events offers the opportunity to find even more frequently the progenitor star in archive images. In a few cases the progenitor star is a yellow supergiant star. The estimated position in the HR diagram of these stars is not compatible with the theoretical tracks of classical single-star models. According to several authors (e.g. [130], the mass loss during the red supergiant phase could be underestimated , so it is important to study the effects on mass loss of the massive stars even when rotation is not considered. For all these considerations we need the main set of stellar evolutionary tracks for massive stars with actual mass loss implemented.

In the Fig. 4.1 we can see the new set of tracks calculated for the chemical composition Z=0.017 and Y=0.26 for the masses in the range from 10 to 120 $M_{\odot}$. The different color lines correspond to the 10, 12, 15, 20, 30, 40, 50, 60, 80, 100 and 120 $M_{\odot}$.

The evolutionary tracks for the chemical composition of Z=0.008 and Y=0.26 (Large Magellanic Cloud), are presented in Fig. 4.2. With different color lines

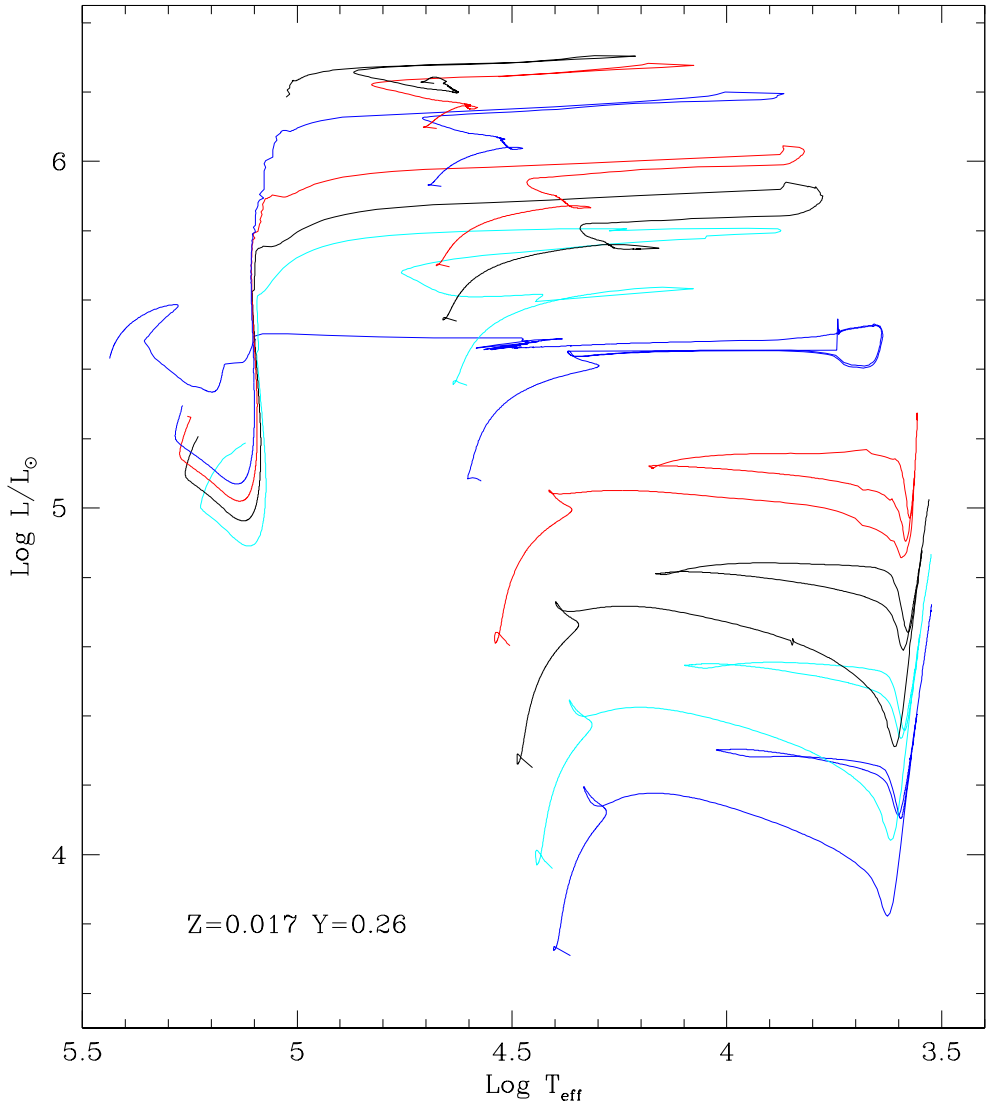

Figure 4.1— Evolutionary tracks in the Hertzsprung-Russel diagram for model with stellar masses in the range of 10 $M_{\odot}$ to 120 $M_{\odot}$. The chemical composition is Z=0.017 and Y=0.26.

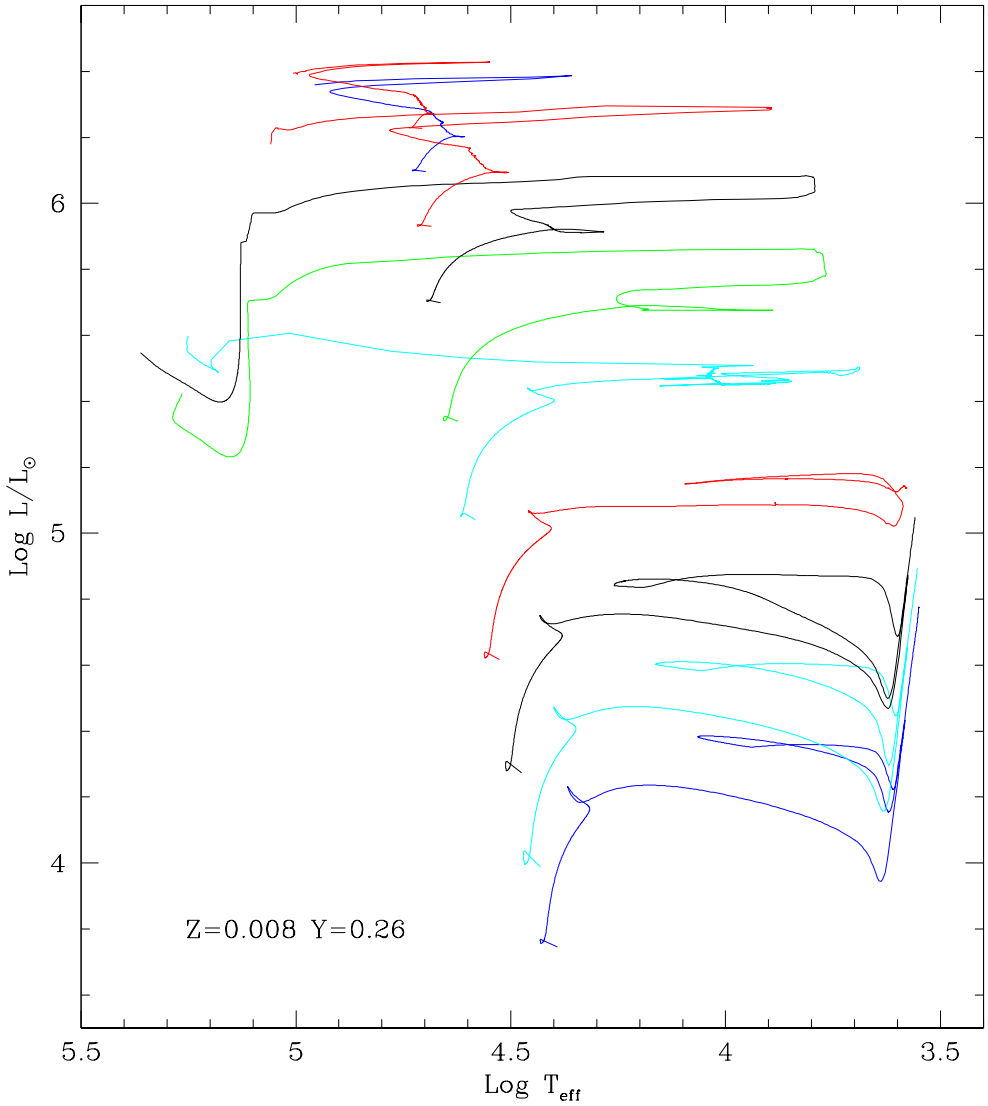

Figure 4.2— Evolutionary tracks in the Hertzsprung-Russel diagram for model with stellar masses in the range of 10 $M_\odot$ to 120 $M_\odot$. The chemical composition is Z=0.008 and Y=0.26.

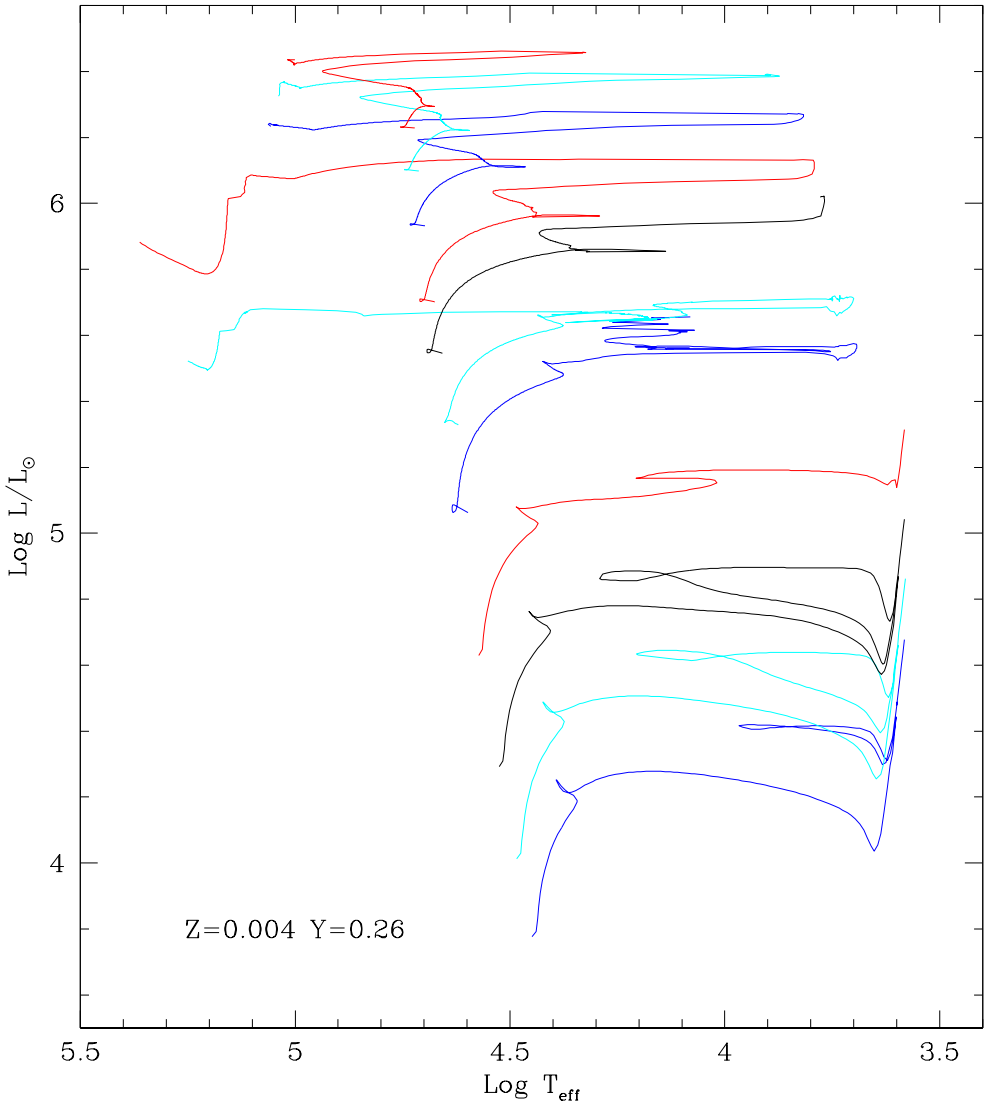

Figure 4.3— Evolutionary tracks in the Hertzsprung-Russel diagram for model with stellar masses in the range of 10 $M_\odot$ to 120 $M_\odot$. The chemical composition is Z=0.004 and Y=0.26.

tracks for 10, 12, 15, 20, 30, 40, 60, 80, 100 and 120 $M_\odot$ are presented. For the same masses the evolutionary tracks for chemical composition of Z=0.004 and Y=0.26, which corresponds to the Small Magellanic Cloud chemical composition, are computed and shown in Fig. 4.3.

In the graphics we can notice that the core helium burning phase of model stars evolved with mass loss is characterized by an apparently erratic location in the HR diagram, which is the result of the extreme sensitivity of the models to many structural properties. Several criteria for blueward and/or redward movements in the HR diagram have been suggested (e.g. Chiosi [29], Chiosi & Maeder [30]). Generally speaking, four internally competing effects can be distinguish:

- the classical mirror expansion that responds to the core contraction
- the increasing size of the He core by outward shifting of the H-burning shell and the increasing size of the fractional mass of the He core by mass loss, which favours redward evolution up to some critical value and blueward evolution afterward (Giannone et al. [62])
- the homogenization of the envelope by large intermediate convective zones, which (if present) tends to limit the increase of the stellar radius
- a large luminosity-to-mass ratio, which favours the envelope expansion

In particular, the second point is regulated by mass loss during the post main sequence stages and more precisely at low effective temperatures. Several plausible scenarios are generated by the competition between the various factors discussed above an we will discuss them in the following sections.

It is important to notice, that if a star becomes a red supergiant at the very beginning of the core He-burning phase, the lifetime of its red supergiant will be larger then the one of a star which will begin to transform its central helium already in the blue part of the HR diagram and enters its red supergiant stage in a more advanced evolutionary stage. Therefore, red supergiant lifetimes depend on the way the star evolves into the red part of HR diagram after the main sequence phase.

4.3 Masses below 20 $M_\odot$

Below about 20 $M_\odot$ the mass loss in the blue or the red is never large enough to remove the outer layers and to produce a definitive blueward motion. After the main sequence the star may either become a blue supergiant and later on a red supergiant, or it may first become a red supergiant and then undergo

a blue loop during which the Cepheid instability trip may be crossed on an appreciable time scale.

Several plausible scenarios are generated by the competition between the various factors discussed above. Here we give a short overview.

- **Case A**: to the first case we will refer as case A because of the historical importance of the classification suggested by Chiosi & Summa [31] in their pioneer study on the effects that instability criteria on massive stars can be taken as representative for the general evolution of stars in this mass range.

  The models move to the red side of the HR diagram after finishing H-burning in the core within the Kelvin-Helmholtz time scale, spend a fraction of their He-burning phase near the Hayashi line, make a blue loop to the high temperature region of the HR diagram, and spend a fraction of the He-burning time near the tip of the loop. Finally, they return to the red before exhausting helium in the core, and remain there for the rest of their life. This evolution is often indicated by O-BSG-RSG-YSG-RSG.

  In the original work of Chiosi & Summa [31] this case is obtained adopting the Ledoux criterion for the neutrality condition in the occurence of semi-convection. A 20 $M_{\odot}$ stellar sequence at constant mass was calculated. The resulting scenario accounts both for the blue supergiants, because of the extended loop and supergiants, because this model spends a fraction of the stationary He-burning lifetime at low effective temperatures. Moreover, because this scenario has a red phase before looping back to the blue, the surface abundances are altered by the deep penetration of the envelope convection, which mixes CNO processed material up to the surface. The inclusion of mass loss, slightly modifies the above scheme by affecting the extension of the loop.

  Our models, as well as the models from Bressan et al. [20] computed with overshoot both in the convective core and the convective envelope follow the case A evolution.

- **Case B**: this case is refered to as case B for the identical reasons as case A. After the H-burning phase the models get in thermal equilibrium while igniting helium in the core somewhere to the red of the main sequence band. These model evolve slowly towards the red side of the HR diagram on the time scale of cenral He-burning and terminate the core He-burning phase in the red. This kind of evolution is indicated by O-BSG-YSG-RSG.

  Evolutionary models following case B show in the HR diagram a stationary phase after leaving the main sequence, somewhere inbetween this

and the Hayashi limit. Thus, they can account for the distribution of supergiant stars in the HR diagram, but fail to match the observations of surface abundances, because if they start core He-burning in the blue, and spend a part of the lifetime of this phase at relatively high temperatures and part in the red, it is not possible for a single star to show variations of the surface abundances if rotationaly mixing is not included.

- **The blue-red evolution**: these models follow the case A evolution until the first arrival at the Hayashi track. However, they never return to the high temperature region, and spend the whole He-burning life time as red supergiants. This kind of evolution is named O-BSG-RSG because these models have no equilibrium configuration in the middle of the HR diagram between the main sequence band and the Hayashi limit. This behaviour is characteristic for models with overshoot only from the core. Langer [94] found that a small amount of overshoot (0.2 H_p) from the convective core inhibits the originally very extended loops.

- **The blue-red-blue evolution** or the SN1987A progenitor evolution:

  As we mentioned before the important factor governing the blueward evolution from the red supergiant stage is the mass fraction occupied by the helium core. Typically, when the mass fraction of the helium core becomes greater than about 60-70% of the total actual mass, the star evolves back to the blue part of the HR diagram. This is what happens in the rotating 20 $M_\odot$ stellar model with $v_{ini} = 300km/s$, in which the helium burning occupies more then 65% of the total mass. This was calculated for pre-supernova evolutionary models by Hirschi et al. [75].

In Fig. 4.4 we present models computed with and without overshoorting for 6, 8, 10, 12 and 15 $M_\odot$, in order to analyze the effect of overshooting on the stellar evolutionary track. The blue lines indicate models computed without overshooting and the red one with overshooting. The core hydrogen burning phase of all stars possessing a convective core on the zero age main sequence is affected by convective overshoot. Because of the larger cores, the models run at higher luminosities and live longer than the classical ones. They also extend the main sequence band over a wider range of T_{eff}; this trend increases with stellar mass (Alongi et al. [5], Bertelli et al. [13], Maeder & Meynet [108]). The overluminosity caused by overshoot during the core hydrogen burning phase still remains during the shell hydrogen and core helium burning phases because of the larger size of the hydrogen exhausted core. As a consequence of the higher luminosity, the lifetime of the helium burning phase gets shorter in spite of the larger mass of the convective core.

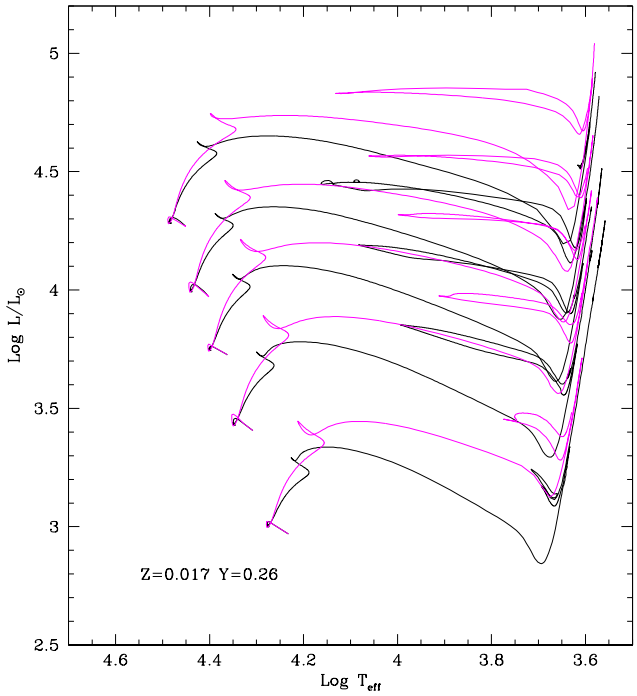

Figure 4.4— Evolutionary tracks in the Hertzsprung-Russell diagram for models with masses in the range of 6 $M_\odot$ to 15 $M_\odot$. The black lines correspond to models without overshooting, while the magenta curves indicate the result of claculations with overshooting.

4.4 Masses between 25 $M_\odot$ and 60 $M_\odot$

For all masses greater than about 25 $M_\odot$ mass loss plays the key role and strongly affects stellar evolution. In this mass range, mass loss on and near the main sequence is not high enough to remove the complete outer envelope, and therefore the star rapidly becomes a red supergiant because the intermediate convective zone is small or absent. The star spends a part of the helium burning phase as a red supergiant, where it can expect a lifetime longer than that calculated from a constant-mass model. In this mass range, the high stellar winds in the red supergiant stage progressively remove the outer envelope and the star evolves to the blue due to the increasing size of the helium core. Whether or not this will actually occuer is entirely determined by the competition between the time scale of mass loss (rate) and the nuclear burning time scale. With insufficient mass loss, a star may not be able to leave the red supergiant region. If a blue loop occurs, a star may then spend part of the He phase as a blue supergiant. It is interesting to note that such a blue supergiant could be differentiated from supergiants on their first crossing by their pulsation properties and surface abundances. If the mass loss is high enough, the star may lose all the ennvelope and become a good candidate for a Wolf-Rayet stage. This will likely occur in the mass range 40-60 $M_\odot$. In this range of mass is faced the complex situation that mass loss on or near the main sequence favors the formation of red supergiant, whereas heavy mass loss in the red may shorten the lifetime of red supergiants, since the star turns either into a blue supergiant and/or a Wolf-Rayet star. [30]

4.5 Masses larger then 60 $M_\odot$

The winds responsible for peeling during the main sequence and early shell H-burning phases are strong enough to remove all stellar outer layers, leaving a bare helium core. As we can see in the figures 4.1, 4.2, 4.3, so for three different metallicity, the evolution towards the red supergiant stage is prevented and therefore the star always remains on the left half of the HR diagram. Zones that were initially in the core are exposed at the stellar surface, where they lead to large spectroscopically observable changes of chemical abundances. During the blue supergiant phase, these stars are located in the region of lumionous blue variables. As a result of the very high mass loss rates [92] the remaining part of the envelope is ejected and the stars evolve directly as bare cores, identifiable as Wolf-Rayet stars (more deteils in section 4.8). Observational evidence for such an evolutionary connection is given by P Cygni [92].

4.6 Evolutionary scenarios

Although our evolutionary tracks do not reach into the presupernova phase, we sketch here schemactically the evolutionary scenarios at solar metallicity for single massive stars. Our models can be followed until the Red Supergiant phase (RSG), until the Wolf-Rayet phase or until the Luminous Blue Variable phase (LBV). Massive stars follow the sequences as shown below [106]:
10 - 25 $M_\odot$: O -RSG - (Cepheid loop, M $< 15\ M_\odot$) RSG - SN (SNIIp)
25 - 30 $M_\odot$: O - (BSG) - RSG - BSG (blue loop) - RSG - SN(SNIb, SNIIL)
30 - 40 $M_\odot$: O - BSG - RSG - LBV?- WNE - WCE - SN(SNIb)
40 - 60 $M_\odot$: O - BSG - LBV $\Leftrightarrow$ WNL - (WNE) - WCL-E - SN(SNIb)
- WCL-E - WO - SN (SNIc)
60 - 90 $M_\odot$: O - Of/WNL $\Leftrightarrow$ LBV - WNL (H poor) - WCL-E - SN(NIIn?)
M $> 90\ M_\odot$: 0 - Of - WNL - (WNE) - WCL - WCE - SN (Hypernova low Z)

The sign $\Leftrightarrow$ means back and forth motions between two stages. Of-stars are 0-type star showing emission lines. The various types of supernovae are tentatively indicated (review by Smartt [152] for more details). Wolf-Rayet (WR) are presented in a section 4.8 and for more details see Crowther [35].

The limits between the various scenarios depend on metallicity Z and rotation. As we saw above this different scenario can be classified in three families: below about 30 $M_\odot$, stars go through a red giant stage; above about 40 $M_\odot$ stars go through a Luminous Blue Variable and a Wolf-Rayet (WR) phase; in the intermediate mass range, between 30 and 40 $M_\odot$, stars can possibly (but not necessarily) go through the tree phases, RSG, LBV and WR.

4.7 Red supergiants

Stars in the mass range of 10 to 25 $M_\odot$ which are in their He burning phase are called red supergiants (RSGs). Until recently, stellar evolution models only poorly described the location of Galactic RSGs in the Hertzsprung-Russell diagram, where theoretical models were unable to produce stars as cool and luminous as required by observations (Massey [117]). Several reasons might be the explanation for these discrepancies: the molecular opacities of RSGs are only poorly known, the approximations within the mixing-length theory do not apply to the near-sonic velocities of the convective layers, the highly extended atmospheres of RSGs may not be treated as plane-parallel in theoretical description (Levesque et al. [100]). Similar deviations between theorey and observations have been reported for RSGs in the Magellanic Clouds (Massey & Olsen 2003 [118]).

The situation improved with moderate-resolution optical spectrophotome-

try and the new MARCS stellar atmosphere models (Gustafsson et al. [68]). Levesque et al. ([99], [100]) determined the properties of RSGs in our Galaxy and in the Magellanic Clouds to be compared with evolutionary tracks. They infered significantly higher effective temperatures and uncovered a better agreement between the new temperatures and bolometric corrections with stellar evolutionary models. The tracks used for the comparison with Galactic RSGs have been taken from the Geneva group with initial rotation rates in the range of 0 to 300 kms^{-1} at solar metallicity (Meynet & Maeder [126]). To investigate the effects of metallicity Levesque et al. [100] studied the RSGs in the Magellanic Clouds and provided evidence for significant visual extinction because of circumstellar dust. The observed effective temperatures of K supergiants are approximately the same in the SMC, LMC and Milky Way but the lower abundance of TiO leads to effective temperatures which are lower for M supergiants of the same spectral subtype. RSGs in the Magellanic Clouds are in average not as cool as Galactic RSGs, which is consistent with the shifting of the rightmost extension (the Hayashi limit)of the evolutionary tracks to higher effective temperatures at lower metallicities. The observed average spectral subtypes of RSGs in these galaxies shift from $M2I$ in the Milky Way to $M1I$ in the LMC and $K5 - K7I$ in the SMC. The updated physical properties by Levesque et al. ([99], [100]) made the location of RSGs compatible with the predictions of stellar evolution. There is now an excellent agreement between Milky Way supergiants and evolutionary tracks, which reproduce accurately this stage of massive star evolution in the Milky Way.

We note that our tracks until 20 $M_{\odot}$ are calculated with the same code as the tracks of Bertelli et al. [15], so here it has been shown that the according tracks are compatible with observations of RSGs as discussed above.

4.8 Wolf-Rayet stars

As we mentioned above very massive stars pass through the Wolf-Rayet (WR) stage before they finally explode as supernovae or, possibly γ-ray bursts. The WR stars are important sources of ionizing photons, momentum, and chemical elements. Wolf-Rayet stars are the bare core of initially massive star, whose H-rich envelope has been removed by strong stellar winds or through Roche lobe overflow in a close binary system. For more details see the review by Crowther [35].

Conti [32] first proposed that a massive O star may lose a significant amount of mass via stellar winds, revealing first the H-burning products at its surface, and subsequently the He-burning products. The surface composition is used to assign the evolutionary stage of these objects and to classify these stars.

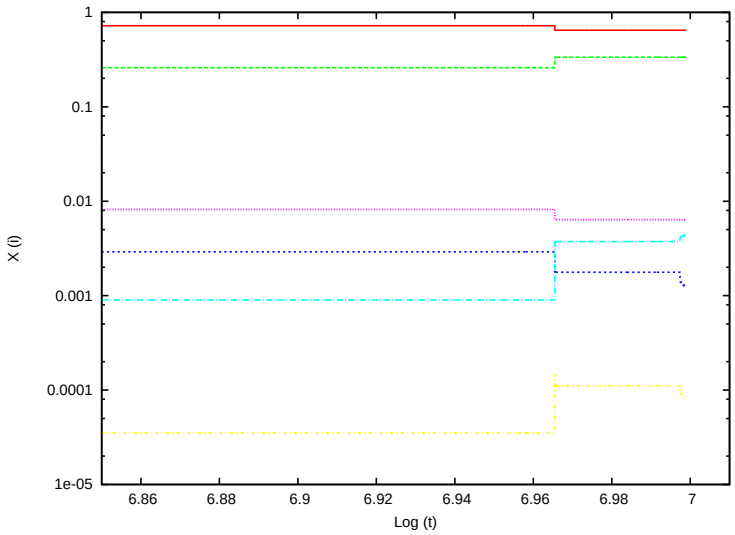

Figure 4.5— The chemical structure of a 20 $M_{\odot}$ star as a funtion of the age in years. The abundances (by mass) of various elements are indicated on a logarithmic scale. The initial chemical composition of the model was chosen to be Z=0.017 and Y=0.26. We use the following color scheme: H in red, ^{4}He in green, ^{16}O in magenta dotted, ^{12}C in purple, ^{14}N cyan dashed-dotted, ^{13}C in yellow.

WR stars, whose spectra are dominated by strong emission lines, are generally grouped into three sequences according to their spectra: WN, WC and WO. The spectra of the WN stars exhibit transition lines of He and N ions with little evidence of C; those of WC stars predominately show lines of He and C with little evidence of N; finally the spectra of the rarer WO stars are dominated by lines of O. The WN stars are commonly separated into the further groups according to whether or not evidence of significant H is detected. Broadly speaking, the separation corresponds to that between early (WNE - little or no hydrogen) and late (WNL - some significant hydrogen) WN stars.

In this section we will not analyze the lifetimes of WR stars and the WR/O and WN/WC number ratios. From the literature it is known that these stars are strongly influenced by rotational mixing and this is exacly the reason why we need a functional rotating code to analyze very massive stars. We will just present the surface abundances of the non rotating models for showing how even for nonrotating models stars evolve into the Wolf-Rayet phase in the HR diagram.

In massive stars, the variation of the surface abundances in the course of

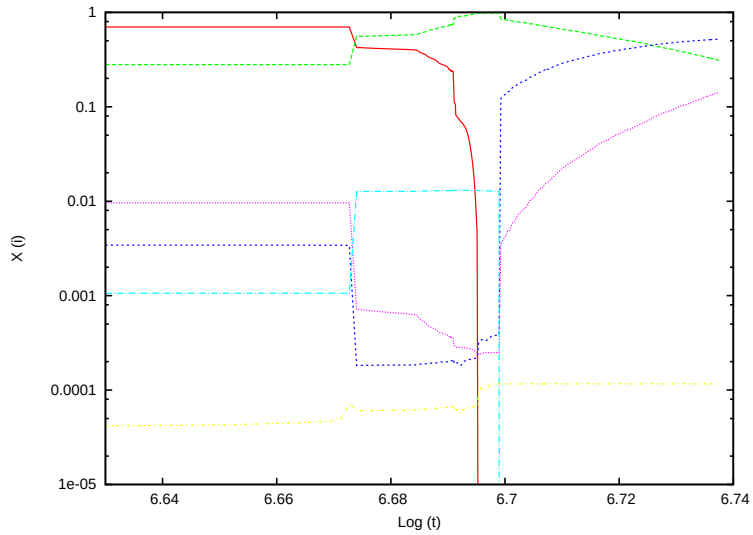

Figure 4.6— The chemical structure of a 40 $M_{\odot}$ star as a funtion of the age in years. The abundances (by mass) of various elements are indicated on a logarithmic scale. The initial chemical composition of the model was chosen to be Z=0.017 and Y=0.26. We use the following color scheme: H in red, ^{4}He in green, ^{16}O in magenta dotted, ^{12}C in purple, ^{14}N cyan dashed-dotted, ^{13}C in yellow.

the evolution is affected by the occurance of mass loss. Layers of the deep interiors can be exposed to the surface under the effect of stellar winds, thus enableing direct observations of the products of the main nuclear burning. This depends of the efficiency of mass loss and central mixing, because central mixing determines the convective core. The bigger the convective core, the easier is the exhibition of nuclearly processed material at the surface. For the assumed mixing (in our case overshooting and mass loss as a function of the age) the variations in the surface abundances (by mass) of ^{1}H,^{4}He,^{12}C,^{13}C,^{14}N and ^{16}O are shown in figures 4.5, 4.6, 4.7, 4.8 respectively for 20, 40, 60 and 80 $M_{\odot}$. In all figures we can identify the hydrogen abundance by the red lines. Furthermore, we indicate the different nuclei by ^{4}He in green, ^{16}O in magenta dotted, ^{12}C in purple, ^{14}N cyan dashed-dotted, ^{13}C in yellow.

A WR star is any star that has $log(T_{eff}/K) \geq 4.0$ and a surface hydrogen mass fraction $X \leq 0.4$. It is assumed that a WR star is initially a WNL star. When $X \leq 0.001$ it becomes a WNE star. The star becomes a WC star when $X \leq 0.001$ and $(x_C + x_O)/y \geq 0.03$, where x_O, x_C and y are the surface number fractions of carbon, oxygen and helium.

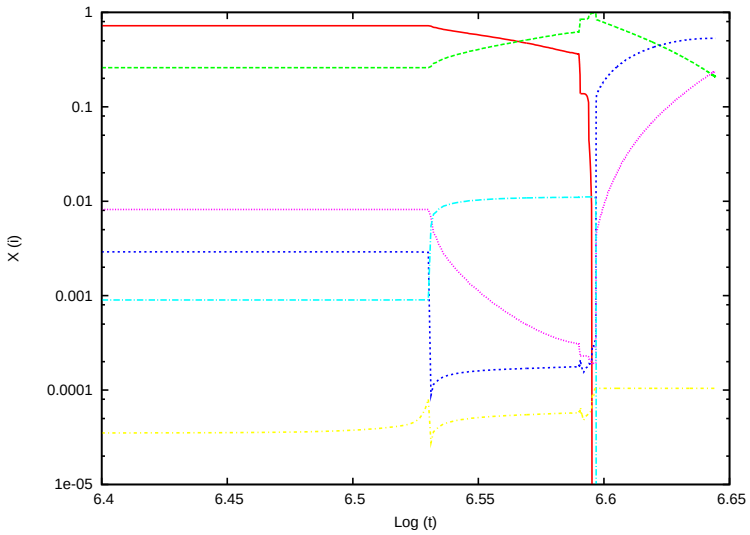

Figure 4.7— The chemical structure of a 60 $M_{\odot}$ star as a funtion of the age in years. The abundances (by mass) of various elements are indicated on a logarithmic scale. The initial chemical composition of the model was chosen to be Z=0.017 and Y=0.26. We use the following color scheme: H in red, ^{4}He in green, ^{16}O in magenta dotted, ^{12}C in purple, ^{14}N cyan dashed-dotted, ^{13}C in yellow.

Not all massive stars evolve through the whole sequence, they may appear as WR objects of the various types according to their initial mass, efficiency of mass loss, and size of the convective cores. If we anlayze the tracks for Z=0.017 and Y=0.26 we can conclude that stars with initial masses greater then 60 $M_{\odot}$, may become a WN stars even during the central hydrogen burning and WC stars during the central helium phase. Stars with initial masses in the range 40 to 60 undergo the WN phase at the very end of central hydrogen burning phase. As we can see in figures 4.7 and 4.8 in the case of 60 $M_{\odot}$ star and 80 $M_{\odot}$, the surface abundance of ^{14}N becomes higher than the abundances of ^{12}C and ^{16}O already during the last 25% of the core hydrogen burning phase while the star appears in the HR diagram as a LBV object. For the 40 $M_{\odot}$ this is manifest only towards the very end of central hydrogen burning as we can see in Fig.4.6. We can see that for stars with 20 $M_{\odot}$ and lower masses, the mass loss rates are not high enough to expose the surface layers with low hydrogen abundance. So for models without rotation they will not undergo the WR phase.

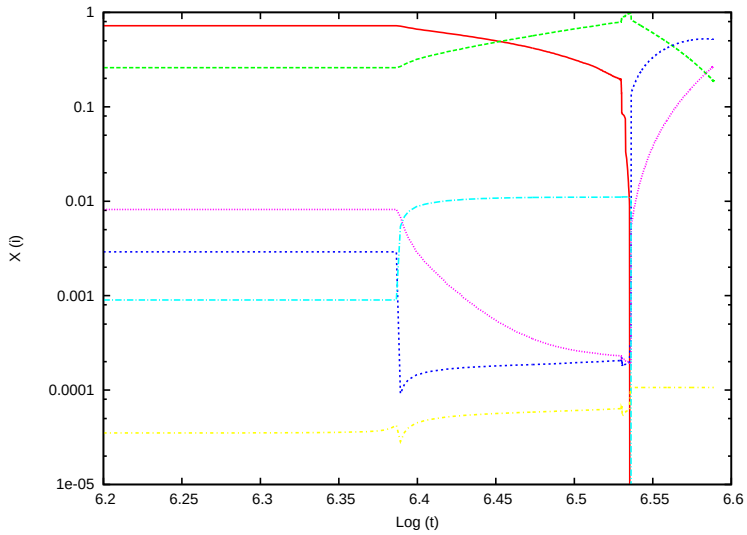

Figure 4.8— The chemical structure of a 80 $M_{\odot}$ star as a funtion of the age in years. The abundances (by mass) of various elements are indicated on a logarithmic scale. The initial chemical composition of the model was chosen to be Z=0.017 and Y=0.26. We use the following color scheme: H in red, ^{4}He in green, ^{16}O in magenta dotted, ^{12}C in purple, ^{14}N cyan dashed-dotted, ^{13}C in yellow.

4.9 Luminosity blue variables

Finally, we note that our tracks for very massive stars as visible in Figs. 4.1, 4.2 and 4.3 are compatible with the observations of Luminous Blue Variables stars (LBVs). LBVs are evolved, luminous hot stars that experience eruption events and episodes of increased mass loss. During such outburst they move in the Hertzsprung-Russell diagram from their normal hot quiescent state to lower temperatures. Changes in the brightness of different amplitudes are known to occur for LBVs. Some LBVs correspond to initial masses of $25M_{\odot}$ and final masses as low as $\sim 10M_{\odot} - 15M_{\odot}$.

In order to confront our theoretically calculated tracks with observations, Fig. 4.9, adapted from Smith et al. [153], shows the positions on the HR diagram of well-studied LBVs in the Milky Way and nearby galaxies, as well as some related stars. It borrows from similar diagrams presented by Wolf [172], de Jager [37] (more details in Smith et al. [153]), but includes additional stars and updated values from the literature. LBVs generally reside in the shade dareas of the diagram, either along the diagonal quiescent S Doradus instability

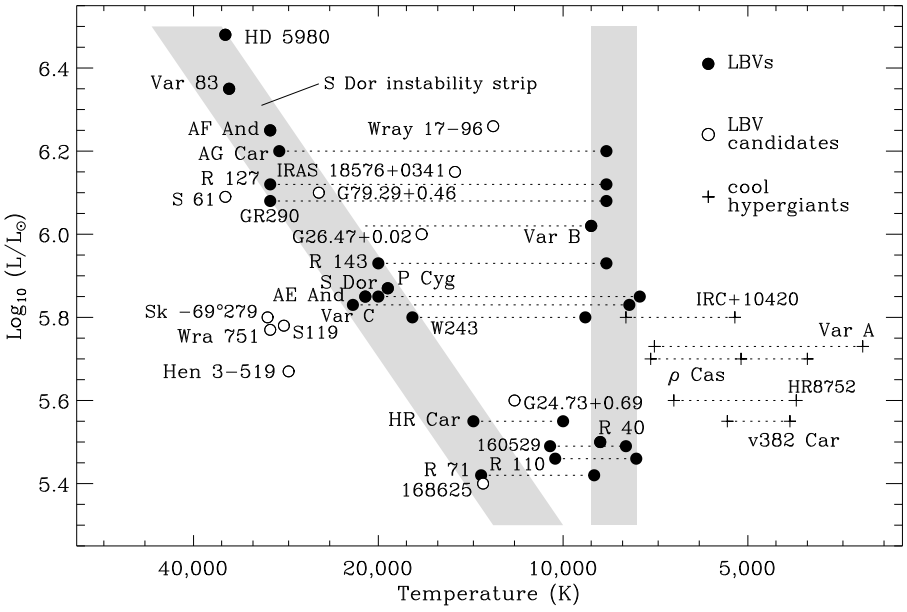

Figure 4.9— Observed LBVs in the Hertzprung-Russel diagram. Figure taken from Smith et al. [153].

strip [172] or along the constant temperature vertical stripe while in outburst (Davidson [36]). The dotted line represent their transit between quiescence and their outburst state or visual maxiumum. Their effective temperatures vary from 30 000 K, corresponding to spectral type late O/early B, for the luminous classical LBVs to only ∼15 000K, coressponding to late B spectral types, for the less luminous LBVs. Object from both subgroups transit redwards to T_{eff} not lower then ∼8 000, coressponding to spectral types A to F, when they are "in outburst" or viual maximum. Wolf [172] noted taht the amplitudes of the S Doradus excursions become larger with increasing luminosity, and suggested that the most luminous LBVs could be cosmological distance indicators. Normal blue supergiants are also observed in and to the right of the S Doradus instability striip, but they may not be close to their Eddington limit and therefore not to be subjected to the instability that characterizes LBVs. The cool or yellow hypergiants (YHGs) just below the Humphreys-Davidson limit [80], [79] are included ad these may somehow represent a distinct lack of LBVs in the range $5.6 - 5.8 log(L/L_{\odot})$.

We can conclude that our evolutionary tracks sucesfully covers the range of the LBVs for the $log(L/L_{\odot}) < 6.3log(L/L_{\odot})$ on the schematic HRD that we can see in Fig. 4.9. Stellar evolutionary theory predicts that LBV's have the largest allowed mass by gravity: if they were any larger, gravity would be insuddicient to balance the radiation pressure and they would blow away the excess mass through stellar wind. As they are, they barely mantain hydrostatic equilibrium because their stellar wind constantly ejects matter. For this reason there are usually nebulae around such stars, created by outbursts; η Carinae is the nearest and best studied example. After having completely shed their outer envelope, LBVs are supposed to become WR stars and eventually explode as Ib/c SNe. It is worth to note that while the maximum initial mass is thought to be $\sim 150M_{\odot}$, WR stars do not have masses in exceed of 20 $M_{\odot}$. Therefore, very massive stars are supposed to remove a burden of 30 $M_{\odot}$-130 $M_{\odot}$ during their lifetime before the Wr phase. This would maen that the mass loss must be especially efficient during the late evolutionary stages. Alternatively, one could tentatively aaume that LBVs may somehow be able to explode as supernovae before having depleted their outer hydrogen envelope.

CHAPTER 5

Models with mass loss and rotation

In this chapter we present the very first results of our new implementation. Here, we focus on a number of selected models and describe some general observations without entering a deep discussion which is beyond the scope of this work. First we discuss models with 10 $M_{\odot}$ and the same chemical composition but with different rotation rates to point out the general effects of rotation. Then we investigate tracks for different initial masses and finally, we also vary the metallicity. In addition, we present a few tracks that include overshooting. We close our discussion with an survey of results available in the literature, and in a comparison, we set our findings in relation to the avaliable tracks. Before presenting our calculations we introduce the critical rotation rate of stars in order to quantify angular velocities.

5.1 Critical velocities

For every star one can define a critical angular velocity Ω_{crit}, sometimes called break up velocity. If a star rotates with this angular velocity, the centrifugal force equals the gravitational force at the equator. Hence, the star is marginally stable to mass shedding from the equator. This critical velocity can be easily derived form the expression for the effective gravity at the equator assuming

rigid rotation (see equation (3.11)). Then the effective gravity reads

$$g_{eff}(\theta = \pi/2) = \sqrt{-\frac{GM}{R_e^2} + \Omega^2 R_e} \tag{5.1}$$

with the equatorial radius R_e. Setting this expression to zero yields

$$\Omega_{crit} = \sqrt{\frac{GM}{R_{e,crit}^3}}. \tag{5.2}$$

This angular velocity can be converted to an linear velocity via

$$v_{crit} = \Omega_{crit} R_{e,crit}. \tag{5.3}$$

From the surface equation (3.7) one finds that at the critical rotation rate the equatorial radius is given by

$$R_{e,crit} = \frac{3}{2} R_{p,crit} \tag{5.4}$$

and thus

$$\Omega_{crit} = \sqrt{\frac{GM}{(1.5 R_{p,crit})^3}}. \tag{5.5}$$

Note that for simplicity in the following we assume that the polar radius $R_{p,crit}$ is approximately given by the polar radius of the corresponding nonrotating star, which is a fair approximation because the changes of the polar radius due to rotation are very small (but see [106] for a more consistent description). It is convenient to characterize the rotation rate of a star by the fraction of the critical angular velocity because it allows an easy assessment of how fast a star rotates, i.e. how strong is the impact of rotation on the star's structure. Therefore, in the following we will use angular velocity realtive to the critical one, Ω/Ω_{crit}, to specify the rotation rate of a star.

5.2 Rotating models on the main sequence

After describing the basics of stellar rotation and detailing the approach to treat stellar rotation numerically we present in this section the first results of our new implementation of stellar rotation. These models are thought to be a testbed for the code. We discuss the evolutionary tracks for stars with 10 $M_\odot$ and with a chemical composition of Z=0.017 and Y=0.26, taking into account the effects of rotation and local conservation of angular momentum as discussed in chapter 4.

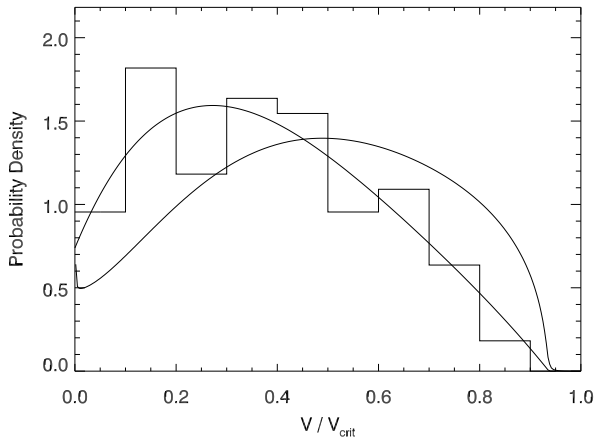

Figure 5.1— Probability distribution of linear velocities as the fraction of the critical velocity of rotating young B stars. Note that the inclination angle is unknown. Figure taken from [77].

These models include in particular the effect of mass loss due to stellar rotation as sketched in chapter 4. We calculated the tracks assuming initally uniform rotation with an angular velocity of $\Omega = 0.5\Omega_{crit}$ and $\Omega = 0.6\Omega_{crit}$, where Ω_{crit} is the critical angular velocity as defined in the previous section. These angular velocities correspond to linear velocities of v_{ini} =261 km/s and v_{ini} =312 km/s.

The choice of v_{ini}/v_{crit} is based on the peak of the velocity distribution of young B stars in Huang et al. [78] as we can see in Fig. 5.1. This initial rotation rate corresponds to the mean MS velocities comprised between 110 and 220 km/s for the stars that are not magnetically braked ($M_{ini} \geq 1.7M_{\odot}$). These values are well within the range of those observed in the Galaxy (Huang & Gies [77])

In Fig. 5.2 we can see mainly the core hydrogen burning evolution of the stars modeled with our new code. It takes about 90% of the whole lifetime of stars and is therefore the evolutionary phase which can be most compared with observations. The blue line indicates the track for the nonrotating star. The other two curves correspond to the rotating stellar models. The red one belongs to the star rotating initially with 50% of its critical velocity, while the cyan line marks the star with 60% of the critcial velocity.

One observes a clear reduction in the effective temperature, which is stronger for initially higher rotation rates. The tracks evolve nearly parallel in the HR

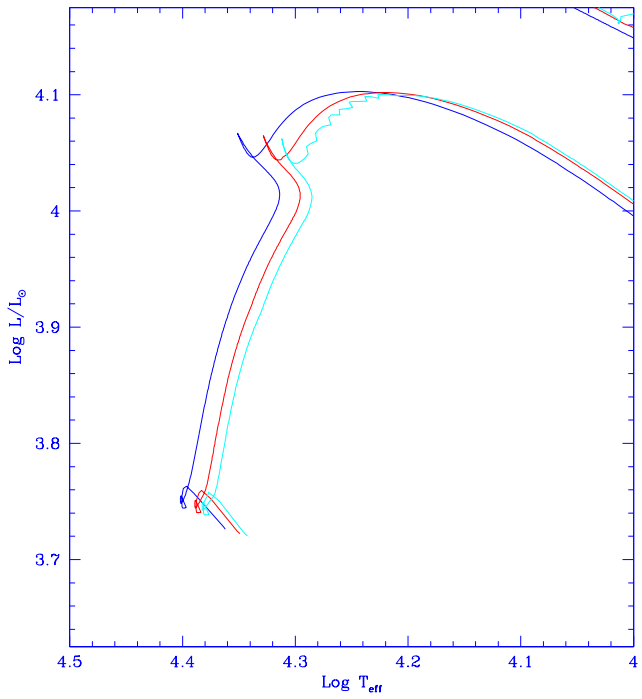

Figure 5.2— Main sequence evolution in the Hertzsprung-Russell diagram for three stars of the same chemical composition with the same mass of 10 $M_{\odot}$. The blue line denotes a nonrotating star. The red and the cyan curves correspond to stars that rotate initially with 50% and 60% of their critical velocity.

diagram during the core hydrogen burning. Note that the differences between the two rotating models are nearly as large as the difference between the non-rotating star and the model spinning with 50% Ω_{crit} leading to the conclusion that stellar rotation becomes increasingly effective with initially higher rotation rates. These findings are in agreement with the reduction of the effective temperature, which has been reported by other authors (see e.g Meynet & Maeder [123]). The wiggles beyond the main sequence phase for the track with 60% Ω_{crit} are likely to be connected to numerical problems of the atmosphere treatment but remain unexplored at this point.

It is furthermore noticeable in Fig. 5.2 that the luminosities on the zero-age main sequence are lowered for rotating stars, also in agreement with findings

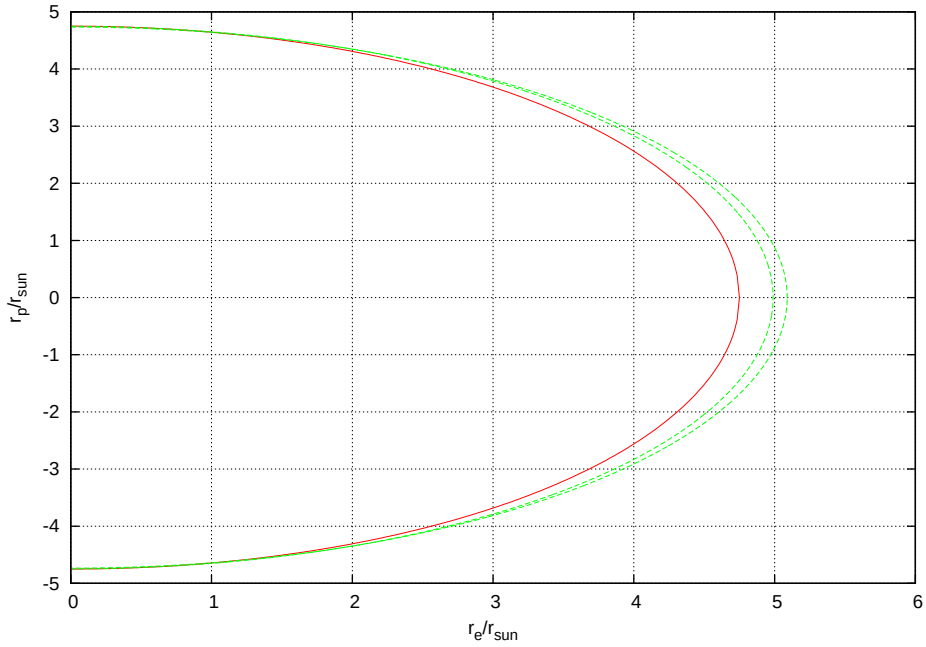

Figure 5.3— Surface of three stars on the zero age main sequence with the same chemical composition and the same mass. The snapshot illustrates the effects of rotation when comparing the polar radius r_p to the equatorial radius r_e. The dashed lines correspond to stars rotating with 50% and 60% of its critical velocity.

in the literature. Note also that the turn-off point is shifted towards lower luminosities for rotating stellar models. Analyzing the presented tracks in more details reveals that the lifetime on the main sequence is slightly lengthens for rotating stars. This behavior can be also seen in the temporal evolution of the central density or the central temperature (not shown here). The changes in the lifetime can be understood intuitively. The lifetime enhancement is a consequence of the decrease of the effective temperature and luminosity in rotating models due to the decreased effective gravity. The small shift of the tracks towards lower luminosity and effective temperatures on and close to the zero age main sequence is an effect of atmospheric distorsions and of the lowering of the effective gravity as it was pointed out in the past by Kippenhahn & Thomas [86], Maeder & Peytremann [113] . At this stage the stars are still nearly homogeneous.

Finally, before discussing the whole evolutionary track, we illustrated by a

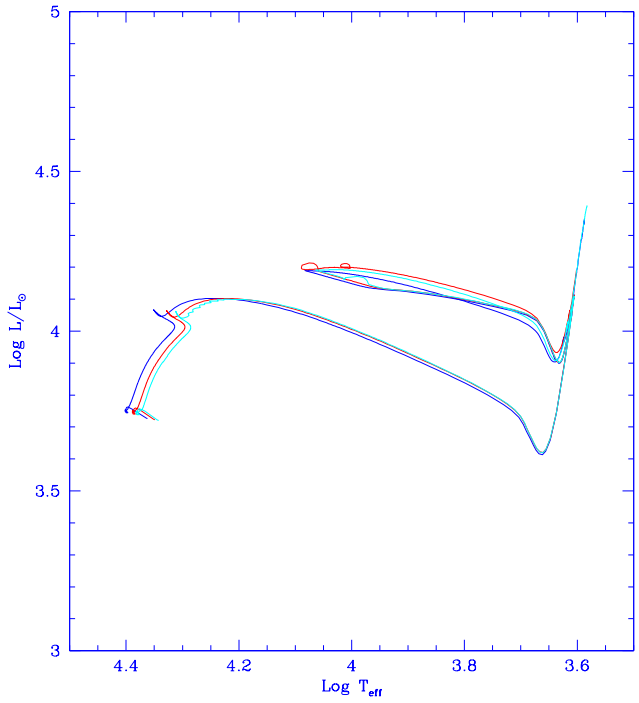

Figure 5.4— Whole evolutionary track in the Hertzsprung-Russell diagram for three stars of the same chemical composition with the same mass of 10 $M_{\odot}$. The blue line denotes a nonrotating star. The red and the cyan curves correspond to stars that rotate initially with 50% and 60% of their critical velocity.

snapshot the effects of rotation exemplary in the first stellar model on the zero age main sequence. In Fig. 5.3 the surface of the considered stars is shown. One can clearly recognize the flattening due to rotation by comparing the location of the equator for the different stars. While the polar radii coincide to a high precision for all three models, the radii at the equator deviate significantly from the spherical, nonrotating model (inner most line). (The outermost curve corresponds to the model spinning with 60% of the critical rotation rate.)

The equatorial radii for the rotating models are a few per cent larger than the polar radii. It is apparent that the structural changes due to rotation get increasingly stronger for higher rotation rates (compare the difference in the models with 0 and 50% of the critical rotation rate with the deviations in the

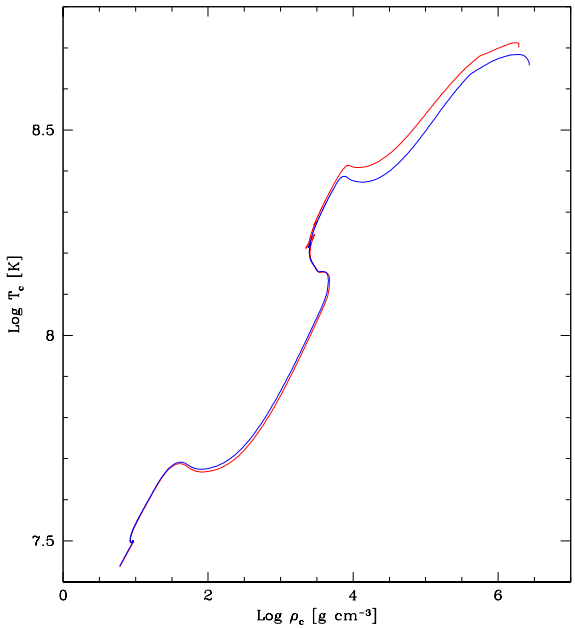

Figure 5.5— Central temperature as a function of the central density for a nonrotating model (blue line) and for a model rotating with 50% of its critical velocity (red line).

radii of the models with 50% and 60% of the break up velocity). Note that in all models considered in this thesis the Roche approximation is adopted meaning that the gravitational potential is assumed to be spherical symmetric. This can be considered to be a fair approximation as long as the core does not spin extremely fast showing significant deviations from spherial symmetry.

In the Fig. 5.4 we present the complete evolutionary tracks for 10 $M_{\odot}$ and a chemical composition of Z=0.017 and Y=0.26 computed without overshooting and with mass loss. The blue line indicates as before the nonrotating model and the cyan and red line the models with rotation as defined in a Fig. 5.2. We can notice slight differences in the luminosities between the rotating and nonrotating tracks, in the sense that rotational models tends towards higher luminosities after the main sequence evolution. But this difference is very small in our models which may be explained by two points. First, the chosen rotation rates are not extremely high and thus the effects of rotation are still small. Second, rotational mixing is not yet switched on for these calculations and therefore

we may miss the physics necessary to increase the luminosity significantly as found in other computations. Rotational mixing has the effect to bring fresh hydrogen fuel into the convective core, slowing down its decrease in mass during the main sequence. For a given value of the central hydrogen content the mass of the convective core in the rotating model is therefore larger than in the nonrotating model and therefore the stellar luminosity is higher (e.g. Heger et al. [72], Meynet & Maeder [124]). Rotational mixing also transports helium and other hydrogen burning products (essentially nitrogen) into the radiative envelope. The helium enrichment lowers the opacity. This contributes to the enhancement of the stellar luminosity and favours the blueward track Maeder & Meynet [124]. Obviously this effect can not be expected from our tracks because rotationaly mixing is not yet used here.

Fig. 5.5 displays the central temperature as a function of the central density for the rotating stellar evolution model (with 50% of the critical velocity) and for the nonrotating reference model. The plot covers the phase the initial hydrogen burning to the phase of carbon burning. It is evident that the stars follow approximately the same curves until helium is exhausted in the core. This is understandable from the fact that the rotation rates are not very high. The star initially rotates uniformly. This implies that even if the rotation rates were critical (determined at the stellar surface), the core would still spin relatively slow in terms of distortions due to centrifugal forces. One could also consider a break up velocity for every mass shell and would find the stellar core to rotate slowly in this respect. This explains why the curves are initially on top of each other. As the core contracts in the course of the evolution, it spins up because of the conservation of angular momentum. Then rotational effects become noticeable in the core and the central density is lower in comparison to central density in the nonrotating model.

5.3 Evolutionary tracks with rotation at different Z, with different masses and with overshooting

After analyzing in detail the evolutionary tracks calculated for 10 $M_{\odot}$, we present the set of tracks for 6 $M_{\odot}$, 8 $M_{\odot}$, 9 $M_{\odot}$, 10 $M_{\odot}$, 12 $M_{\odot}$ and 20 $M_{\odot}$ for the same chemical composition as before. The blue lines represent the evolutionary tracks without rotation, without overshooting and with mass loss. The red ones denote the tracks rotating initially with 50% of thier critical velocity. They are computed including mass loss but without overshooting.

We can conlude that the tracks are following the same pattern and that every rotating track differs from its nonrotating counterpart in the same way that we explained for 10 $M_{\odot}$ models. So in general the rotating models are shifted

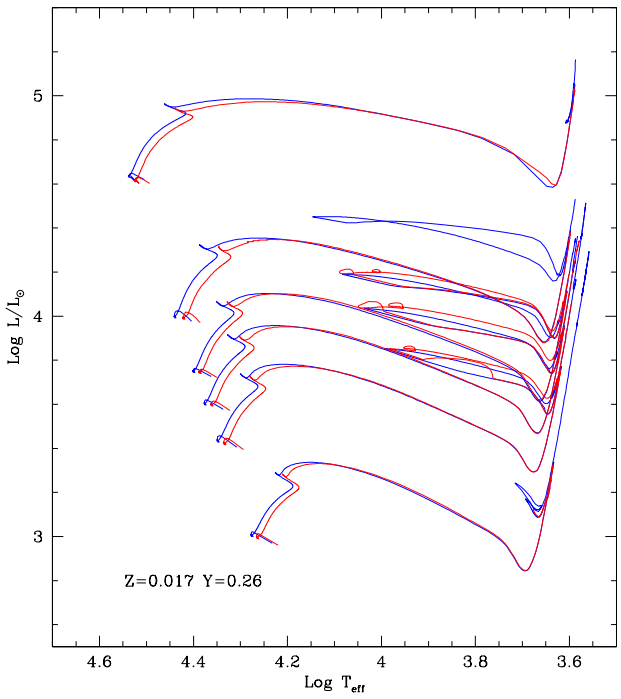

Figure 5.6— Evolutionary tracks in the Hertzsprung-Russell diagram for stars with 6 $M_\odot$, 8 $M_\odot$, 9 $M_\odot$, 10 $M_\odot$, 12 $M_\odot$ and 20 $M_\odot$. Blue lines indicate models without rotation, red curves correspond to stars rotating initially with 50% of their critical velocity. In these calculations no overshooting is included.

during the main sequence evolution towards lower luminosites and effective temperatures. In general we can say that their main sequence lifetime duration is affected by rotation at least in two ways. Rotation increases the quantity of hydrogen burnt in the core. The hydrostatic effects of rotation make a star of a given initial mass to behave as a nonrotating star of smaller initial mass. These effects tend to increase the main sequence lifetime.

The stars in this mass range become red supergiants and rotation does not change qualitatively their behaviour. We just notice that for the star with initially 12 $M_\odot$, rotating track shows a reduction of the blue loop. This can be understood in the following way. The blue extensions of the loops mainly depend on the potential of the core $\Phi \sim M_c/R_c$. There is a critical value of the

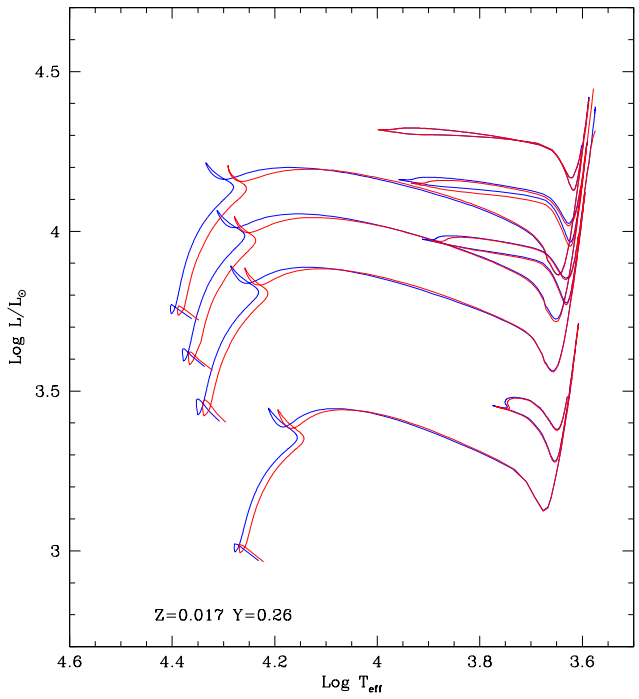

Figure 5.7— Evolutionary tracks in the Hertzsprung-Russell diagram for stars with 6 $M_{\odot}$, 8 $M_{\odot}$, 9 $M_{\odot}$ and 10 $M_{\odot}$. Blue lines indicate models without rotation, red curves correspond to stars rotating initially with 50% of their critical velocity. In these calculations overshooting is included. The chemical composition is Z=0.017 and Y=0.26.

potential such that $\Phi_{crit}(M)$ increases with mass. If $\Phi_c < \Phi_{crit}(M)$ then the blue evolution is favoured, otherwise the redward evolution. The core potential grows with the core mass like $\Phi \sim M_c^{0.4}$. Any effect which increases the core mass and therefore Φ_c also favours a redward evolution instead of a blue loop. Rotation can reduce the blue loops because of the core extension. In the case of mass loss that can also reduce the blue loops, Φ_c remains the same, while $\Phi_{crit}(M)$ becomes smaller since the total mass M is smaller.

In the Fig.5.7 we present our first tracks including overshooting, mass loss and rotation for the same chemical composition as in the previous figures. The red lines represent again the rotation tracks with the same initial angular velocities as for the tracks computed without overshooting. The blue lines mark

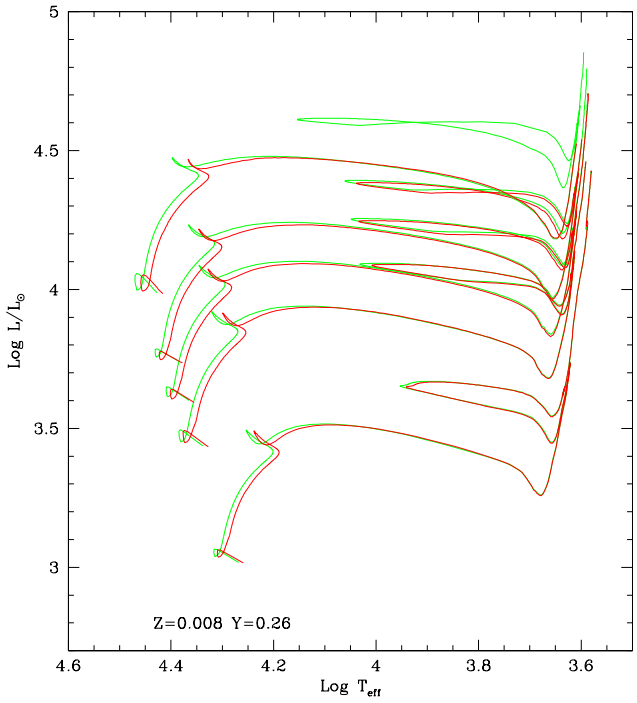

Figure 5.8— Evolutionary tracks in the Hertzsprung-Russell diagram for stars with 6 $M_\odot$, 8 $M_\odot$, 9 $M_\odot$, 10 $M_\odot$ and 12 $M_\odot$. Green lines indicate models without rotation, red curves correspond to stars rotating initially with 50% of their critical velocity. In these calculations overshooting is included. Note that a different metallicity is assumed (Z=0.008 and Y=0.26).

the tracks without rotation. The tracks are computed for the 6 $M_\odot$, 8 $M_\odot$, 9 $M_\odot$ and 10 $M_\odot$, and we can notice that the tracks differ from the ones without overshooting as we explained in chapter 5. But, the general trend caused by rotation of lowering the effective temperature and luminosity, and therefore increasing the lifetime during the main sequence is the same as for those tracks visible in Fig. 5.6. So the effect of rotation on the tracks with and without overshooting is the same.

The conclusions are the same also for a different metallicity of Z=0.008 and Y=0.26. In the Fig. 5.8 we present the tracks for the 6 $M_\odot$, 8 $M_\odot$, 9 $M_\odot$, 10 $M_\odot$ and 12 $M_\odot$. Green lines identify the models without rotation. The red

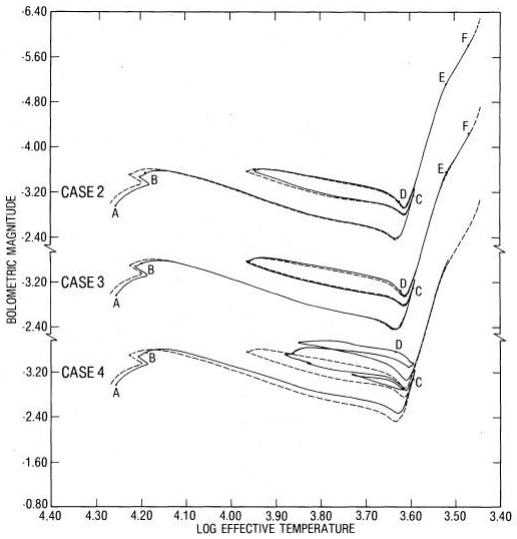

Figure 5.9— Tracks for stars with 7 $M_\odot$. The different lines coorespond to different distributions of angular momentum. See main text for explainations. Figure is taken from [51].

curves indicate the rotation models with the same rotational rate as before. So even if the metallicity is changed, the influence of rotation on the evolutionary tracks remains. We can again notice the same situation for the 12 $M_\odot$ that misses the blue loop.

5.4 Comparision with other models

Kippenhahn et al. [84] investigated rapidly rotating stars ($v \geq 400 km/s$) and followed their evolution until central helium exhaustion. They did not consider mass loss or any mixing of the composition due to rotation, but included the centrifugal force according to Kippenhahn & Thomas [86]. They compared two different assumptions for the transport of angular momentum inside the star. In the first, angular momentum is locally conserved in all radiative regions and uniform rotation is enforced in convective regions. In the second, rigid rotation is enforced also in all radiative zones which are chemically homogeneous.

Compositional mixing from the core into the envelope is inhibited in their work by μ-barrier. The μ-barriers do not allow any mixing between the core and the envelope during central helium burning as in core hydrogen burning. Thus, no angular momentum is lost from the core and these models end up

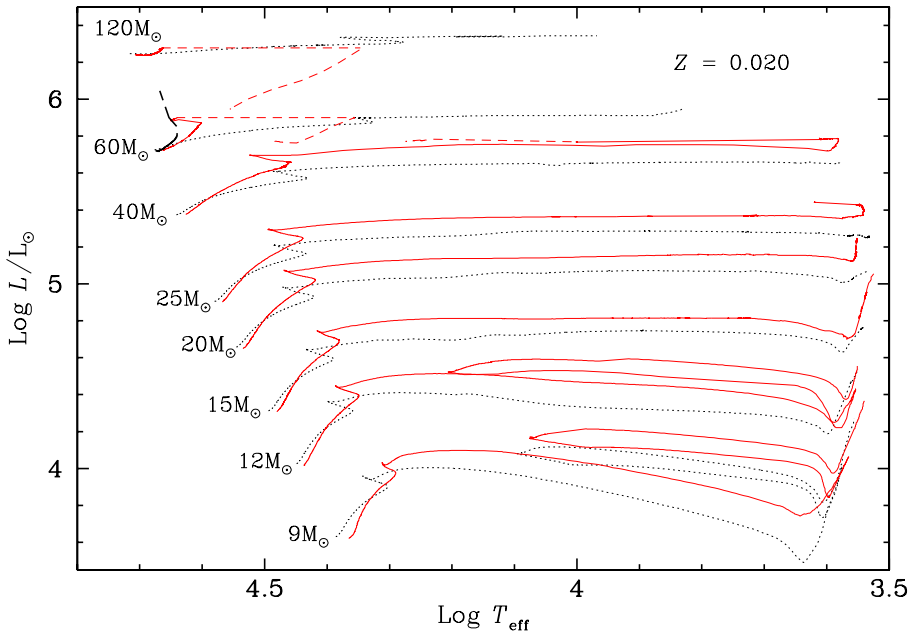

Figure 5.10— Tracks in the range from 9 $M_\odot$ to 120 $M_\odot$ in the Hertzsprung-Russel diagram. Figure is taken from [124]

with rapidly spinning cores which already become secularly unstable to triaxial deformations (Ostriker & Bodenheimer [132] at the end of central helium burning.

Similarly to our result, Kippenhahn et al. [84] found that the lifetime of the stars during core hydrogen burning increases due to the hydrostatic effect of centrigugal forces by only 4% and during central helium burning by 11%. In their work this hydrostatic effect by itself was already sufficient to significantly change the evolution of their models in the HR diagram during central helium burning and causes bigger loops, the effect that we do not notice in our models with rotation.

Endal & Sofia [51] followed the evolution of 7 $M_\odot$ and 10 $M_\odot$ stars with a ZAMS rotational velocity of 210 km/s. They used the Schwarzschild criterion for convection and did not include mass loss. In their work, the μ barrier above the convective hydrogen-burning core supresses mixing and transport of angular momentum completely. Their stellar cores therefore lose very little

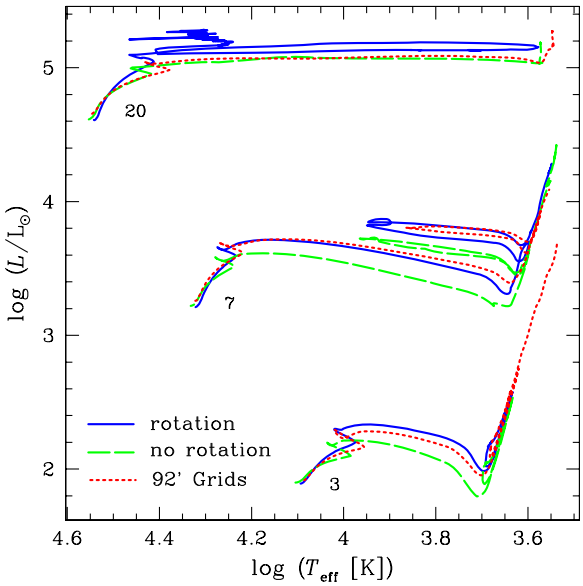

Figure 5.11— Tracks of 3 $M_\odot$, 7 $M_\odot$, and 20 $M_\odot$ in the Hertzsprung-Russel diagram. Figure is taken from [46].

angular momentum during the central hydrogen burning. In Endal & Sofia [51] during the central helium burning the angular momentum loss from the core is greater than in Kippenhahn & Thomas [86], but a big amount of angular momentum is still retained in the core at core helium exhaustion. From the core helium depletion until the end of the calculations, i.e., before carbon ignition they find a reduction of the specific angular momentum by only $\sim 0.2dex$ in the helium and C/O core relative to the specific angular momentum on the ZAMS. In Fig.5.9 we see the sequences of models that were computed for a 7 $M_\odot$ star; one sequence for a nonrotating star (case 0), and three sequences for rotating stars with different assumptions about the redistribution of angular momentum in an evolving star (case 2-4). Case 3 represents an extreme because of the assumption of no redistribution of angular momentum.

Case 2 shows an intermediate and more likely possibility that, while circulation currents redistribute the angular momentum in chemically homogeneous radiative regions, such currents are switched off in homogeneous regions by gradients in the mean molecular weight (Mestel [121]). In convective regions, the high viscosity associated with turbulence may lead to a solid-body rotation. Case 4 represents an alternative possibility where the mass motions in convec-

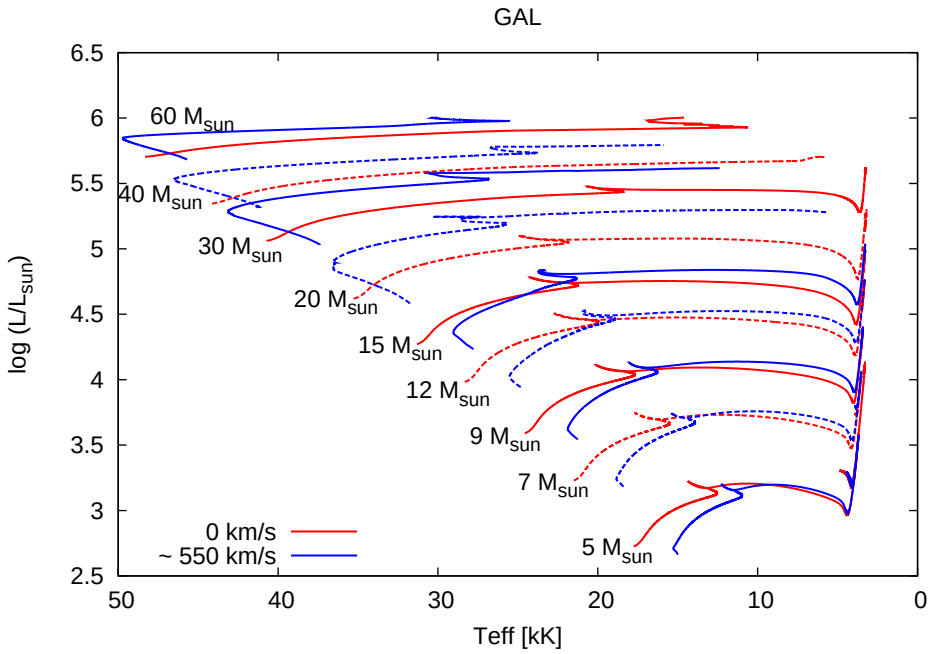

Figure 5.12— Tracks for stars from 5 $M_\odot$ to 60 $M_\odot$ in the Hertzsprung-Russel diagram. Figure is taken from [22]

tive regions tend to equalize the specific angular momentum in such regions. This would be the same if the circulation produced by convection preserves the angular momentum of the convective elements and has, to some extent, been found out by calculations (Tayler [161]). In the tracks it is easy to notice that like in our work the effect of rotation is to lengthen the timescale for the evolution. The case 4 track presents multiple loops as Kippenhahn et al. [84] already indicated.

Meynet & Maeder [123] used a prescription for the Eddington-Sweet circulation in the "aysymptotic regime" according to Zahn (1992) and a Richardson criterium modified for thermal effects. They computed the hydrogen burning evolution for mass of $9M_\odot$ to 60 $M_\odot$. They find a strong inhibiting effect of the μ-gradients on the rotationally induced mixing and angular momentum transport process, and only modest effects due to the centrifugal forces. In the following years they apply futher changes to the physics of rotationally induced mixing discussed in the series of papers about stellar evolution with rotation

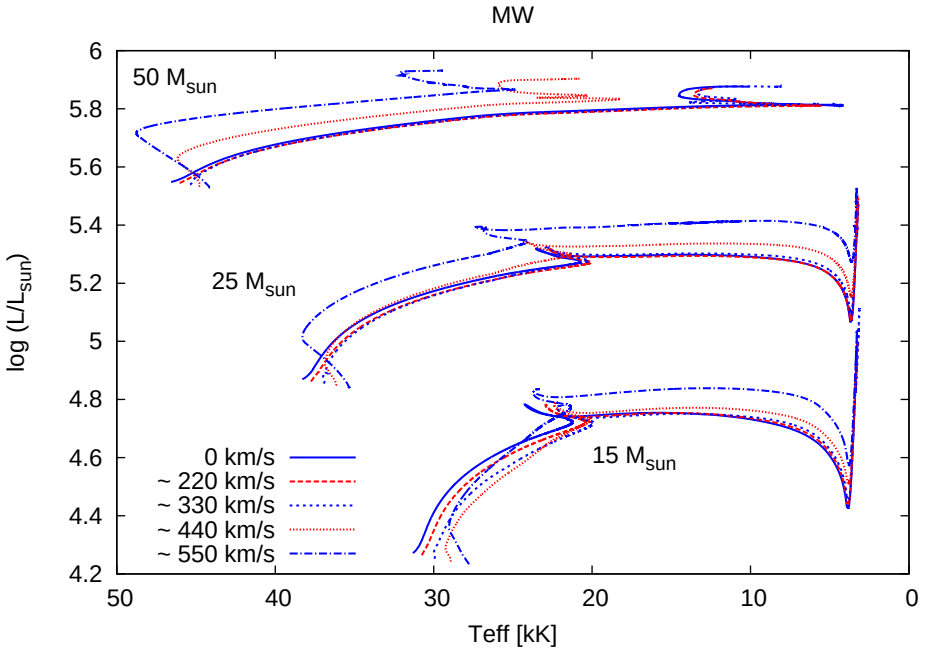

Figure 5.13— Tracks for stars from 15 $M_{\odot}$ to 50 $M_{\odot}$ in the Hertzsprung-Russel diagram. The models are computed for different rotation rates. Figure is taken from [22]

done by the Geneva group. In the Fig. 5.10 we want to show the tracks calculated by this group with the inclusion of the hydrostatic effetcs of rotation, transport of angular momentum, mixing and transport of chemical elements, meridional circulation and shear turbulence and mixing (for more deteils see Meynet & Maeder 2000 [124]). Evolutionary tracks for nonrotating models are represented by dotted lines and for rotating models are shown with solid lines. These rotational models have an initial velocity v_{ini} of 300 km/s. We can clearly see the effects explained before due to rotational mixing that are leading the rotating tracks towards higher luminosities. These tracks as ours also produce on and near the zero age main sequence a small shift of the tracks towards lower luminosities and effective temperatures.

In the Fig. 5.11 we present the newest tracks calculated by the Geneva group by Ekström et al. [46]. We can see the comparision between the rotating models, shown with blue lines, nonrotating models (dashed green lines) and Schaller et al. [148] grids models. Since Schaller's grids many physical inputs have changed

but still the most striking difference is, if we compare the green curve with the red curve, the extension of the main sequence band which is reduced in the present rotating grid as a consequence of the smaller core overshoot (0.10 in the rotatin grid instead of 0.20 in the 1992's one), We will return to this interesting result.

We also want to discuss the rotation evolutionary tracks calculated by a different group (Brott et al. [22]). They use a one-dimesional hydrodynamic stellar evolution code that takes into account the physics of rotation, magnetic fields and mass loss. This code has been described extensively by Heger et al. [72]. Recent improvements are presented in Petrovic et al. [137] and Yoon et al. [178]. In Fig. 5.12 evolutionary tracks for various masses and for the Milky Way metallicity are presented. As we can see, the blue lines are nonrotating models and red lines show the rotating ones computed with ~ 550 km/s so with almost critical velocity. In our models this would correspond to $0.9 \cdot \Omega_{crit}$. We can see the huge difference compared to the models computed by Geneva group. Here they conclude that rotational mixing does effect the surface abundances of those elements that are so fragile that relatively low temperatures in the stellar envelope are sufficient to induce nuclear reactions on them. However, they showed that for stars less massive than 15 $M_{\odot}$ mixing is not efficient enough to significantly alter the structure of the star. As a consequence, the effect of rotation on the coressponding evolutionary tracks in the HR diagram remains limited. This is exactly the same result that we obtained but we need to mention our currently limited input physics where just the hydrostatic effects of rotation and the effects on mass loss are computed. So the found coindidence may be due to the current lack of rotational mixing. Brott et al. (2011) concluded that the effect of rotational mixing becomes more important than the influence of the reduced effective gravity in rapid rotators which are more massive than about 15 $M_{\odot}$. Then towards the cool edge of the main sequence, the rotating stars become more luminous than the nonrotating ones. The main effect of rotation is an effective increase of the size of the stellar core.

We can see the situation in more detail, in Fig. 5.13 for stars more massive than $15M_{\odot}$ for different rotation velocities. We can notice that actually the effects of rotation become important just if the rotational velocities are approaching the critical ones. If not the situation is the same as for masses below $15M_{\odot}$ where the reduced effective gravity is more important then the rotational mixing and then there is a limited difference between the rotating and nonrotating models in the HR diagram. This is very different form the Geneva models where the importance of rotatinal mixing is found to be crucial even for intermediate stars and for 50% of the critical velocity. There is no doubt, that approaching the critical veocities and higher masses, rotation may

crucially affect the surface abundances and the evolutionary tracks in general. There is not yet a consensus among different groups at which mass at which rotation rate the two effects dominate over each other.

5.5 Interplay overshooting - rotation

We can not compare in a direct way our calculated rotationing models and the ones from Maeder group and Langer group. The physics implemented in the code for computing their models as we showed in the previous section are more sophisticated. But, in this work we made a crucial and significant step by including stellar rotation that opens enormous possibilities for implementing all the effects related to rotation such as the transport of chemical elements, the transport of angular momentum, magnetic fields and so on. So even if we can not compare directly the tracks, we can draw already some conlusions.

Obviously comparing our tracks with the Geneva group even for comparable rotation rates (they are using 40 % of the critical velocity and we 50 %) there is a big difference in the tracks with and without rotation. Their tracks are significantly more luminous with respect to their nonrotating counterpart. This according to theory is due to rotational mixing and due to the fact that in rotating models convective cores are larger than in the nonrotating case and therefore the stellar luminosity is higher. As we pointed out before, our tracks are not tested for rotational mixing so this can be the reason. But then the question arises why our tracks agree with the rotation tracks calculated by the Langer group by Brott et al. [22] for the same rotational rates. As we saw in the previous section they concluded that for the tracks below 15 solar masses rotational effects are not important at these rotational rates. The differences between the tracks of Ekström et al. and Brott et al. may be explained by different choices of the overshoot parameters, from which we may conclude that for larger overshoot parameters the effects of rotational mixing decrease.

Smartt et al. [152] discussed that the newer Geneva models differ in the treatment of mixing and convection in the models which affects the vigour of the nuclear burning in the stars and therefore the luminosity. For example they use a smaller overshooting parameter than the older Geneva models as mixing is now also provided by rotation. Therefore, the rotating models agree with the final luminosities obtained Smartt et al. [152], but the luminosities of non-rotating stars were 0.3 dex lower. He emphasise and we also noticed that the new rotating Geneva models are artificially pushed to lower luminosities as the mixing efficiencies (from overshooting) have been significantly reduced. Otherwise employing the same mixing parameters as previously employed and adding rotational mixing would push all the luminosities too high to be consistent with

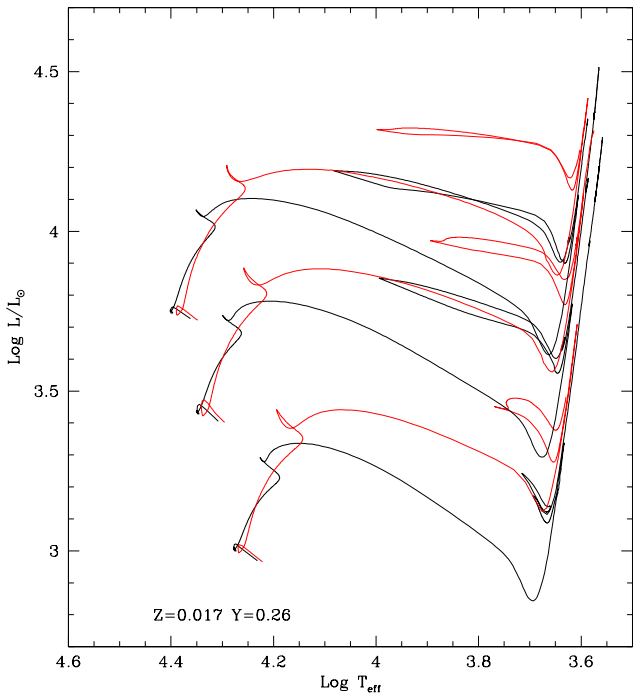

Figure 5.14— Tracks for stars with masses of 6 $M_\odot$, 8 $M_\odot$and 10 $M_\odot$. Black lines show models without rotation and without overshooting. Red curves illustrate models with rotation and overshooting. The initial rotation rate is 50% of the critical rotation rate.

observed HR diagram.

To discuss in more detail this point that we also noticed in comparing roughly our tracks with the Geneva tracks, we present the tracks calculated for the chemical composition with Z=0.017 and Y=0.26, where the black lines represent the models without rotation and overshooting but with mass loss, and the red one the models with rotation and overshooting and mass loss. The tracks are computed for 6 $M_\odot$, 8 $M_\odot$ and 10 $M_\odot$.

As we can see from Fig. 5.14 overshooting can mimic the behaviour of rotating tracks because rotational mixing and overshooting have the same effect on the size of the convective core making it larger. This directly manifests itself in a higher luminosity. But this interplay between overshooting and rotation is very important in explaining the luminosity of a star and it needs to be under-

stood in more detail. We stress that more attention should be paid to this. It is important that at some point the different groups find a qunatitative agreement of the behavior of evolutionary tracks for a given mass, rotation rate and chemical composition. Obviously, rotation remains the crucial ingredient of stellar evolution because their effects on very massive star and rapidly rotating stars are enormous, on which the different groups agree. Moreover, all groups agree that stellar rotation plays an important role to explain the observed surface abundances. These are all points that should be investigate in future work.

CHAPTER 6

Summary, conclusions and outlook

In the introduction of this thesis we argue why stellar rotation is a crucial ingredient in stellar evolution models. Our arguments are substantiated by both observational facts and more theorectical hints towards an important role of stellar rotation in particular for massive stars. From the observational point of view it is evident that stars do rotate. This can be in particular infered from spectroscopic measurements. Furthermore, the asymmetries of stellar winds are likely to be explained by deviations from spherical symmetry due to rotation. Another hint towards rotation are the observed surface abundances of several types of stars, which seem to require an additional mixing process in stars that may rely on rotation. In addition, we sketch the existing results of astroseismology, which allow to have a look deep inside the stellar interior and which have provided evidence for stellar rotation, especially for fast rotating stellar cores.

From the more theoretical side we motivate the study of stellar rotation by the consideration of the number ratio between blue and red supergiants and also by the population of Wolf-Rayet stars. Moreover, the observational data in the context of supernovae hint towards a substantial role of stellar rotation in supernova progenitors. Here we also mention the role of rotation in massive stars for the explaination of long, soft Gamma Ray Bursts. From all these points the necessity of the inclusion of rotation in stellar evolutionary models is obvious. The main purpose of our work is therefore the implementation of stellar rotation in a stellar evolution code.

In order to lay out the starting point we provide a rather general and basic description of the equations governing stellar structure and stellar evolution. Some details of the numerical implementation are also discussed in chapter 2. We stress that the first challenge and one major achievement of our work is the recovery, the preparation and the adaption of a version of the existing Padova stellar evolution code that can be used as a basis for the implementation of stellar rotation. In particular, it is important to make a code available that includes the lastest developments of input physics and that runs robustly for massive stars. The results of these "test" runs are presented in chapter 4. The tracks discussed there are obtained from our code that includes in particular a proper description of mass loss and of overshooting. Details on the concrete modeling of these effects are briefly summarized in chapter 2. We obtain tracks in the mass range from 10 to 120 $M_{\odot}$ with three different metallicities in the range of Z=0.004 to Z=0.017.

As the major goal of this thesis we present in chapter 3 the implementation of stellar rotation. First we mention some historical developments in the context of stellar rotation. In particular, we describe in general effects of rotation on the stellar structure and review methods that have been used in the past to tackle this problem. Then it is argued that physical processes (horizontal turbulence) are likely to lead to a shellular rotation law inside stars. The according differential rotation law has constant angular velocities on isobars, i.e. on nonspherical surfaces. We present a description of these surfaces by considering the involved forces. At this point we stress that throughout the whole work we are assuming the Roche approximation to be a valid description of the gravitational force. This means that the gravitational potential is assumed to be spherical symmetric. Based on these propositions we outline how the common stellar structure equations in a Lagrangian form are modified by the inclusion of shellular rotation. The crucial advantage of this procedure is the fact that the problem is formally kept one-dimensional, and therefore allows to use an existing stellar evolution code without rotation as the basis for the implementation of rotational effects. The underlying concept of the modified formulation of the stellar structure equations is based on the consideration of isobars, i.e. nonspherical surfaces, that are considered to replace the "classical" concept of spherical mass shells in "nonrotating" models. As mentioned, in the case of shellular rotation the different isobars rotate with constant angular velocities. In the due to rotation modified set of stellar structure equations certain quantities need to be employed as averages over isobars in order to keep the description one-dimensional. This includes in particular the effective gravity subsuming gravitational and centrifugal forces, and other derived quantities. We also stress that the radial coordinate of a mass shell is replaced by a more

abstract radial coordinate which is defined via the volume of a deformed isobar.

The latter two complications, averaging over deformed isobars and the meaning of the new radial coordinate, are the main challenges for the implementation of rotation in an existing code which requires additional numerical infrastructures that provide the corresponding modules. A special difficulty arises from the fact that the function describing isobars (over which has to be avearged and which determine the new radial coordinate) is only implicitly given. Hence, any operation involving an isobar requires the numerical solution of the corresponding equation including the prior determination of the parameter specifying the equation, which has to be accomplished numerically as well. This is frequently the case as any evaluation of the source terms of the stellar structure equations requires these processes. (In more detail, certain quantities like the effective gravity are requested as functions of the mass shell, the angular velocity and the new radial coordinate. The latter three parameters however determine the surface equation to be solved only implicitly. Hence, the parameter set specifying an isobar has to be found by an appropriate numerical algorithm to then allow the numerical solution of the equation under consideration.) In our new implementation we compute tables that contain the needed dependencies between requested and given parameters and employ an interpolation scheme to obtain the according quantities needed for setting up the source terms of the modified stellar structure equations. Note that two tables have to be calculated. One table for the first stellar model where we impose uniform rotation with a given angular velocity. As the stellar model evolves a second table has to be invoked, which has to be constructed under the constraint of the conservation of the angular momentum of each mass shell. In chapter 3 we focus on a clear and detailed presentation of the numerical procedure as there is no decription of these issues available in the literature. We also detail the modifications applied for the treatment of the stellar atmosphere.

We are able to obtain the first results with our new implementation of stellar rotation. Here we consider stars which rotate with 50% and 60% of their critical velocity, the rotation rate where a star is marginally stable to loosing mass by centrifugal forces. We observe a decrease of the effective temperature of rotating stars in comparison to nonrotating models with the same mass and metallicity. Furthermore, we find a slight reduction of the luminosity of rotating stars and an increase of the lifetime during hydrogen burning. We note that after the main sequence the luminosities of rotating stars are not significantly higher than in nonrotating stars. Comparing models with and without overshooting a similar behavior of the resulting tracks is observed. We investigate also the effect of rotation for different initial masses of stars and find in general the same behavior. Furthermore, we run models with a different chemical compostion

and uncover qualitatively the same behavior for these stars. Also a review of results available in the literature is provided in chapter 5 and we discuss our tracks in comparison to the outcomes of other groups and find an overall qualitatively consistent picture, though many details also among the different groups remain still unclear. A more thorough, quantitative comparison of our findings to other works is not yet meaningful because the considered physics in the different models vary too much. This includes for instance rotational mixing and the transport of angular momentum.

These differences also indicate the plans for the future of our project. Beside a more detailed analysis and comparison of our models, which is beyond the scope of this work, this includes several developments. The consideration of rotational mixing and transport of angular momentum appears as a natural next step. This requires some additional numerical modules, and, in particular, the tables used for the hydrostatic effects of rotation need to be extended to arbitrary angular momenta if the conservation of angular momentum of single mass shells is given up. Moreover, the numerical stability should be improved for models rotating close to the critical angular velocity which could not yet be achieved by our implementation most likely because of difficulties in the treatment of the atmosphere. Also, more massive rotating stars should be considered with our new implementation. Overall, exciting developments lie ahead, which challenge especially the progress of theoretical models of stellar evolution. New observations and in particular the upcoming results of astroseismology require continuous efforts in the modeling of stellar evolution. Thus, despite lively research over the last decades the field of stellar evolution is about to enter a new era towards a more fundamental understanding of stellar processes.

Bibliography

[1] C. Aerts. Core Overshoot and Nonrigid Internal Rotation of Massive Stars: Current Status from Asteroseismology. In F. Bresolin, P. A. Crowther, & J. Puls, editor, *IAU Symposium*, volume 250 of *IAU Symposium*, pages 237–244, June 2008.

[2] C. Aerts, A. Thoul, J. Daszyńska, R. Scuflaire, C. Waelkens, M. A. Dupret, E. Niemczura, and A. Noels. Asteroseismology of HD 129929: Core Overshooting and Nonrigid Rotation. *Science*, 300:1926–1928, June 2003.

[3] T. Aikawa. On Schwarzschild's theory of stellar rotation. *Sci. Rep. Tohoku Univ. Eighth Ser.*, 53:21–29, 1970.

[4] D. R. Alexander and J. W. Ferguson. Low-temperature Rosseland opacities. ApJ, 437:879–891, December 1994.

[5] M. Alongi, G. Bertelli, A. Bressan, and C. Chiosi. Effects of envelope overshoot on stellar models. *A&A*, 244:95–106, April 1991.

[6] N. Baker and R. Kippenhahn. Untersuchungen über rotierende Sterne. III. Meridionale Zirkulation bei nichtstarrer Rotation. ZAp, 48:140, 1959.

[7] B. Barbuy, J. R. de Medeiros, and A. Maeder. Carbon, nitrogen and oxygen abundances in yellow supergiants. *A&A*, 305:911, January 1996.

[8] P. G. Beck, J. Montalban, T. Kallinger, J. De Ridder, and C. et al. Aerts. Fast core rotation in red-giant stars as revealed by gravity-dominated mixed modes. Nature, 481:55–57, January 2012.

[9] T. R. Bedding and H. Kjeldsen. Observations of solar-like oscillations. *Communications in Asteroseismology*, 150:106, June 2007.

[10] T. R. Bedding, B. Mosser, D. Huber, and J. et al. Montalbán. Gravity modes as a way to distinguish between hydrogen- and helium-burning red giant stars. Nature, 471:608–611, March 2011.

[11] R. Behrend and A. Maeder. Formation of massive stars by growing accretion rate. *A&A*, 373:190–198, July 2001.

[12] K. Belkacem, R. Samadi, M.-J. Goupil, L. Lefèvre, F. Baudin, S. Deheuvels, M.-A. Dupret, T. Appourchaux, R. Scuflaire, M. Auvergne, C. Catala, E. Michel, A. Miglio, J. Montalban, A. Thoul, S. Talon, A. Baglin, and A. Noels. Solar-Like Oscillations in a Massive Star. *Science*, 324:1540–, June 2009.

[13] G. Bertelli, A. Bressan, and C. Chiosi. Setting the clock of stellar models. ApJ, 392:522–529, June 1992.

[14] G. Bertelli, L. Girardi, P. Marigo, and E. Nasi. Scaled solar tracks and isochrones in a large region of the Z-Y plane. I. From the ZAMS to the TP-AGB end for 0.15-2.5 $\{M\}_{\&sun;}$ stars. *A&A*, 484:815–830, June 2008.

[15] G. Bertelli, E. Nasi, L. Girardi, and P. Marigo. Scaled solar tracks and isochrones in a large region of the Z-Y plane. II. From 2.5 to 20 $M_{\odot}$ stars. *A&A*, 508:355–369, December 2009.

[16] J. E. Bjorkman and J. P. Cassinelli. Equatorial disk formation around rotating stars due to Ram pressure confinement by the stellar wind. ApJ, 409:429–449, May 1993.

[17] P. Bodenheimer. Rapidly Rotating Stars. VII. Effects of Angular Momentum on Upper-Main Models. ApJ, 167:153, July 1971.

[18] E. Böhm-Vitense. Über die Wasserstoffkonvektionszone in Sternen verschiedener Effektivtemperaturen und Leuchtkräfte. Mit 5 Textabbildungen. ZAp, 46:108, 1958.

[19] I. A. Bonnell, M. R. Bate, and H. Zinnecker. On the formation of massive stars. MNRAS, 298:93–102, July 1998.

[20] A. Bressan, F. Fagotto, G. Bertelli, and C. Chiosi. Evolutionary sequences of stellar models with new radiative opacities. II - Z = 0.02. *A&AS*, 100:647–664, September 1993.

[21] A. G. Bressan, C. Chiosi, and G. Bertelli. Mass loss and overshooting in massive stars. *A&A*, 102:25–30, September 1981.

[22] I. Brott, S. E. de Mink, M. Cantiello, N. Langer, A. de Koter, C. J. Evans, I. Hunter, C. Trundle, and J. S. Vink. Rotating massive main-sequence stars. I. Grids of evolutionary models and isochrones. *A&A*, 530:A115, June 2011.

[23] I. Brott, C. J. Evans, I. Hunter, and A. et al. de Koter. Rotating massive main-sequence stars. II. Simulating a population of LMC early B-type stars as a test of rotational mixing. *A&A*, 530:A116, June 2011.

[24] C. J. Burrows, J. Krist, J. J. Hester, and R. et al. Sahai. Hubble Space Telescope Observations of the SN 1987A Triple Ring Nebula. ApJ, 452:680, October 1995.

[25] E. Cappellaro, R. Evans, and M. Turatto. A new determination of supernova rates and a comparison with indicators for galactic star formation. *A&A*, 351:459–466, November 1999.

[26] Carciofi, A. C. and Domiciano de Souze, A. and Magalhães, A. M. and Bjorkman, J. E. and Vakili, F. On the Determination of the Rotational Oblateness of Achernar. ApJ, 676:L41–L44, March 2008.

[27] G. R. Caughlan and W. A. Fowler. Thermonuclear Reaction Rates V. *Atomic Data and Nuclear Data Tables*, 40:283, 1988.

[28] S. Chandrasekhar. The equilibrium of distorted polytropes. I. The rotational problem. MNRAS, 93:390–406, March 1933.

[29] C. Chiosi. Structure and Evolution of Massive Stars. In S. D'Odorico, D. Baade, & K. Kjaer, editor, *The Most Massive Stars*, page 27, 1981.

[30] C. Chiosi and A. Maeder. The evolution of massive stars with mass loss. ARA&A, 24:329–375, 1986.

[31] C. Chiosi and C. Summa. On the Evolution of OB Stars from the Main Sequence to the Helium Exchaustion Phase. Ap&SS, 8:478–496, September 1970.

[32] P. S. Conti. On the relationship between Of and WR stars. *Memoires of the Societe Royale des Sciences de Liege*, 9:193–212, 1976.

[33] T. G. Cowling. The Condition for Turbulence in Rotating Stars. ApJ, 114:272, September 1951.

[34] P. A. Crowther. Stellar Winds from Massive Stars. In D. Vanbeveren, editor, *The Influence of Binaries on Stellar Population Studies*, volume 264 of *Astrophysics and Space Science Library*, page 215, 2001.

[35] P. A. Crowther. Physical Properties of Wolf-Rayet Stars. ARA&A, 45:177–219, September 2007.

[36] K. Davidson. The relation between apparent temperature and mass-loss rate in hypergiant eruptions. ApJ, 317:760–764, June 1987.

[37] C. de Jager. The yellow hypergiants. *A&AR*, 8:145–180, 1998.

[38] C. de Jager, H. Nieuwenhuijzen, and K. A. van der Hucht. Mass loss rates in the Hertzsprung-Russell diagram. *A&AS*, 72:259–289, February 1988.

[39] J. De Ridder, C. Barban, F. Baudin, and F. et al. Carrier. Non-radial oscillation modes with long lifetimes in giant stars. Nature, 459:398–400, May 2009.

[40] L. Deng and D. R. Xiong. How to define the boundaries of a convective zone, and how extended is overshooting? MNRAS, 386:1979–1989, June 2008.

[41] P. A. Denissenkov. Turbulent diffusive mixing in early B-type main sequence stars. *A&A*, 287:113–130, July 1994.

[42] A. Domiciano de Souza, P. Kervella, S. Jankov, L. Abe, F. Vakili, E. di Folco, and F. Paresce. The spinning-top Be star Achernar from VLTI-VINCI. *A&A*, 407:L47–L50, August 2003.

[43] R. G. Eastman, S. E. Woosley, T. A. Weaver, and P. A. Pinto. Theoretical light curve of a Type 2p supernova. ApJ, 430:300–310, July 1994.

[44] A. S. Eddington. Circulating currents in rotating stars. *The Observatory*, 48:73–75, March 1925.

[45] A. S. Eddington. Internal circulation in rotating stars. MNRAS, 90:54, November 1929.

[46] S. Ekström, C. Georgy, P. Eggenberger, G. Meynet, N. Mowlavi, A. Wyttenbach, A. Granada, T. Decressin, R. 3, U. Frischknecht, C. Charbonnel, and A. Maeder. Grids of stellar models with rotation. I. Models from 0.8 to 120 $M_{\&sun;}$ at solar metallicity (Z = 0.014). *A&A*, 537:A146, January 2012.

[47] S. Ekström, G. Meynet, A. Maeder, and F. Barblan. Evolution towards the critical limit and the origin of Be stars. *A&A*, 478:467–485, February 2008.

[48] J. J. Eldridge, R. G. Izzard, and C. A. Tout. The effect of massive binaries on stellar populations and supernova progenitors. MNRAS, 384:1109–1118, March 2008.

[49] J. J. Eldridge and J. S. Vink. Implications of the metallicity dependence of Wolf-Rayet winds. *A&A*, 452:295–301, June 2006.

[50] A. S. Endal and S. Sofia. The evolution of rotating stars. I - Method and exploratory calculations for a 7-solar-mass star. ApJ, 210:184–198, November 1976.

[51] A. S. Endal and S. Sofia. The evolution of rotating stars. II - Calculations with time-dependent redistribution of angular momentum for 7- and 10-solar-mass stars. ApJ, 220:279–290, February 1978.

[52] J. Faulkner, I. W. Roxburgh, and P. A. Strittmatter. Uniformly Rotating Main-Sequence Stars. ApJ, 151:203, January 1968.

[53] J. Fliegner and N. Langer. Models of rotating Wolf-Rayet stars. In K. A. van der Hucht & P. M. Williams, editor, *Wolf-Rayet Stars: Binaries; Colliding Winds; Evolution*, volume 163 of *IAU Symposium*, page 326, 1995.

[54] J. Fliegner, N. Langer, and K. A. Venn. Boron in main sequence B stars: a critical test for rotational mixing. *A&A*, 308:L13–L16, April 1996.

[55] S. Frandsen, F. Carrier, C. Aerts, D. Stello, T. Maas, M. Burnet, H. Bruntt, T. C. Teixeira, J. R. de Medeiros, F. Bouchy, H. Kjeldsen, F. Pijpers, and J. Christensen-Dalsgaard. Detection of Solar-like oscillations in the G7 giant star xi Hya. *A&A*, 394:L5–L8, October 2002.

[56] C. Fransson, A. Cassatella, R. Gilmozzi, R. P. Kirshner, N. Panagia, G. Sonneborn, and W. Wamsteker. Narrow ultraviolet emission lines from SN 1987A - Evidence for CNO processing in the progenitor. ApJ, 336:429–441, January 1989.

[57] D. B. Friend and D. C. Abbott. The theory of radiatively driven stellar winds. III - Wind models with finite disk correction and rotation. ApJ, 311:701–707, December 1986.

[58] I. Fukuda. A statistical study of rotational velocities of the stars. PASP, 94:271–284, April 1982.

[59] A. W. Fullerton. Observations of Hot-Star Winds. In J. P. De Greve, R. Blomme, & H. Hensberge, editor, *Stellar Atmospheres: Theory and Observations*, volume 497 of *Lecture Notes in Physics, Berlin Springer Verlag*, page 187, 1997.

[60] T. J. Galama, P. M. Vreeswijk, and J. et al. van Paradijs. An unusual supernova in the error box of the γ-ray burst of 25 April 1998. Nature, 395:670–672, October 1998.

[61] C. Georgy, G. Meynet, R. Walder, D. Folini, and A. Maeder. The different progenitors of type Ib, Ic SNe, and of GRB. *A&A*, 502:611–622, August 2009.

[62] P. Giannone, K. Kohl, and A. Weigert. Entwicklung in engen Doppelsternsystemen IV. ZAp, 68:107, 1968.

[63] D. R. Gies and D. L. Lambert. Carbon, nitrogen, and oxygen abundances in early B-type stars. ApJ, 387:673–700, March 1992.

[64] R. Gilmozzi, A. Cassatella, J. Clavel, C. Fransson, R. Gonzalez, C. Gry, N. Panagia, A. Talavera, and W. Wamsteker. The progenitor of SN1987A. Nature, 328:318–320, July 1987.

[65] L. Girardi, A. Bressan, C. Chiosi, G. Bertelli, and E. Nasi. Evolutionary sequences of stellar models with new radiative opacities. VI. Z=0.0001. *A&AS*, 117:113–125, May 1996.

[66] D. O. Gough. A new measure of the solar rotation. MNRAS, 196:731–745, September 1981.

[67] L. Gratton. Circolazione interna e instabilità nelle binarie strette. Mem. Soc. Astron. Italiana, 17:5, 1945.

[68] B. Gustafsson, B. Edvardsson, K. Eriksson, M. Mizuno-Wiedner, U. G. Jørgensen, and B. Plez. A Grid of Model Atmospheres for Cool Stars. In I. Hubeny, D. Mihalas, & K. Werner, editor, *Stellar Atmosphere Modeling*, volume 288 of *Astronomical Society of the Pacific Conference Series*, page 331, January 2003.

[69] M. Haft, G. Raffelt, and A. Weiss. Standard and nonstandard plasma neutrino emission revisited. ApJ, 425:222–230, April 1994.

[70] G. Handler, J. M. Matthews, and J. A. et al. Eaton. Asteroseismology of Hybrid Pulsators Made Possible: Simultaneous MOST Space Photometry and Ground-Based Spectroscopy of γ Peg. ApJ, 698:L56–L59, June 2009.

[71] A. Heger and N. Langer. Presupernova Evolution of Rotating Massive Stars. II. Evolution of the Surface Properties. ApJ, 544:1016–1035, December 2000.

[72] A. Heger, N. Langer, and S. E. Woosley. Presupernova Evolution of Rotating Massive Stars. I. Numerical Method and Evolution of the Internal Stellar Structure. ApJ, 528:368–396, January 2000.

[73] A. Heger, S. E. Woosley, and H. C. Spruit. Presupernova Evolution of Differentially Rotating Massive Stars Including Magnetic Fields. ApJ, 626:350–363, June 2005.

[74] A. Herrero, R. P. Kudritzki, J. M. Vilchez, D. Kunze, K. Butler, and S. Haser. Intrinsic parameters of galactic luminous OB stars. *A&A*, 261:209–234, July 1992.

[75] R. Hirschi, G. Meynet, and A. Maeder. Stellar evolution with rotation. XII. Pre-supernova models. *A&A*, 425:649–670, October 2004.

[76] I. D. Howarth, K. W. Siebert, G. A. J. Hussain, and R. K. Prinja. Cross-correlation characteristics of OB stars from IUE spectroscopy. MNRAS, 284:265–285, January 1997.

[77] W. Huang and D. R. Gies. Stellar Rotation in Young Clusters. I. Evolution of Projected Rotational Velocity Distributions. ApJ, 648:580–590, September 2006.

[78] W. Huang, D. R. Gies, and M. V. McSwain. A Stellar Rotation Census of B Stars: From ZAMS to TAMS. ApJ, 722:605–619, October 2010.

[79] R. M. Humphreys and K. Davidson. The luminous blue variables: Astrophysical geysers. PASP, 106:1025–1051, October 1994.

[80] R. M. Humphreys and D. B. McElroy. The initial mass function for massive stars in the Galaxy and the Magellanic Clouds. ApJ, 284:565–577, September 1984.

[81] I. Hunter, I. Brott, N. Langer, D. J. Lennon, P. L. Dufton, I. D. Howarth, R. S. I. Ryans, C. Trundle, C. J. Evans, A. de Koter, and S. J. Smartt.

The VLT-FLAMES survey of massive stars: constraints on stellar evolution from the chemical compositions of rapidly rotating Galactic and Magellanic Cloud B-type stars. *A&A*, 496:841–853, March 2009.

[82] N. Itoh, S. Mitake, H. Iyetomi, and S. Ichimaru. Electrical and thermal conductivities of dense matter in the liquid metal phase. I - High-temperature results. ApJ, 273:774–782, October 1983.

[83] S. Jackson. Rapidly Rotating Stars. V. The Coupling of the Henyey and the Self-Consistent Methods. ApJ, 161:579, August 1970.

[84] R. Kippenhahn, E. Meyer-Hofmeister, and H. C. Thomas. Rotation in Evolving Stars. *A&A*, 5:155, March 1970.

[85] R. Kippenhahn and H.-C. Thomas. Integralapproximationen für die Zustandsgleichung eines entarteten Gases. ZAp, 60:19, 1964.

[86] R. Kippenhahn and H.-C. Thomas. A Simple Method for the Solution of the Stellar Structure Equations Including Rotation and Tidal Forces. In A. Slettebak, editor, *IAU Colloq. 4: Stellar Rotation*, page 20, 1970.

[87] R. Kippenhahn and A. Weigert. *Stellar Structure and Evolution*. 1990.

[88] R. Kippenhahn, A. Weigert, and E. Hofmeister. Methods in Computational Physics 7,129. 1967.

[89] W. Krogdahl. Stellar Rotation and Large-Scale Currents. ApJ, 99:191, March 1944.

[90] R. P. Kudritzki, A. Pauldrach, and J. Puls. Radiation driven winds of hot luminous stars. II - Wind models for O-stars in the Magellanic Clouds. *A&A*, 173:293–298, February 1987.

[91] R.-P. Kudritzki and J. Puls. Winds from Hot Stars. ARA&A, 38:613–666, 2000.

[92] H. J. G. L. M. Lamers, P. Korevaar, and A. Cassatella. The ejection of shells in the stellar wind of the hypergiant P Cygni (B1 Ia/+/). *A&A*, 149:29–40, August 1985.

[93] N. Langer. Mass-dependent mass loss rates of Wolf-Rayet stars. *A&A*, 220:135–143, August 1989.

[94] N. Langer. Evolution of massive stars in the Large Magellanic Cloud - Models with semiconvection. *A&A*, 252:669–688, December 1991.

[95] N. Langer. Coupled mass and angular momentum loss of massive main sequence stars. *A&A*, 329:551–558, January 1998.

[96] N. Langer, J. Fliegner, A. Heger, and S. E. Woosley. Nucleosynthesis in rotating massive stars. *Nuclear Physics A*, 621:457–466, February 1997.

[97] N. Langer, G. García-Segura, and M.-M. Mac Low. Giant Outbursts of Luminous Blue Variables and the Formation of the Homunculus Nebula around eta Carinae. ApJ, 520:L49–L53, July 1999.

[98] N. Langer and A. Maeder. The problem of the blue-to-red supergiant ratio in galaxies. *A&A*, 295:685, March 1995.

[99] E. M. Levesque, P. Massey, K. A. G. Olsen, B. Plez, E. Josselin, A. Maeder, and G. Meynet. The Effective Temperature Scale of Galactic Red Supergiants: Cool, but Not As Cool As We Thought. ApJ, 628:973–985, August 2005.

[100] E. M. Levesque, P. Massey, K. A. G. Olsen, B. Plez, G. Meynet, and A. Maeder. The Effective Temperatures and Physical Properties of Magellanic Cloud Red Supergiants: The Effects of Metallicity. ApJ, 645:1102–1117, July 2006.

[101] C. C. Lovekin, R. G. Deupree, and C. I. Short. Surface Temperature and Synthetic Spectral Energy Distributions for Rotationally Deformed Stars. ApJ, 643:460–470, May 2006.

[102] R. E. Luck. The chemical composition of late-type supergiants. III - Carbon, nitrogen, and oxygen abundances for 19 G and K Ib stars. ApJ, 219:148–164, January 1978.

[103] L. S. Lyubimkov. Observational manifestations of early mixing in B- and O-type stars. Ap&SS, 243:329–349, September 1996.

[104] A. I. MacFadyen and S. E. Woosley. Collapsars: Gamma-Ray Bursts and Explosions in "Failed Supernovae". ApJ, 524:262–289, October 1999.

[105] A. Maeder. Tables for massive star evolution at various metallicities. *A&AS*, 84:139–177, July 1990.

[106] A. Maeder. *Physics, Formation and Evolution of Rotating Stars*. 2009.

[107] A. Maeder and V. Desjacques. The shape of eta Carinae and LBV nebulae. *A&A*, 372:L9–L12, June 2001.

[108] A. Maeder and G. Meynet. Grids of evolutionary models from 0.85 to 120 solar masses - Observational tests and the mass limits. *A&A*, 210:155–173, February 1989.

[109] A. Maeder and G. Meynet. New models of Wolf-Rayet stars and comparison with data in galaxies. *A&A*, 287:803–816, July 1994.

[110] A. Maeder and G. Meynet. The Evolution of Rotating Stars. ARA&A, 38:143–190, 2000.

[111] A. Maeder and G. Meynet. Stellar evolution with rotation. VII. . Low metallicity models and the blue to red supergiant ratio in the SMC. *A&A*, 373:555–571, July 2001.

[112] A. Maeder and G. Meynet. Stellar evolution with rotation and magnetic fields. II. General equations for the transport by Tayler-Spruit dynamo. *A&A*, 422:225–237, July 2004.

[113] A. Maeder and E. Peytremann. Stellar Rotation. *A&A*, 7:120, July 1970.

[114] A. Maeder and J.-P. Zahn. Stellar evolution with rotation. III. Meridional circulation with MU -gradients and non-stationarity. *A&A*, 334:1000–1006, June 1998.

[115] P. Marigo and L. Girardi. Evolution of asymptotic giant branch stars. I. Updated synthetic TP-AGB models and their basic calibration. *A&A*, 469:239–263, July 2007.

[116] C. L. Martin and D. Arnett. The Origin of the Rings around SN 1987A: an Evaluation of the Interacting-Winds Model. ApJ, 447:378, July 1995.

[117] P. Massey. MASSIVE STARS IN THE LOCAL GROUP: Implications for Stellar Evolution and Star Formation. ARA&A, 41:15–56, 2003.

[118] P. Massey and K. A. G. Olsen. The Evolution of Massive Stars. I. Red Supergiants in the Magellanic Clouds. AJ, 126:2867–2886, December 2003.

[119] N. Mauron and E. Josselin. The mass-loss rates of red supergiants and the de Jager prescription. *A&A*, 526:A156, February 2011.

[120] N. D. McErlean, D. J. Lennon, and P. L. Dufton. Galactic B-supergiants: A non-LTE model atmosphere analysis to estimate atmospheric parameters and chemical compositions. *A&A*, 349:553–572, September 1999.

[121] L. Mestel. Rotation and stellar evolution. MNRAS, 113:716, 1953.

[122] G. Meynet, S. Ekström, A. Maeder, R. Hirschi, C. Georgy, and C. Beffa. Developments in Physics of Massive Stars. In F. Bresolin, P. A. Crowther, & J. Puls, editor, *IAU Symposium*, volume 250 of *IAU Symposium*, pages 147–160, June 2008.

[123] G. Meynet and A. Maeder. Stellar evolution with rotation. I. The computational method and the inhibiting effect of the μ-gradient. *A&A*, 321:465–476, May 1997.

[124] G. Meynet and A. Maeder. Stellar evolution with rotation. V. Changes in all the outputs of massive star models. *A&A*, 361:101–120, September 2000.

[125] G. Meynet and A. Maeder. Stellar evolution with rotation. X. Wolf-Rayet star populations at solar metallicity. *A&A*, 404:975–990, June 2003.

[126] G. Meynet and A. Maeder. Stellar evolution with rotation. X. Wolf-Rayet star populations at solar metallicity. *A&A*, 404:975–990, June 2003.

[127] G. Meynet and A. Maeder. Stellar evolution with rotation. XI. Wolf-Rayet star populations at different metallicities. *A&A*, 429:581–598, January 2005.

[128] D. Mihalas, D. G. Hummer, B. W. Mihalas, and W. Daeppen. The equation of state for stellar envelopes. IV - Thermodynamic quantities and selected ionization fractions for six elemental mixes. ApJ, 350:300–308, February 1990.

[129] E. A. Milne. The equilibrium of a rotating star. MNRAS, 83:118–147, January 1923.

[130] T. Moriya, N. Tominaga, S. I. Blinnikov, P. V. Baklanov, and E. I. Sorokina. Supernovae from red supergiants with extensive mass loss. MNRAS, 415:199–213, July 2011.

[131] E. J. Öpik. Rotational currents. MNRAS, 111:278, 1951.

[132] J. P. Ostriker and P. Bodenheimer. On the Oscillations and Stability of Rapidly Rotating Stellar Models. 111. Zero-Viscosity Polytropic Sequences. ApJ, 180:171–180, February 1973.

[133] J. P. Ostriker and J. W.-K. Mark. Rapidly rotating stars. I. The self-consistent-field method. ApJ, 151:1075–1088, March 1968.

[134] S. P. Owocki and K. G. Gayley. ThePhysics of Stellar Winds Near the Eddington Limit. In A. Nota & H. Lamers, editor, *Luminous Blue Variables: Massive Stars in Transition*, volume 120 of *Astronomical Society of the Pacific Conference Series*, page 121, 1997.

[135] J. C. B. Papaloizou and J. A. J. Whelan. The structure of rotating stars:the J2 method and results for uniform rotation. MNRAS, 164:1, 1973.

[136] D. M. Peterson, C. A. Hummel, T. A. Pauls, J. T. Armstrong, J. A. Benson, C. G. Gilbreath, R. B. Hindsley, D. J. Hutter, K. J. Johnston, and D. Mozurkewich. Imaging the Effects of Rotation in Altair and Vega. In A. Richichi, F. Delplancke, F. Paresce, & A. Chelli, editor, *The Power of Optical/IR Interferometry: Recent Scientific Results and 2nd Generation*, page 43, 2008.

[137] J. Petrovic, N. Langer, S.-C. Yoon, and A. Heger. Which massive stars are gamma-ray burst progenitors? *A&A*, 435:247–259, May 2005.

[138] M. H. Pinsonneault, S. D. Kawaler, S. Sofia, and P. Demarque. Evolutionary models of the rotating sun. ApJ, 338:424–452, March 1989.

[139] N. Prantzos and S. Boissier. On the relative frequencies of core-collapse supernovae sub-types: The role of progenitor metallicity. *A&A*, 406:259–264, July 2003.

[140] W. H. Press, S. A. Teukolsky, W. T. Vetterling, and Flannery B. P. *Numerical Recipes In Fortran 77 & 90 - The Art of Scientific Computing, 2ed, Vol 1 & 2.* 1992.

[141] G. Randers. Large-Scale Motion in Stars. ApJ, 94:109, July 1941.

[142] G. Randers. On the Rotation of Stars with Convective Core. ApJ, 95:454, May 1942.

[143] F. J. Rogers and C. A. Iglesias. The OPAL Opacity Code: New Results. In S. J. Adelman & W. L. Wiese, editor, *Astrophysical Applications of Powerful New Databases*, volume 78 of *Astronomical Society of the Pacific Conference Series*, page 31, 1995.

[144] R. A. Rossiter. On the detection of an effect of rotation during eclipse in the velocity of the brigher component of beta Lyrae, and on the constancy of velocity of this system. ApJ, 60:15–21, July 1924.

[145] I. W. Roxburgh, J. S. Griffith, and P. A. Sweet. On Models of Non Spherical Stars I. The Theory of Rapildy Rotating Main Sequence Stars. With 3 Figures in the Text. ZAp, 61:203, 1965.

[146] I.-J. Sackmann and S. P. S. Anand. Structure and Evolution of Rapidly Rotating B-Type Stars. ApJ, 162:105, October 1970.

[147] B. Salasnich. Diffusive mixing in stellar interiors: an applications to alpha-enhanced models. *PhD Thesis, Universita degli studi di Padova*, 2000.

[148] G. Schaller, D. Schaerer, G. Meynet, and A. Maeder. New grids of stellar models from 0.8 to 120 solar masses at Z = 0.020 and Z = 0.001. *A&AS*, 96:269–331, December 1992.

[149] H. Schlattl, A. Heger, H. Oberhummer, T. Rauscher, and A. Csótó. Sensitivity of the C and O production on the 3α rate. Ap&SS, 291:27–56, April 2004.

[150] M. Schwarzschild. On Stellar Rotation. II. ApJ, 106:427, November 1947.

[151] A. Slettebak, II G. W. Collins, T. D. Parkinson, P. B. Boyce, and N. M. White. A system of standard stars for rotational velocity determinations. ApJS, 29:137–159, May 1975.

[152] S. J. Smartt, J. J. Eldridge, R. M. Crockett, and J. R. Maund. The death of massive stars - I. Observational constraints on the progenitors of Type II-P supernovae. MNRAS, 395:1409–1437, May 2009.

[153] N. Smith, J. S. Vink, and A. de Koter. The Missing Luminous Blue Variables and the Bistability Jump. ApJ, 615:475–484, November 2004.

[154] E. A. Spiegel and J.-P. Zahn. The solar tachocline. *A&A*, 265:106–114, November 1992.

[155] H. C. Spruit. Dynamo action by differential rotation in a stably stratified stellar interior. *A&A*, 381:923–932, January 2002.

[156] K. Z. Stanek, T. Matheson, P. M. Garnavich, and P. et al. Martini. Spectroscopic Discovery of the Supernova 2003dh Associated with GRB 030329. ApJ, 591:L17–L20, July 2003.

[157] P. A. Strittmatter, J. W. Robertson, and D. J. Faulkner. Evolution of rapidly rotating stars with mass loss. *A&A*, 5:426–430, May 1970.

[158] J. C. Suárez, A. Moya, P. J. Amado, S. Martín-Ruiz, C. Rodríguez-López, and R. Garrido. Seismology of β Cephei Stars: Differentially Rotating Models for Interpreting the Oscillation Spectrum of ν Eridani. ApJ, 690:1401–1411, January 2009.

[159] I. P. A. Sweet and A. E. Roy. The structure of rotating stars. MNRAS, 113:701, 1953.

[160] P. A. Sweet. The importance of rotation in stellar evolution. MNRAS, 110:548, 1950.

[161] R. J. Tayler. Convection in rotating stars. MNRAS, 165:39, 1973.

[162] K. A. Venn. Atmospheric Parameters and LTE Abundances for 22 Galactic, A-Type Supergiants. ApJS, 99:659, August 1995.

[163] K. A. Venn, D. L. Lambert, and M. Lemke. The abundance of boron in evolved A- and B-type stars. *A&A*, 307:849–859, March 1996.

[164] H. Vogt. Zum Strahlungsgleichgewicht der Sterne. *Astronomische Nachrichten*, 223:229, January 1925.

[165] H. von Zeipel. The radiative equilibrium of a rotating system of gaseous masses. MNRAS, 84:665–683, June 1924.

[166] N. R. Walborn. Evolutionary Helium and CNO Anomalies in the Atmospheres and Winds of Massive Hot Stars. In K. Nomoto, editor, *IAU Colloq. 108: Atmospheric Diagnostics of Stellar Evolution*, volume 305 of *Lecture Notes in Physics, Berlin Springer Verlag*, page 70, 1988.

[167] J. Wasiutynski. Studies in Hydrodynamics and Structure of Stars and Planets. *Astrophysica Norvegica*, 4:1–497, 1946.

[168] K. Weis, W. J. Duschl, D. J. Bomans, Y.-H. Chu, and M. D. Joner. The bipolar structure of the LBV nebula around HR Carinae. *A&A*, 320:568–574, April 1997.

[169] A. Weiss, J. J. Keady, and Jr. N. H. Magee. A Collections of Los Alamos Opacity Tables for All Temperatures. *Atomic Data and Nuclear Data Tables*, 45:209, 1990.

[170] A. Weiss and H. Schlattl. Age-luminosity relations for low-mass metal-poor stars. *A&AS*, 144:487–499, June 2000.

[171] J. C. Wheeler, R. P. Harkness, E. S. Barker, A. L. Cochran, and D. Wills. Supernovae 1983i and 1983v - Evidence for abundance variations in type Ib supernovae. ApJ, 313:L69–L73, February 1987.

[172] B. Wolf. Empirical amplitude-luminosity relation of S Doradus variables and extragalactic distances. *A&A*, 217:87–91, June 1989.

[173] S. E. Woosley. Gamma-ray bursts from stellar mass accretion disks around black holes. ApJ, 405:273–277, March 1993.

[174] S. E. Woosley and J. S. Bloom. The Supernova Gamma-Ray Burst Connection. ARA&A, 44:507–556, September 2006.

[175] S. E. Woosley and A. Heger. The Progenitor Stars of Gamma-Ray Bursts. ApJ, 637:914–921, February 2006.

[176] S. E. Woosley, A. Heger, T. A. Weaver, and N. Langer. SN 1987A - Presupernova Evolution and the Progenitor Star. *ArXiv Astrophysics e-prints*, May 1997.

[177] D.-R. Xiong. The evolution of massive stars using a non-local theory of convection. *A&A*, 167:239–246, October 1986.

[178] S.-C. Yoon, N. Langer, and C. Norman. Single star progenitors of long gamma-ray bursts. I. Model grids and redshift dependent GRB rate. *A&A*, 460:199–208, December 2006.

[179] J.-P. Zahn. Circulation and turbulence in rotating stars. *A&A*, 265:115–132, November 1992.